Summer 5-2012

Synthesis, Modification, and Characterization of Spherical SBA-15 Ordered Mesoporous Silica and Evaluation in High Performance Liquid Chromatography

Alexander P. Giaquinto
Seton Hall University

Synthesis, Modification, and Characterization of Spherical SBA-15 Ordered Mesoporous Silica and Evaluation in High Performance Liquid Chromatography

By:

Alexander Paul Giaquinto

Dissertation submitted to the Department of Chemistry and Biochemistry of Seton Hall University in partial fulfillment of the requirement for the degree of

DOCTOR OF PHILOSOPHY

in

Chemistry

May, 2012

South Orange, New Jersey

This work is dedicated to:

My loving parents:

Alexander and Elizabeth Giaquinto

My guardian Angel:

Pilar Cruz

My Friend:

Steven Ciasulli

We certify that we have read this thesis and that in our opinion it is sufficient in scientific scope and quality as a dissertation for the degree of Doctor of Philosophy

APPROVED

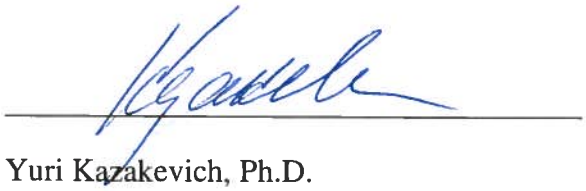

Yuri Kazakevich, Ph.D.
Research Adviser

Alexander Fadeev, Ph.D.
Member of Dissertation Committee

Nicholas H. Snow, Ph.D.
Member of Dissertation Committee

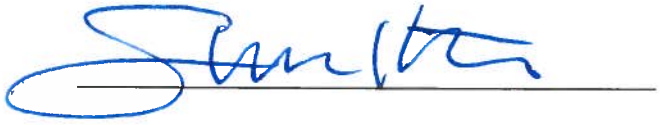

Stephen P. Kelty, Ph.D.
Chair, Department of Chemistry and Biochemistry

Abstract

SBA-15 mesoporous silica is characterized by hexagonally ordered non-intersecting parallel pores. In stark contrast, silica gel, commonly utilized in high performance liquid chromatography as a stationary phase, consists of many interconnected channels created by the spaces between primary particles. There has been much research regarding the importance of the geometry and characteristics of porous silica in chromatography, however, since the advent of ordered materials in the early 1990's, most of the investigations into use of ordered material have failed to extensively study the effects of the highly ordered porous structure on retention mechanisms. In this study, we attempt to evaluate the effect of the characteristic parallel non-intersecting pores of SBA-15 on the thermodynamics and kinetics aspects of retention.

To achieve our goal, it was necessary to transform the native rope-like morphology of SBA-15 into the more commonly used and efficient sphere. The effects of temperature and synthesis time were evaluated. Following modification, characterization by low temperature nitrogen adsorption, thermogravimetric analysis and optical microscopy were utilized to evaluate pore structure, bonded layer characteristics and morphology.

Suitable spherical SBA-15 packed into stainless steel columns were fully characterized for void volume and interparticle volume. Based on the results produced by kinetic studies, the evidence of column obstruction showed a reduced value for the diffusion of benzene as compared to commercial silicas, while surface specific retention studies resulted in the evaluation of reduced accessible surfaces. The obstruction of the pore volume, thus limiting the surface area, is most likely attributed to a combined effect of long narrow pores, which in the spherical particles, tend to bend or twist, and to which an uneven modified layer creates instances of pore blockage of the mobile phase.

Acknowledgement

This dissertation serves, for me, as a reminder of the great things we can achieve in life; of the possibilities offered up to us and the heights we can reach if only we trust in ourselves and the guidance and love of others.

First and foremost I would like to thank my mentor and my friend, Dr. Yuri Kazakevich, for the years of guidance, knowledge and wisdom he has given to me; for the patience and kindness he has shown, and for being the epitome of what a scientist should be. I doubt he will ever truly know the impact he has had on my life and on my ability to write this dissertation. I want to thank him for being a true mentor to me, for trusting in me and allowing me the chance to grow as a scientist and a person.

I would like to thank my co-mentor, Dr. Fadeev, for the years of guidance, trust, and patience he has shown me. I am truly grateful for all of the wisdom he has imparted on me during the past several years. It has been my honor to study under him and to learn all that I have.

I would also like to acknowledge and thank Dr. Snow for being on my dissertation committee, and for always being a positive force in our research laboratory. Dr. Snow has offered valuable scientific advice to me over the years, and his input into this project is much appreciated. He has taught me much over the last several years and I will always be grateful.

I would also like to extend my thanks to the department of Chemistry and Biochemistry, the students and faculty, for all of their help and support throughout these last years of my life.

I would like to specially thank my mother and father for the years of support, unconditional love, and true encouragement. You have given me strength and confidence in myself – the greatest gifts a person can ask for. I am blessed to have parents like you and I will always love you.

Lastly, I would like to thank my angel and fiance, Constanza Del Pilar Cruz. To be honest, I would not be writing this acknowledgement if it were not for you. Your love has brought me back from the depths of despair; from the dark places of this earth from which there is seldom return. I am alive- renewed, hopeful, bright-eyed, and vibrant because of your love and belief in me. I thank you from the bottom of my heart and I will always love you and remember what you have done for me.

Table of Contents

PART I Synthesis, Modification and Characterization of Spherical SBA-15 Ordered Mesoporous Silica

1. Introduction 1

1.1 Chemistry of Porous Silica 2

1.2 SBA-15 Ordered Mesoporous Silica 6

1.2.1 Synthesis Parameters 9

1.2.2 Self-assembly of P123 Micelles and Silica Species 10

1.2.3 Particle Formation and Morphology 12

1.3 Surface Modification 13

1.4 Methods of Characterization 16

1.4.1 Low Temperature Nitrogen Adsorption 16

1.4.1.1 Surface Area and BET Theory 16

1.4.1.2 Pore Volume, Size, and Size Distribution 21

1.4.2 Thermogravimetric Analysis 28

2. Scope of Research 30

3. Experimental 32

3.1 Synthesis of Spherical SBA-15 Silicas 32

3.2 Modification of Spherical SBA-15 Silicas 34

3.3 Methods of Characterization 36

3.3.1 Equipment 36

3.3.1.1 Low Temperature Nitrogen Adsorption 36

3.3.1.2 Thermogravimetric Analysis 36

3.3.1.3 Elemental Analysis 37

3.4 Materials 37

4. Results and Discussion 38

4.1 Synthesis of Spherical SBA-15 38

4.2 The C constant and Cross-sectional Area of Nitrogen 58

4.3 Characterization of Modified Silica 61

4.4 Pore Structure and Tortuosity 70

5. Conclusions 73

6. References 75

PART II: Evaluation of Spherical SBA-15 in High Pressure Liquid Chromatography

1. Introduction 79

1.1 Chromatographic Theory 80

1.2 Retention Mechanism and Surface Specific Retention Factor 87

1.3 Porous Silica in High Performance Liquid Chromatography 89

1.3.1. Geometry 90

1.3.1.1 Particle Morphology and Size 90

1.3.1.2 Surface Area 91

1.3.1.3 Pore Structure 94

1.4 Ordered Silica in High Performance Liquid Chromatography 98

2. Scope of Research 100

3. Experimental 101

3.1 Experimental Design 102

3.2 HPLC 103

3.2.1 Systems 103

3.2.2 Methodology 104

3.2.3 Experimental Conditions 104

3.2.4 Analytes 104

3.3 Sedimentation and Column Packing Method 105

3.4 Column Characterization 107

3.5 Methylene Selectivity 108

3.6 Materials 110

4. Results and Discussion 111

4.1 Adsorbent Characterization 111

4.2 Flow Rate Studies 123

4.3 Kinetic Studies 133

4.4 Methylene Selectivity 145

4.5 Surface Specific Retention 157

5. Conclusions 172

6. References 174

Appendixes 179

List of Figures

1. Example of pore created by the space between primary spherical particles. 5
2. SEM images of fibrous SBA-15. The left view shows the hexagonal order while the right image shows the long range order and non-intersecting parallel pores. 7
3. Fibrous (non-spherical) SBA-15 nitrogen adsorption isotherm (top) and pore size distribution (bottom) showing the characteristic parallel adsorption/desorption branches of the hysteresis and narrow pore size distribution as a result of the highly-ordered cylindrical pore structure. 8
4. The assembly of Pluronic P123. Spherical micelles of P123, with PPO cores and PEO segments interacting with the aqueous environment through hydrogen bonding and Coulombic interactions. Co-assembly into hexagonally ordered cylindrical micelle aggregates with interactions from added silicate species. Condensation of silica around ordered micelles and calcination to give final ordered material. 10
5. Classification of isotherms type I through VI. The isotherms most common isotherms referenced are type I (microporous solids), type II (nonporous solids) and type IV (mesoporous solids). Types III and V refer special cases of types II and IV, respectively, where weak interactions between adsorbate and adsorbent are present. The hysteresis loop seen in type IV and V is characteristic of mesoporous solids with pores between 20 and 500Å. 17
6. Nitrogen adsorption and desorption isotherm on porous silica (left) highlighting the direction of adsorption (blue trace) and desorption (red trace) with the identification of the BET region (0.05 to 0.25) where adsorption of the monolayer is complete. On the right is the pore size distribution which shows the distribution of the pore volume as a function of pore radius. 20
7. Overlay of nitrogen adsorption isotherms for 3 hypothetical porous solids with uniform cylindrical pores of 25 angstrom, 50 angstrom and 75 angstrom for each sample respectively. 24

8. Nitrogen adsorption/desorption isotherm for a synthesized batch of spherical SBA-15 silica. Notice the striking similarity between this experimentally determined isotherm for spherical SBA to the expected isotherm for a hypothetical porous solid with uniform, cylindrical pores in figure 7. 25
9. **On the left**: cross-section of a cylindrical pore with a radius r_p, showing the relationship between the "inner core" of the radius, r^k and the adsorbed film if thickness, t. **On the right**: the relationship between r_m of the Kelvin equation and the inner core radius, r^k, for a cylindrical pore with a hemispherical meniscus. θ is the contact angle. For a hemispherical meniscus, the contact angle,θ = 0, so cosθ=1 and $r_m=r^k$. 27
10. Synthesis Scheme showing the general flow of the procedure. Adjustments to temperature and duration of reaction, ageing, and treatment steps can be made (with best results from staying within the limits presented, especially within the reaction step). The reaction can be followed by both ageing and treatment, or just treatment. 35
11. S-1-10 nitrogen adsorption isotherm (top) and pore size distribution. 40
12. S-1-3 adsorption isotherm (top) and pore size distribution (bottom) 41
13. Nitrogen adsorption isotherm (top) and pore size distribution for S-1-9. 42
14. Nitrogen adsorption isotherm (top) and pore size distribution (bottom) for S-1-30. 43
15. Nitrogen adsorption isotherm and pore size distribution for S-1-17 46
16. Nitrogen adsorption isotherm and pore size distribution for S-1-19 47
17. Pore size distribution for S-1-4 (120^{o}C 12 hours) 49
18. Nitrogen adsorption isotherm and pore size distribution for S-1-26 53
19. S-1-29 Nitrogen adsorption isotherm and pore size distribution 54
20. Nitrogen adsorption isotherm and pore size distribution for S-2-36 55
21. TEM of S-1-10 C8 (left) and S-1-29 (right) and S-2-36 (bottom) 56
22. SEM of S-1-2 (75oC ,10 hours) with CTAB (Left) and (right) without CTAB 57
23. Plot of experimentally determined modified layer height versus theoretical 66
24. Plot of % Carbon versus %WL. The slope is equal to the fraction of carbon in the cleaved group. 67
25. Overlay of nitrogen adsorption isotherms for S-1-29 (bare, C1-C18).

Ideally, the hysteresis should get thinner and move slightly to the left, but it should not completely change shape. This is an indication there may be some sort of blockages inside the modified pores. 71

26. Comparison of TGA decomposition of P123 surfactant from the pores of spherical SBA-15 (red) and fibrous SBA-15 (blue). The weight loss curve for spherical SBA-15 shows a two-step process requiring greater energy for the decomposition of the surfactant from the pores. This comparison demonstrates the possible effect spherical morphology can have on the obstruction of the porous space in spherical SBA-15. 72
27. Chromatogram displaying retention time t_R, dead time t_o, reduced retention time t_R' and the peak variance, σ. 84
28. Low Temperature Adsorption Nitrogen Isotherm of a porous silica sample and description of the how pore volume, pore size and BET surface area are calculated 93
29. Cross section of an analytical column portraying the pore volume arising from interconnected, intraparticle pores within the particles (V_p) as well as the interparticle pore volume (V_{ip}) from the spaces in-between the particles columns inside the column. 95
30. Example of the extrapolation of V_R vs $MW^{1/3}$ for polystyrene standards to zero in the determination of V_{ip}. 109
31. Pore size distribution for SBA-16 modified with C8 114
32. Pore size distribution of Gemini C18. 115
33. Pore size distribution of fibrous SBA-15 116
34. Pore size distributions of SBA-29C8 (left) and SBA 36 (right) 117
35. t-plot for spherical SBA batch 29 showing the absence of micropores 121
36. Interparticle and void volume as determined on SBA batch 36 122
37. Effect of flow on peak shape and retention on C8 SBA batch 10. 125
38. Retention of benzene at varying flows on SBA-3C8 126
39. Nitrogen isotherm for SBA-36. 128
40. Effect of flow rate on retention and peak shape as seen using C8 modified batch 29 129
41. Flow studies as performed on the Luna C18 column 50 x 2.00mm. 130

42. Effect of flow rate on bare silica SBA batch 36. Mobile phase used was hexane. 131
43. H/u curves for SBA-10C8, -26C8, and Luna C18 136
44. Comparison of H/u curves for 70/30 MeCN and MeOH on SBA-26C8. 138
45. H/u curve for SBA-29C8 140
46. Plot of peak variance vs. retention time for SBA-29C8 141
47. Plot of peak variance against retention time for Luna C18 column. 143
48. H/u (top) and Plot of peak variance vs. retention time (bottom) for SBA-36 146
49. H/u (left) and plot of peak variance for SBA-3C8 147
50. Methylene selectivity results for SBA-10C8 149
51. Methylene selectivity plots for SBA-29C8 150
52. Methylene selectivity plots for SBA-26C8 151
53. Methylene selectivity plots for Gemini C18 152
54. Methylene selectivity vs %MeOH for Gemini C18 and SBA -10C8, -26C8, and -29C8. 153
55. Plot of selectivity of Ethylbenzene to toluene for both SBA-10C8 and Gemini C18 153
56. Slope of lnk on n_c versus % MeCN 156
57. Comparison of traditional retention factors at 70% MeOH 160
58. Comparison of surface specific retention factors at 70% MeOH 161
59. Comparison of traditional retention factors at 70% MeCN 162
60. Comparison of surface specific retention factors at 70% MeCN 163
61. Comparison of Surface specific retention factor for SBA-26C8 after weighing the adsorbent 166
62. Comparison of surface specific retention for SBA 26C8 after weighing the adsorbent in the column 167
63. Overlay of isotherms for bare SBA 29 and C1-C18 modified samples. Shows the shift of the desorption isotherm 169

List of Tables

PART I

I.	Molar ratios for different spherical and fibrous SBA-15 syntheses.	33
II.	Synthesis Results: Effect of temperature.	39
III	Synthesis results: Effect of heating time.	45
IV	Synthesis results. Single Ageing time and temperature	48
V	Final synthesis results	52
VI	Correction for cross-sectional area of nitrogen based on correlation of C constant to geometric relationship in cylindrical pores	60
VII	Calculation bonding densities for modified spherical SBA-15 silicas	62
VIII	Calculation of bonded layer thickness and molecular volume of ligand	63
IX	Comparison of bonding densities from % carbon and % weight loss	68
X	TGA data	69

PART II

I	Packing Densities for Slurry packed columns	106
II	Adsorbent Geometry	112
III	Column Geometry	119
IV	Determination of Obstruction factor	144
V	Column characteristics for commercial and SBA-15 (batch 26) columns	159

VI Surface specific Retention for SBA batch 26 calculated with weighed column mass. 165

VII Weighed mass of adsorbent for SBA Batch 26 and 36 171

Appendixes

A1 Methylene Selectivity data for GeminiC18 in MeOH

A2 Methylene Selectivity data for SBA 10C8 in MeOH

A3 Methylene Selectivity data for SBA 29C8 in MEOH

A4 Methylene Selectivity data for GeminiC18 in MeCN

A5 Methylene Selectivity data for SBA 10C8 in MeCN

A6 Methylene Selectivity data for SBA 29C8 in MeCN

A7 Example of Vip determination

A8 Example of Nitrogen Isotherm Mathcad Calculations

1. INTRODUCTION

Ordered mesoporous silicas have been the focus of much attention since the discovery of the M41 family of materials by the mobile corporation in 1992 [1]. Through the use of surfactants as structure directing agents, these silicas are characterized by large surface areas and narrow pore size distributions [1]. MCM-41, for example, is prepared with the use of cationic surfactants in a basic solution giving hexagonally ordered porous solids with pores sizes of 20 to 30Å [2]. Using non-ionic tri block copolymers in acidic media, Zhao and co-workers were successful in synthesizing a family of highly ordered mesoporous Santa Barbara Amorphous (SBA) silicas with pore sizes up to 300 angstrom [3]. In particular, SBA-15, has been synthesized with large surface areas and a highly ordered hexagonal mesostructure with thick uniform walls using triblock copolymer poly(ethylene oxide)-poly(propylene oxide)-poly (ethylene oxide) (PEO_{20}-PPO_{70}-PEO_{20}) as a structure directing agent [4]. The greater hydrothermal stability and overall mechanical strength offered by the thick pore walls, as well as large surface area and tunable pore size, make SBA-15 a desirable potential stationary phase in liquid chromatography. As such, there has been extensive research into the synthesis of spherical SBA-15 silica and subsequent evaluation for use in high performance liquid chromatography [5-11]. While the native particle morphology of SBA-15 is that of an irregular, rectangular shape on the order of a few micrometers [4], control of the particle morphology has been reported [12], albeit with compromise of the porous structure integrity [13]. As SBA-15 is characterized by long, relatively narrow non-intersecting hexagonally oriented pores, roughly 1000 times longer than they are wide, it is of particular interest how the spherical particle morphology affects the porous structure. Further, as reverse phase chromatography is the most common utilized mode of liquid chromatography, the effect of surface modification, to our

knowledge, has not been rigorously studied in spherical SBA-15 silicas to date. However, in order to fully understand the effects of various synthetic routes and conditions on the porous structure, a brief discussion of silica chemistry, surface modification, as well as methods used to characterize and evaluate porous silicas is necessary.

1.1 Chemistry of Porous Silica

Reaction mechanisms must be considered if sol-gel chemistry is to be developed as anything other than art [14]. Generally, there are 3 basic stages involved in the formation of silica gel: 1) the polymerization of the silicic acid monomer to form particles, 2) the growth of the particles, and 3) the linking of the particles into branched chains and networks extending through the liquid medium ultimately thickening into a gel [15]. Involved in the initial stages of polymerization are the hydrolysis of the silica precursor and subsequent condensation. In the first step of acid catalyzed hydrolysis

$$H_3O^+ + Si(OR)_4 \rightarrow HO\text{-}Si\text{-}(OR)_3 + ROH + H^+$$

with complete hydrolysis producing $Si(OH)_4$ (mono silicic acid), however in real situations it is unlikely that complete hydrolysis would be achieved, as mono silicic acid is quite unstable in concentrations over 100-200 ppm and will undergo rapid condensation:

$$Si(OR)_3OH + HOSi(OR)_3 \rightarrow (RO)_3Si\text{-}O\text{-}Si(OR)_3 + H2O \quad \textit{or,}$$

$$Si(OR)_3OR + HOSi(OR)_3 \rightarrow (RO)_3Si\text{-}O\text{-}Si(OR)_3 + ROH$$

As can be seen either water or alcohol can be produced by the condensation reaction [14]. As mentioned, in real systems hydrolysis and condensation are taking place at the same time and

thus, rates for the polymerization can become quite complicated [14]. However, a general picture can be painted as to the rules governing the polymerization of silica gel. According to Iler, silicic acid monomer in solution will polymerize by condensation to produce dimers and higher molecular weights species of silicic acid, the rate of which is proportional to the concentration of H^+ ion at a pH below 2 and to OH^- at a pH greater than 2 [15]. Since there is a strong tendency to polymerize in such a way to minimize uncondensed SiOH groups while maximizing the formation of siloxane bonds (Si-O-Si), early polymerization usually results in ring-like structures and finally large cyclic polymers which condense internally and ultimately produce spherical units [15]. The resulting spheres then develop into larger particles depending on their size and the pH of the solution. Below the isoelectric point of silica (~2.2), particles will not grow larger than 2 to 4 nm and will begin to collide and aggregate into chains and gel networks. At high pH's, especially above 7, particles will begin to grow through a process of Ostwald ripening where smaller particles, more soluble by the fact of their radius of curvature, will dissolve and be re-deposited on larger particles [15]. As the particles are negatively charged at high pH, this process will continue without aggregation, unless salts are added. Therefore, by thus controlling the conditions of the reaction solution, the silica sol or gel can be manipulated to produce singular non porous particles or secondary porous particles consisting of the aggregated small nanometer-sized primary particles.

Although the above description provides a very general picture of the sol-gel method, it is sufficient to gain an understanding of the nature of porous silica used in high performance liquid chromatography. The porous silica gels used in chromatography are the aggregates of primary particles grown together in chains or networks[16]. Factors affecting the characteristics of the silica gel include the size of the primary particle at the moment of aggregation, the concentration

of particles in solution and the compactness of the network, the pH, salt concentration, and the temperature and time during which the gel is aged or treated [17]. It is from the spaces between the primary particles which give rise to the pores in silica gels (Figure 1). Understanding the types of pores generated in these types of silicas will enhance our understanding of the ordered porous structures of SBA-15. In a discussion on the origins of porous structures, the International Union of Pure and Applied Chemistry describes the class of porous materials , such as the aforementioned silica gel, as arising from the aggregation and subsequent agglomeration of small particles [18]. Therein, description of pore shape, for the sake of simplicity, is preferably described in terms of cylinders, prisms, cavities and windows, slits, or spheres[18]. However, as pores are most often the voids left between solid spheres in contact with eachother, the actual description of pore shape becomes complicated by the existence of pores of different shape, interconnectivity, and a wide pore size distribution which, in essence, necessitates the introduction of descriptors such as “connectivity” and “tortuosity” in order to accurately portray the porous structure [18]. Interestingly, with the advent of ordered mesoporous silicas, we now had a porous solid which can be accurately portrayed by descriptions of cylindrical pores and for which the assumptions of pore structure and geometry actually apply while the complications arising from tortuosity and connectivity can be forgotten. However, only through rigorous investigation into the nature of ordered mesoporous silicas will we be able to confirm the applicability of the cylindrical pore model and ultimately confirm that complexities such as connectivity and tortuosity as concepts belonging only to the amorphous silica gel.

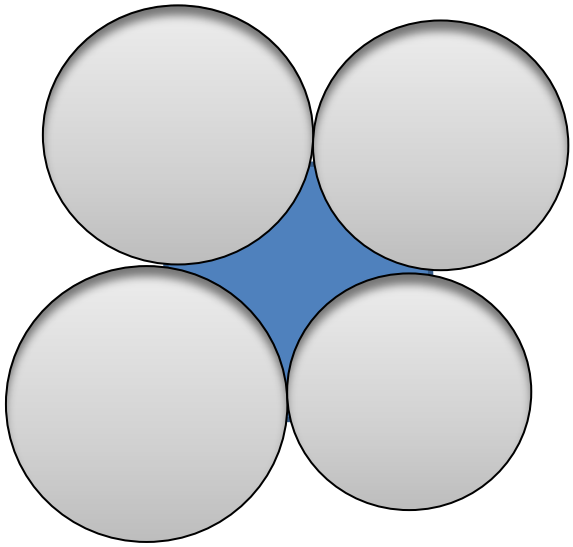

Figure 1. Example of pore created by the space between primary spherical particles.

1.2 SBA-15 Ordered Mesoporous Silica

In contrast to the networking of small primary particles giving rise to the porous structure of secondary silica gel particles, the use of surfactants or tri-block copolymers as structure directing agents results in well-ordered hexagonal mesoporous silica structures, such as SBA-15, exhibiting uniform cylindrical pores and thick pore walls [4]. SBA-15 is synthesized with the use of a nonionic triblock copolymer poly(ethylene oxide)-poly (propylene oxide)- poly(ethylene oxide) PEO_{20}-PPO_{70}-PEO_{20}, commercially known and called herein as P123 [4].

SBA-15 typically shows surface areas ranging from 600 to 1000 m^2/g depending on reaction temperature and duration [4]. Pore diameters are on the level of 40 to 80A, without the use of co-solvents or swelling agents such as trimethylbenzene to increase pore size. As would be expected for silica with cylindrical geometry, the pore size and surface area are inversely proportional to each other; as the pore size decreases, the surface area increases. Pore volumes are typically 0.8 to 1.2 mL/g. However, the most identifiable attribute of SBA-15 is the well-ordered, parallel pore structure, consisting of non-intersecting pores, hexagonally oriented, with a pore width to length aspect ratio of 1:1000 [4] (Figure 2). In terms of characterization, the attribute of the ordered cylindrical pore geometry is most noticeable through an examination of the adsorption isotherm and pore size distribution from low temperature nitrogen adsorption (Figure 3). While we discuss the specifics of the theory behind nitrogen adsorption in the next section, it is quite clear from looking at the pore size distribution in figure 3, that this material possesses a narrow pore size distribution which is a result of the template driven synthesis.

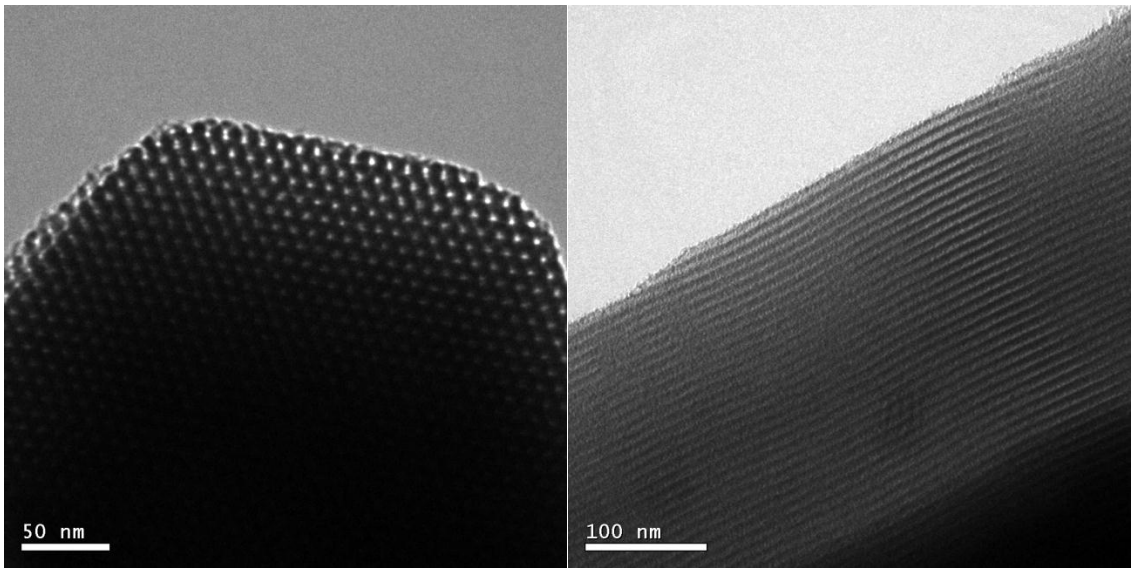

Figure 2. SEM images of fibrous SBA-15. The left view shows the hexagonal order while the right image shows the long range order and non-intersecting parallel pores.

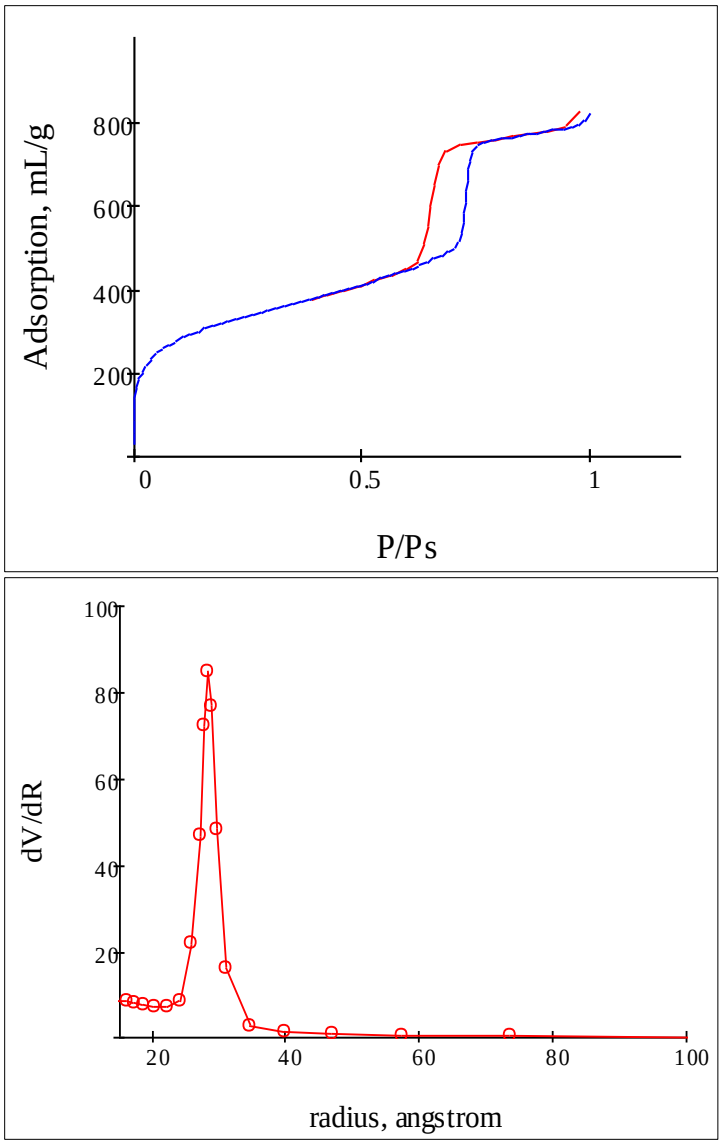

Figure 3. Fibrous (non-spherical) SBA-15 nitrogen adsorption isotherm (top) and pore size distribution (bottom) showing the characteristic parallel adsorption/desorption branches of the hysteresis and narrow pore size distribution as a result of the highly-ordered cylindrical pore structure.

1.2.1 Synthesis Parameters

Non-spherical SBA-15 is typically produced with a reaction temperature of 35^{o}C for 20 hours followed by a static ageing at 80^{o}C for 24 to 48 hours [3,4]. The reaction temperature can be adjusted from 35^{o}C to 80^{o}C and the ageing temperature can be adjusted from 80^{o}C to 140^{o}C. Adjustments to the temperature or time of reaction/ageing will yield changes to pore size, surface area and pore volume, typically with higher temperatures and longer times leading to an increase in pore size and reduction ion surface area [4]. The synthesis of SBA is carried out under acidic conditions (pH~1), as above the isoelectric point of silica, or pH 2.2, no precipitation or formation of silica occurs [4]. Tri-block copolymer P123 weights greater than 6% yield only silica gel, while below 0.5% result in only amorphous silica [4]. Likewise, reaction temperatures over 80^{o}C result in the formation of silica gel, while reaction temperatures under 35^{o}C yield amorphous silica [4].

As mentioned above, pore size can be adjusted by a change in reaction or ageing temperature with greater temperatures yielding increases in pore diameter. It is believed that higher temperatures will increase the hydrophobic domain volume of the PEO segment of the triblock copolymer, reducing its interactions with the surrounding aqueous environment [4]. The relation of synthesis parameters to the porous structure is closely tied to the behavior of the P123 copolymer-silica assembly in solution. In the following section we shall examine more closely the behavior of the P123 micelles in dilute solution and discuss their interactions with the aqueous environment as well as with the silicate species as polymerization is taking place to give a better understanding of the factors affecting pore structure as well as the morphology of SBA-15 during synthesis.

1.2.2 Self-Assembly of P123 Micelles and Silica Species

Mesopore ordering and final morphology are both influenced by the cooperative self-assembly of the inorganic and organic species present during the synthesis of SBA [3]. Long range periodic order is provided through balanced Coulombic, hydrogen bonding, and Van der Waals interactions [3]. Above the critical micelle concentration (0.03 wt% at 25^{o}C), P123 is soluble in dilute solution in water [19]. As the temperature is raised above 15^{o}C, the PPO segments of the polymer becomes increasingly more hydrophobic and the copolymer spontaneously forms dynamic core-shell micelles with the more hydrophobic PPO segments in the core and the hydrated PEO segments making up the surrounding shell [19, 20].

The co-assembly of the P123 copolymer in aqueous solutions in acidic media is enhanced by association of hydronium ions with the alkylene oxide groups which add long range Coulombic interactions [3]. At the pH~1, the silica precursor is positively charged and a cooperative self-assembly of the silica-block-copolymer rich mesophase is expected to take place through an intermediate of the form (SoH+)(X-I+) as the cationic silica interacts preferentially through the halide anion present from the acidic modifier [3,4]. Figure 4 shows a simplified example of the co-assembly process.

In situ small angle X-ray scattering monitoring of the initial stages of the synthesis [21] has confirmed the self-assembly of the copolymer silicate system, as the transformation of P123 micelles from a spherical form to a cylindrical form prior to precipitation of the silicate species, followed by aggregation of the cylindrical micelles into two-dimensional hexagonal structures was observed [21]. Further ordering with the condensation of the silica species resulted in the

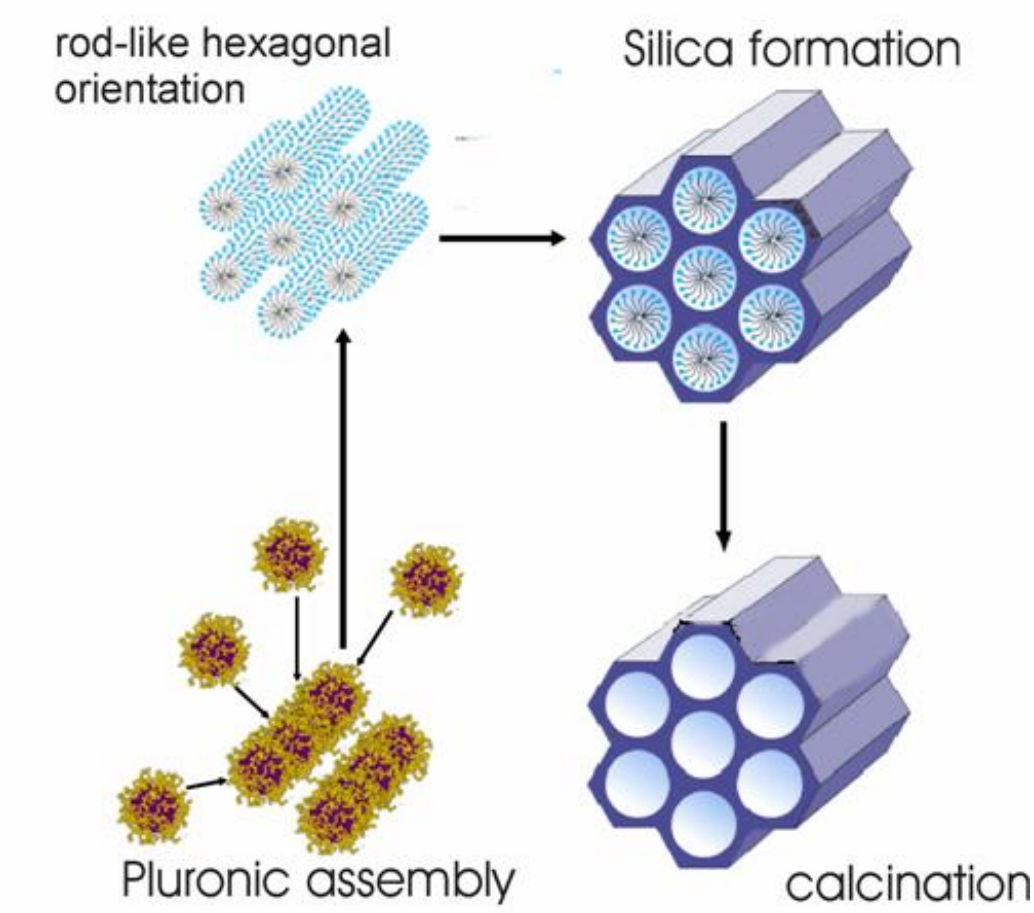

Figure 4. The assembly of Pluronic P123. Spherical micelles of P123, with PPO cores and PEO segments interacting with the aqueous environment through hydrogen bonding and Coulombic interactions. Co-assembly into hexagonally ordered cylindrical micelle aggregates with interactions from added silicate species. Condensation of silica around ordered micelles and calcination to give final ordered material.

cross-linking and covalent bonding between the cylindrical micelles [21]. For the remainder of the initial reaction period and into the ageing/hydrothermal treatment at higher temperatures, silica condensation and densification of the structure continues around the hexagonally ordered cylindrical micelles and comes to a completion with a decrease in the unit cell parameter and increase in the pore size, as the silica wall, highly integrated with the PEO segment of P123 during the reaction and early hydrothermal treatment, ultimately separates from at the high ageing temperatures [21]. These experimental observations agree well with the behavior of PEO as described initially by Stucky and co-workers. The PEO segments which are more closely associated with the inorganic walls than the PPO segments, become more hydrophobic at high temperatures, and resulting in smaller lengths of PEO segments associated with the silica wall, yielding larger pores sizes and smaller pore walls [4].

1.2.3 Particle Formation and Morphology

As we saw with the discussion of sol-gel chemistry, primary silica particles tend to form spheres which is a result of the tendency to minimize surface energy in combination of growth from a nucleation point [22]. However, internal structures with long range order will force the particle to adopt a regular form such as the hexagonal morphology [22]. SBA-15 particles typically take to a rope-like shape about 1μm in size which tend to form wheat like aggregates [3,4]. The question of whether a spherical or a more regular form of morphology is obtained is basically determined by the rate of polymerization in contrast to the rate of the mesostructure (micelle-silicate) formation [12,22]. As we learned with silica gel, polymerization rates are greatly dependent on the pH of the aqueous solution as well as the presence of salts. Likewise, the

condensation rates of SBA-15 can be controlled by several factors including 1) condensation rate of silica, 2) shape of surfactant micelles, 3) concentration of inorganic salts, and 4) stirring rate [12].

According to Zhao, the macroscopic SBA-15 morphology is crucially dependent on the local curvature energy that is present at the interface of the inorganic silica and block copolymer[12]. The addition of co-surfactant can lower the local curvature energy and facilitate curved morphologies [12]. Also, fast condensation rates of silica result in a high local curves energy where the energy penalty for cylinder channel bending is also high, resulting in fiber, rope-like morphologies [12]. Slower condensation rates attainable through co-solvents and adjustment of pH and stirring rates yield a more curved morphology [12, 13, 23]. However, the use of co-surfactants has been shown to lower the long range ordering of the SBA-15 pore structure [24].

1.3 Surface Modification

The terms ‘lyophilic’ and ‘lyophobic’ which from the Greek describe a love (philos) or fear (phobos) of dissolving or mixing with (Lyo), as well as ‘hydrophobic’ and hydrophilic’ (also Greek for “water fearing” and “water loving”, respectively) are words that help qualitatively describe the energy and intensity of interactions at the interface between a solid and liquid [25]. While strong interactions characterize a hydrophilic or polar surface, weak interactions characterize hydrophobic surfaces [25]. As seen with the use of silica in chromatography, silica to be used as a reversed phase stationary phase is modified to convert the polar surface to a hydrophobic one which will exert only dispersive interactions with the analyte [26].

The surface modification of spherical SBA-15 silica in literature has not been rigorously studied, except for simple tests to detect the presence of the bonded phase prior to use in chromatographic studies [5-11]. Several batches of spherical SBA-15 silicas were modified using (N,N-dimethylamino)-alkyldimethylsilanes followed by investigation of the modified silicas for surface coverage, bonded layer thickness and volume of the bonded layer.

The use of (N,N-dimethylamino)-alkyldimethylsilanes for surface modification is expected to produce maximum bonding densities as a result of the island-like type coverage exhibited by dimethylamino alkylsilanes [27]. The bonding densities were calculated:

$$d_b = \frac{6 \times 10^5 (\%C)}{[1200 \times n_c - MW(\%C)} \cdot \frac{1}{S_{BET}} \qquad (1)$$

where $\%C$ is the percent carbon from elemental analysis, n_c is the number of carbons in the grafted ligand and MW is its molecular weight, and S_{BET} is the surface area of the unmodified silica. It has been shown [36] that pore size will affect the confirmation of alkylsilanes bonded to the surface of porous material. Since most of the surface area of porous silica exists inside the pores, i.e. on a concave surface, smaller pores will result in increasing steric hindrance exerted on the bonded ligands decreasing values for bonding density. As a result, the bonded ligands will take on a rigid, liquid-like conformation to compensate for steric hindrance and achieve maximum bonding density [36]. Based on a cylindrical pore model, the critical pore diameter at which (and below) steric hindrance of attached molecules will be a factor is given as

$$D^* = \frac{2l}{L_{min} - d} \qquad (2)$$

where D^* is the critical diameter, l is the length of the bonded ligand, and L_{min} is the minimum distance between anchor points of neighboring bonded ligands [36]. As SBA-15 exhibits cylindrical pores, based on geometric relationship of the bonded ligands to the concave pore surface, the thickness and bonding density of the C18 bonded layer can be expected to be roughly [36]:

$$h = \frac{D}{6} \quad ; \quad p = 0.217D \qquad (3)$$

where h is the bonded layer thickness, p is the bonding density, and D is the pore diameter. The experimental determination of the bonded layer thickness can be calculated from the difference between specific pore volume of modified silica and the specific pore volume before modification, with an applied factor to correct for the weight of the modified layer and relate both volume to 1 gram of bare silica [28]:

$$h = \frac{V_{SiO2} - (V_{mod} \cdot f)}{S_{SiO2}} \qquad (4)$$

$$f = \frac{1}{1 + d_b \cdot S_{SiO2} \cdot MW_{lig}} \qquad (5)$$

where V_{SiO2} and V_{mod} are the specific pore volumes of the bare silica and modified silica respectively; d_b is the bonding density; MW_{lig} is the molecular weight of the bonded ligand and S_{SiO2} is the specific surface area of the bare silica. Also, the volume of the bonded ligand can be calculated

$$V_{MOL} = \frac{V_{BL}}{d_b \cdot S_{BET}} \times 10^6 \qquad (6)$$

where V_{BL} is the volume of the bonded layer from the numerator of Eq. 3.

1.4 Methods of Characterization

1.4.1 Low Temperature Nitrogen Adsorption

1.4.1.1 Surface Area and BET Theory

The specific surface area of a solid is one of the first things that must be determined if any detailed physical chemical interpretation of its behavior as an adsorbent is to be possible [29]. The characterization of surface area, pore volume, pore size and pore size distribution for spherical SBA-15 silicas in this study is provided through the adsorption of nitrogen at 77K which is the temperature of equilibrium between the vapor and liquid phase. In these experiments, the material actually being adsorbed is called the adsorbate, while the solid is the absorbent [30]. Adsorption is brought about by the physical forces acting between the solid and gas molecules including dispersion forces as well as electrostatic (Coulombic) forces in the case of polar solids [30]. The step-wise measurement of nitrogen across a range of relative pressures (P/Po) ending at the saturation pressure results in the adsorption isotherm. The isotherm correlates to the accumulation of adsorbed nitrogen on the surface, and eventually into the porous spaces. The isotherms types I-V, (figure 5) were originally classified by Brunauer, Emmett, and Teller (BET)[30]. Type I describes the adsorption of gas onto a microporous solid, while type II describes adsorption onto a nonporous solid. Type IV and V describe the adsorption onto mesoporous solids and they show the characteristic hysteresis loop. The isotherms for type III and type V are indicative of adsorption onto solids for which there are very weak gas-solid molecular interactions [30]. For the discussion at hand we will be concentrating on type IV, however we will need to briefly discuss the importance of the nonporous isotherm as

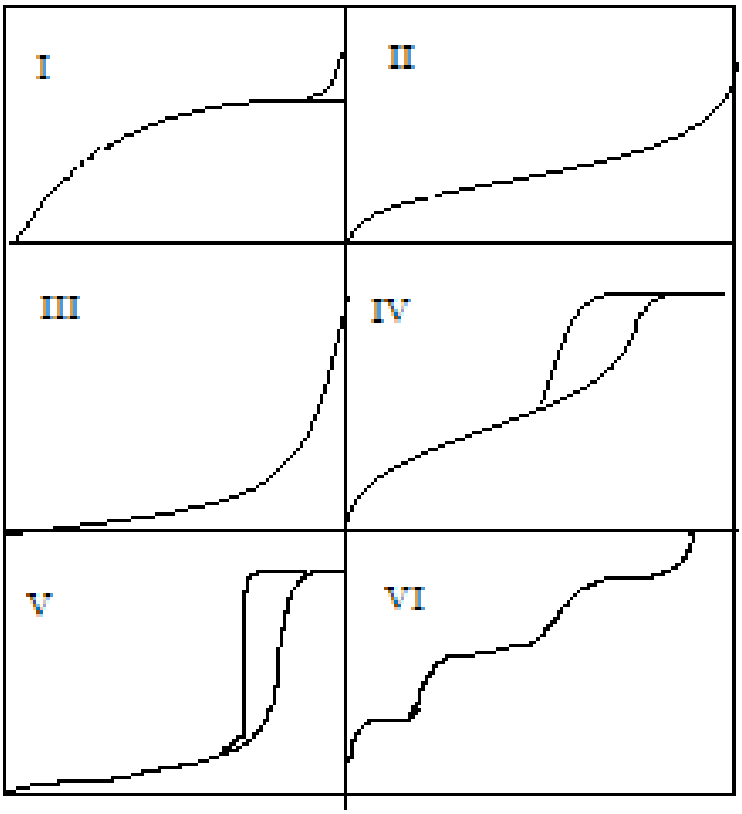

Figure 5. Classification of isotherms type I through VI. The isotherms most common isotherms referenced are type I (microporous solids), type II (nonporous solids) and type IV (mesoporous solids). Types III and V refer special cases of types II and IV, respectively, where weak interactions between adsorbate and adsorbent are present. The hysteresis loop seen in type IV and V is characteristic of mesoporous solids with pores between 20 and 500Å.

it relates to the development and application of the BET theory and calculation of specific surface area.

The process of adsorption is described in terms of an empirical adsorption function n=f(P,T) where n is the amount adsorbed [29]. Thus, experimentally, we can measure the adsorption of nitrogen over a range of pressures, with proper equilibration at each point, all while under constant temperature. Brunauer, Emmett, and Teller showed how to apply the Langmuir equation to multilayer adsorption [29]. The adsorption of a gas on a solid surface is known to proceed with the evolution of energy in the form of heat [30]. The basic assumption of BET is that the Langmuir equation applies to each layer, however, with the added idea that there is a special value to the heat associated with adsorption of the first layer [29]. The original Langmuir kinetic model described the rates of evaporation and condensation as they relate to the adsorption sites existing on the surface [29] and the state of dynamic equilibrium between them. The Langmuir equation in its familiar form

$$\frac{n}{n_m} = \frac{B_p}{1 + B_p} \qquad (7)$$

where n/n_m is the adsorbed amount to the monolayer capacity, and B_p is an empirical constant[30]. To apply the Langmuir equation to multiple layers, BET had to make three assumptions: 1) that in all layers, except the first, the heat of adsorption is equal to the molar heat of condensation (q_L) , 2) that in all layers except the first, the evaporation-condensation conditions are identical, and 3) that when $p=p^o$, the adsorption condenses to a bulk liquid on the surface of the solid (p^o=saturation pressure)[30]. The product of the derivation and assumptions gives the BET equation:

$$\frac{\frac{P}{P_0}}{n\left(1-\frac{P}{P_0}\right)} = \frac{1}{n_m C} + \frac{C-1}{n_m C} \cdot \frac{P}{P_0} \qquad (8)$$

where nm is the monolayer capacity, P/P_0 is the relative pressure and n is the amount adsorbed. The parameter, C, (referred to as the C constant) is related to the heat of adsorption

$$lnC \cong \frac{(q_1 - q_L)}{RT} \qquad (9)$$

where (q_1-q_L) is the net heat of adsorption [30]. As we will discuss later, the adsorption isotherms for modified silicas in the low relative pressure region are less convex than those of bare silica [31], an extreme example of which would be the concave low pressure regions seen with type III isotherms which are characterized by weak interactions. The energy of the adsorption interaction for different surfaces can be compared using the C constant. The use of the BET equation relates only to the linear portion of the adsorption isotherm (relative pressures from 0.05 to 0.25), where the formation of the monolayer is complete. Figure 6 shows the dependence of the amount of nitrogen adsorption on the surface in relation to the relative pressure, as can be seen with the adsorption/desorption branches of the isotherm [26]. In the BET region (P/P_0 of 0.05 to 0.25), the plot of P/P_0 ($1-P/P_0$) versus P/P_0 is a straight line from which the C constant and nm can be calculated:

$$C = \frac{slope}{intercept} + 1 \qquad (10),$$

$$n_m = \frac{1}{slope + intercept} \qquad (11)$$

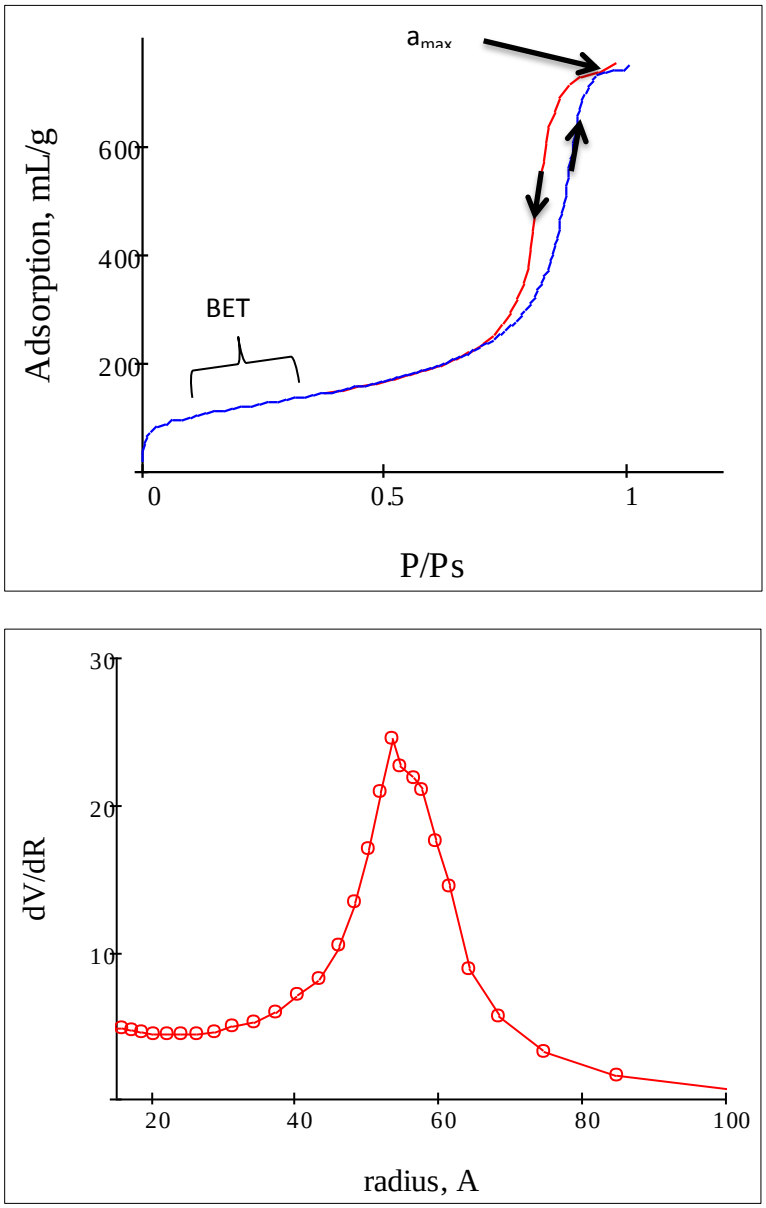

Figure 6. Nitrogen adsorption and desorption isotherm on porous silica (top) highlighting the direction of adsorption (blue trace) and desorption (red trace) with the identification of the BET region (0.05 to 0.25) where adsorption of the monolayer is complete. On the bottom is the pore size distribution which shows the distribution of the pore volume as a function of pore radius.

Finally, the specific surface area in m^2/g can be calculated by

$$S_{BET} = \omega n_m N_A \qquad (12)$$

where N_A is Avogadro's number and ω is the cross-sectional area of molecular nitrogen. It is generally believed that the molecular nitrogen occupies an area of $16.2Å^2$ on the polar silica surface [29,32]. However, modification of the silica surface to be hydrophobic in nature can complicate the value used for the cross-sectional area. As we have discussed with the C constant, the energetic interaction of the adsorbate with the adsorbent is of great importance in adsorption and surfaces exhibiting weaker interactions ultimately result in a change of the effective molecular area of nitrogen occupied on the surface. Amati and Kovats [33,34] showed that the effective cross-sectional area for nitrogen varied from 16.2 to $21Å^2$ as the surface energy of silica decreased by modification [29]. Generally, the relationship of the C constant to the cross-sectional area is such that as the energy of the surface decreases, reflected in lower values of the C constant, the effective cross-sectional area of nitrogen increases. For the purposes of this study, the value used for ω on bare silica will be $16.2A^2$ and on modified silica $21Å^2$ will be used.

1.4.1.2 Pore volume, Size and Size Distribution

The pore volume can be calculated from the maximum adsorption (a_{max}) which can be identified as the flat portion of the adsorption isotherm at the saturation pressure (Figure 6). As can be seen from the isotherm, there is a sharp increase in adsortption after 0.7 P/P^0 which corresponds to the filling of the pores by capillary condensation. The flat portion of the isotherm after capillary condensation is an indication that pores are filled, as no more nitrogen is condensed and

the amount adsorbed levels of yielding the plateau. Thus the pore volume (per gram of adsorbent) is calculated by

$$V_{pore} = a_{max} V_L \qquad (13)$$

V_L is the molar volume of liquid nitrogen in mL/mole and a_{max} is expressed in moles/gram. The study of pore structure is closely connected to the interpretation of the type IV isotherm [30]. While in the low pressure region, the type IV isotherm follows closely to the type II isotherm which allows for the applicability of BET theory to the calculation of surface area, the isotherm shows deviation from the type II as a sharp increase of adsorption occurs at relative pressures of roughly 0.6 to 0.7. The sharp increase is attributable to condensation of the nitrogen in the pores of the absorbent, which will eventually all be filled and the adsorption will reach a maximum (Figure 6). A characteristic feature of the type IV isotherm is the hysteresis loop made up of a adsorption branch (as adsorbate condenses in the pores) and a desorption branch (as adsorbate evaporates out of the pores). The shapes and slopes of the adsorption and desorption branches of the hysteresis will change depending on the structural characteristics of the absorbent [30], however the desorption branch will always show a greater adsorption of the adsorbate compared to the adsorption branch at any given relative pressure of the hysteresis (Figure 6) [30].

In small pore spaces, as nitrogen is absorbed on the pore walls, there is a point at which a meniscus forms and condensation of the liquid inside the pore capillaries can begin. Thermodynamically, the equilibrium vapor pressure, p, over a concave meniscus of liquid must be less than the saturation vapor pressure, p^0, at the same temperature [30]. This implies that the vapor will be able to condense to liquid in the pores before the relative pressure approaches unity

[30]. Relating the radius of the meniscus to the relative pressure is described by the Kelvin equation:

$$ln\left(\frac{P}{P^0}\right) = \frac{-2\gamma V_L}{RT} \cdot \frac{1}{r_m} \qquad (14)$$

where P/P^0 is the relative pressure of vapor in equilibrium with a meniscus having a radius of curvature r_m , while γ and V_L are the surface tension and molar volume of the liquid, respectively [30]. When capillary condensation begins at given P/P^0, wider and wider pores will be filled until the entire system is filled at the saturation pressure [30]. It is interesting to note that in order to equate the radius of meniscus to the pore radius (minus the thickness of the adsorbed film), pores are assumed to be cylindrical [30]. Figure 7 shows a hypothetical or expected isotherm for a porous solid containing cylindrical pores of the same size (3 different pore sizes are shown) and figure 8 shows the actual nitrogen adsorption isotherm for SBA-15. It is clear from the isotherm and pore size distribution that SBA-15 exhibits cylindrical pores of equal size.

From the Kelvin equation, as capillary condensation of nitrogen should occur within a pore at a given pressure, p, determined by the value of the radius of curvature of the meniscus, the calculation of the pore size is possible with the relation of r_m to the pore radius [30]. Figure 9 shows the relationships of the radius of curvature of the meniscus, the inner core radius of the pore, the film thickness, and the pore radius.

The most important characteristic of the nitrogen adsorption isotherm for the determination of the pore size and pore size distribution, as well as the qualitative evaluation of the pore structure, is the position, size and shape of the hysteresis loop. The hysteresis of the isotherm arises from differences in the processes of adsorbate condensation and evaporation and the effect the shape

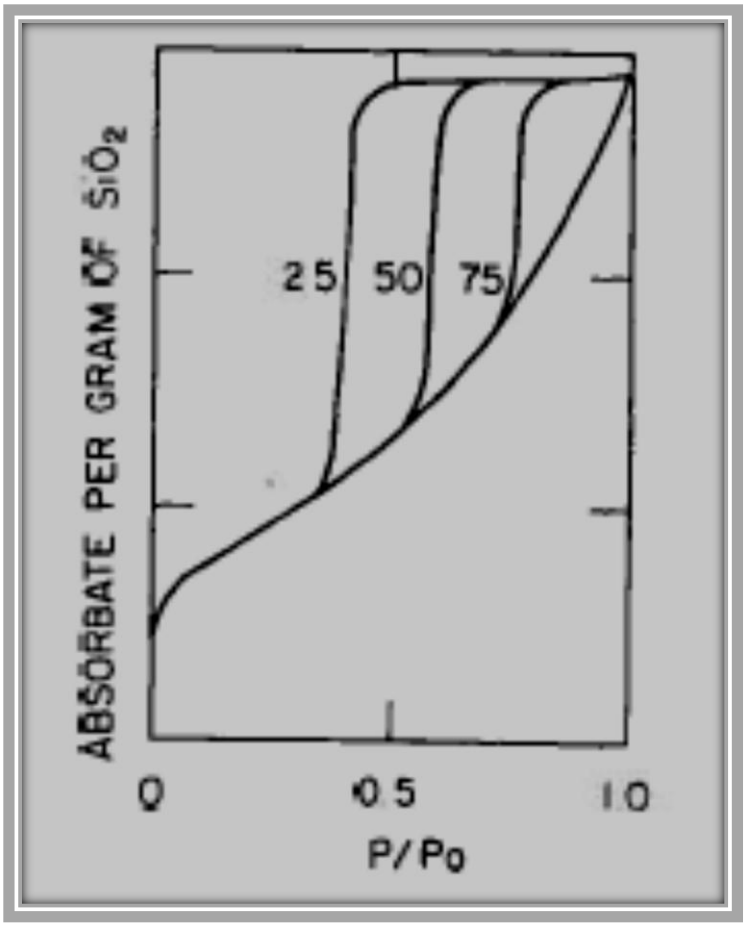

Figure 7. Overlay of nitrogen adsorption isotherms for 3 hypothetical porous solids with uniform cylindrical pores of 25 angstrom, 50 angstrom and 75 angstrom for each sample respectively.

(Copied from R.K. Iler, *Chemistry of Silica: Solubility, Polymerization, Colloid and Surface Properties, and Biochemistry*, Wiley-Interscience, NY, 1979, chapter 5. Silica Gels and Powders: physical characterization p.491).

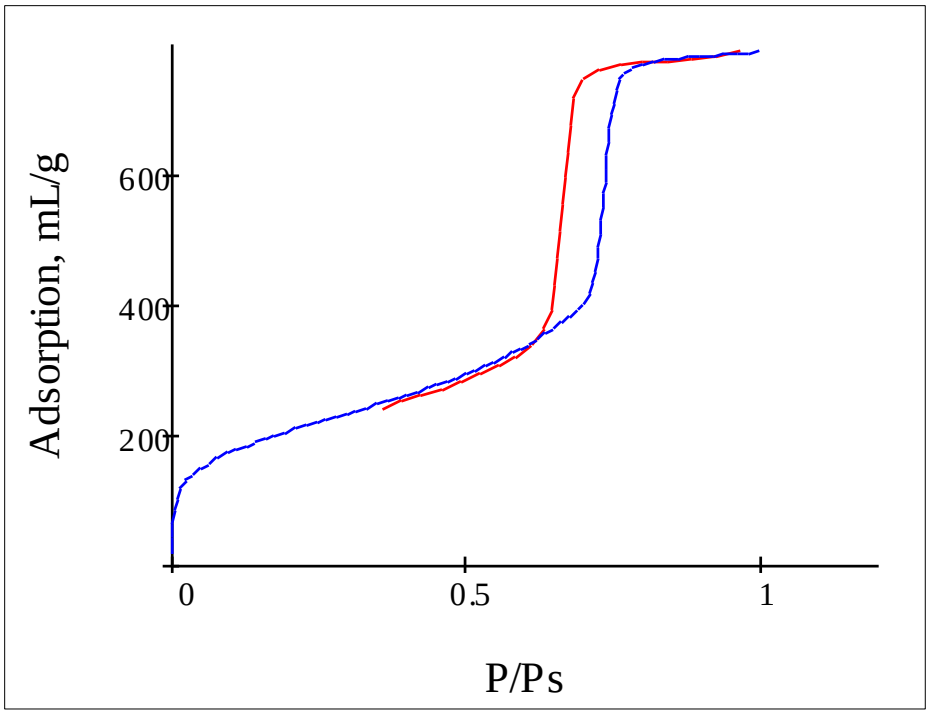

Figure 8. Nitrogen adsorption/desorption isotherm for a synthesized batch of spherical SBA-15 silica. Notice the striking similarity between this experimentally determined isotherm for spherical SBA to the expected isotherm for a hypothetical porous solid with uniform, cylindrical pores in Figure 7.

of the pore has on the meniscus of the condensing adsorbate and subsequent pore filling [30]. The curved interface between a liquid and a vapor is comprised of 2 radii of curvature at right angles from each other, with the mean radius of curvature given by:

$$\frac{1}{r_1}+\frac{1}{r_2}=\frac{1}{r_m} \qquad (15)$$

The filling and evaporation of nitrogen inside the pores, and the relative pressures it is occurring at all depends on the shape of the meniscus and the relationship of its radius of curvature, r_m, to the pore inner core radius, r^k. For example, in a cylindrical pore closed at one end, condensation will begin at the closed end and proceed with a hemispherical meniscus (in which $r_1=r_2=r_m$, and $r_m = r^k$) at a $p/p^0=e^{-2K/rk}$, where K is $\gamma V_L/RT$ of the Kelvin equation. During evaporation, the meniscus is also hemispherical, thus condensation and evaporation happen at the same relative pressures and no hysteresis occurs [30]. However, with a cylindrical pore open at both ends, since condensation begins on the pore walls, the meniscus is cylindrical ($r_1=r^k$; $r_2=\infty$ and $r_m=2r^k$) and condensation proceeds at $p/p^0 = e^{-K/rk}$ [30]. During evaporation, the meniscus is hemispherical and proceeds at $p/p^0= e^{-2K/rk}$. We can see that condensation and evaporation take place at different relative pressures giving rise to the hysteresis loop between adsorption and desorption.

The Kelvin equation is also used for the determination of the pore size distribution. Basically, the evaporation of the liquid from the pores during desorption is segmented across the pore volume, as determined by a_{max}, into sequential steps as pores of certain radii loose condensate while correcting for the contribution of the thinning adsorbed film after the initial pore emptying throughout the process[30]. Through a knowledge of the adsorbed layer thickness, and relation

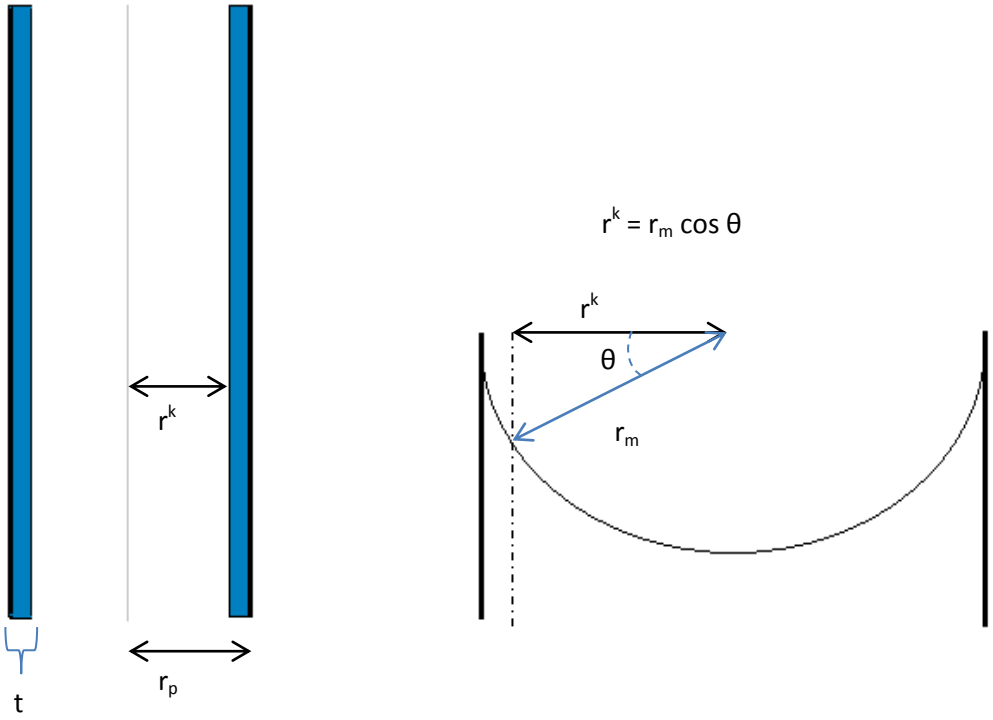

Figure 9. **On the left**: cross-section of a cylindrical pore with a radius r_p, showing the relationship between the "inner core" of the radius, r^k and the adsorbed film if thickness, t. **On the right**: the relationship between r_m of the Kelvin equation and the inner core radius, r^k, for a cylindrical pore with a hemispherical meniscus. θ is the contact angle. For a hemispherical meniscus, the contact angle,$\theta = 0$, so $\cos\theta=1$ and $r_m=r^k$.

of the core radius to the pore radius ($r_p - t = r^k$) all as a function of the relative pressure, the pore size distribution can be plotted.

1.4.2 Thermogravimetric Analysis

Thermogravimetric analysis (TGA) techniques measure the weight loss during heating. Decomposition of bonded alkyl ligands starts slightly before 200^{o}C and will last until about 600^{o}C [26]. Thermogravimetric analysis is a useful tool to determine the presence of material containing carbon, hydrogen, and oxygen on the surface of silica such as surfactants (in the case of templated silicas) and bonded alkyl groups. This method can also yield quantitative results as the weight loss is accurately measured by an internal microbalance, and the percent weight of a sample lost through thermal decomposition can be calculated. Although calculations of bonding density are more accurate when using %C data from elemental analysis, previous work has shown a correlation between weight loss from TGA and % C [35,26]. A plot of %C versus %weight loss will yield a straight line with a slope equal to the carbon fraction of the cleaved ligand [35].

Previous studies have shown that not all of the grafted molecules are removed through ashing techniques, and the use of weight loss to calculate bonding density requires an assumption of the chemical decomposition patter [26]. For example, the degradation of alkyl dimethyl silyl silicas proceed in two steps, with a loss of the hydrocarbon chain at about 250oC, followed by the destruction of the dimethyl silyl group at temperatures up to 450oC [35]. However, the silicon atom left on the silica surface, which may be hydroxylated, complicates the calculation of overall

weight loss [26]. The following equation can be used to calculate bonding density through weight loss:

$$d_b = \frac{w\%}{MW_{lig} S_{SiO2} (100 - w\%)} \qquad (16)$$

where MW_{lig} is the molecular weight of the cleaved group, and S_{SiO2} is the surface area of the silica.

In conclusion, the techniques of LTNA and thermogravimetric analysis are utilized to gain information regarding the physiochemical properties of synthesized silicas. While specific data concerning surface area, pore size and pore size distribution are provided through analysis of nitrogen sorption isotherms, surface chemistry and characteristics of the bonded layer are calculated from measurements made by TGA. By using such techniques, silica synthesis can be guided to produce materials with pore structure and surface chemistry conforming to desired specifications.

II. Scope of Research

This dissertation is mainly concerned with the synthesis, modification and characterization of spherical ordered mesoporous SBA-15 silica suitable for use in high performance liquid chromatography. As the actual study of the synthesized material in liquid chromatography will be discussed in the second part of this dissertation, the first part will concentrate on the methods of synthesis, modification and characterization of spherical SBA-15. Therefore, the main scope of this research is to, first; identify the critical parameters in the synthesis procedure and their effects on the characteristics of the silica produced, second; characterize the synthesized material based on particle morphology, pore size and pore size distribution and select worthy candidates for surface modification, and lastly; characterize the geometry of the modified silicas.

In the first part of this research, the synthesis of spherical SBA-15 presents some interesting challenges. As the normal particle morphology of SBA-15 is that of a fiber, rope-like shape, the adjustment of critical synthetic parameters to yield spherical particles will be undertaken. However, as we identified in the previous section, the rope-like particle shape is a result of the domination of the long range forces originating from the pore ordering surfactant-silicate assembly over the particle formation process. Therefore the particle morphology can only arise from the sacrifice of pore order on some level, even if only minor. We will examine the possibilities of minimizing this sacrifice and producing spherical particles with porous structure representative of fibrous SBA-15.

Surface modification of the synthesized spherical SBA-15 will be studied. In particular, several geometric properties of the modified layer will be investigated, such as the bonding density, thickness of the modified layer and the calculated value for the bonded ligand volume. As SBA-

15 is known to have long, non-intersecting pores, the evaluation of the bonded layer will give insights into the possible tortuosity of these pores in spherical particles.

In the area of characterization, SBA-15 presents us with several interesting situations. As we have discussed, most, if not all, of the assumptions made in the study and characterization of porous materials are based on the use of cylindrical pores. The study of SBA-15 allows for the opportunity to evaluate the veracity of such assumptions as well as to use those assumptions and models to test the cylindrical nature of the pores in spherical SBA-15.

III. Experimental

3.1 Synthesis of Spherical SBA-15 Silicas

Spherical SBA-15 was synthesized with the use of Pluronics P123 (PEO_{20}-PPO_{70}-PEO_{20}) as a surfactant, cetyltrimethylammonium bromide (CTAB) as a co-surfactant, and ethanol as a co-solvent. Tetraethoxysilane (TEOS) was used as the silica source and hydrochloric acid as the acidic modifier. The synthetic procedure basically consists of 3 main stages: the stage post addition of TEOS, called the "reaction"; the static ageing, called the "ageing"; and when applicable the second ageing at elevated temperatures, called the "hydrothermal treatment", or just "treatment". All three of these stages can be adjusted for temperature and time – within certain limits (discussed in sections 1.2.1 and 1.2.2)

Table I lists the molar ratios of the reagents used in the typical synthetic procedure (synth 1), a variation of the typical spherical synthesis (synth 2), as well as the original fibrous SBA-15 procedure. In a typical procedure, 3 grams of P123 was dissolved in 60mL of 1.5M HCl. In a separate vessel, 0.6 grams of CTAB was dissolved in 25 mL of distilled water. Once dissolved, the solutions are combined in a water bath with a magnetic stirrer and maintained at 35^{o}C in a pressure resistant glass bottle with high density Teflon coated polyethylene cap to withstand the pressures generated in the ageing and treatment stages. To this solution, 20 mL of 100% ethanol is added. Once the mixture is at thermal equilibrium, 10 mL of TEOS is added in a drop wise fashion, and the mixture is vigorously stirred (~500 rpm) for 45 min at 35^{o}C (the bottle cap is closed tightly a this point). This is the "reaction" during which hydroxylation and condensation will begin, at rates depending on the volume of ethanol and level of pH. The time of the

Table I. Molar ratios for different spherical and fibrous SBA-15 syntheses.

Method	TEOS	P123	CTAB	HCl	H_20	EtOH
Fibrous	1	0.0168	-----	5.85	203	----
Synth 1	1	0.0115	0.037	2	104	7.8
Synth 2	1	0.0124	0.0197	3.23	120	9

reaction, as well as the temperature may be varied as discussed in 1.2.1. The vessel is removed from the water bath and placed in an 80^{o}C oven or water bath without stirring for 5 hours, after which the vessel is placed into a 120^{o}C oven for 12 hours. These last two steps, the ageing at 80^{o}C and treatment at 120^{o}C can be adjusted for both time and temperature based on the desired result. As discussed in sections 1.2.1 and 1.2.2, increased lengths of time and temperature are expected to yield large pore size. The resulting white precipitate is recovered by filtration with water and dried at 90^{o}C for 24 hours. The sample is then subject to calcination is air at by raising the temperature from 35^{o}C to 500^{o}C over a 2 hour period and holding at 500^{o}C for 8 hours. The final molar ratios of the reactants relative to one mole are shown in Table I.

For comparison, fibrous SBA-15 (non-spherical) was synthesized with 4 grams of P123 and 8.5 grams of TEOS. P123 was dissolved in 30 grams of water and 120 grams of 2M HCl with stirring at 35^{o}C. Once at equilibrium, to this solution was added 8.5 grams of TEOS drop-wise. The solution was allowed to react for 20 hours at 35^{o}C, followed by static ageing at 80^{o}C for 24 hours.

3.2 Modification of Spherical SBA-15 Silicas

To modify the surface of synthesized spherical SBA-15 silica, roughly 1 to 2 grams of material was charged to an glass ampule was put into a clean oven at 100^{o}C overnight. The next day, while the silica was still hot, (N,N-dimethylamino) trimethylsilane (for C1), (N,N-dimethylamino) octyldimethylsilane (for C8), and (N,N-dimethylamino) octadecyldimethylsilane (for C18) was added to until the silica was sufficiently covered (like wet sand) and the ampule was sealed. The sealed ampule was put into a circulating heated water jacket at 60^{o}C for 72

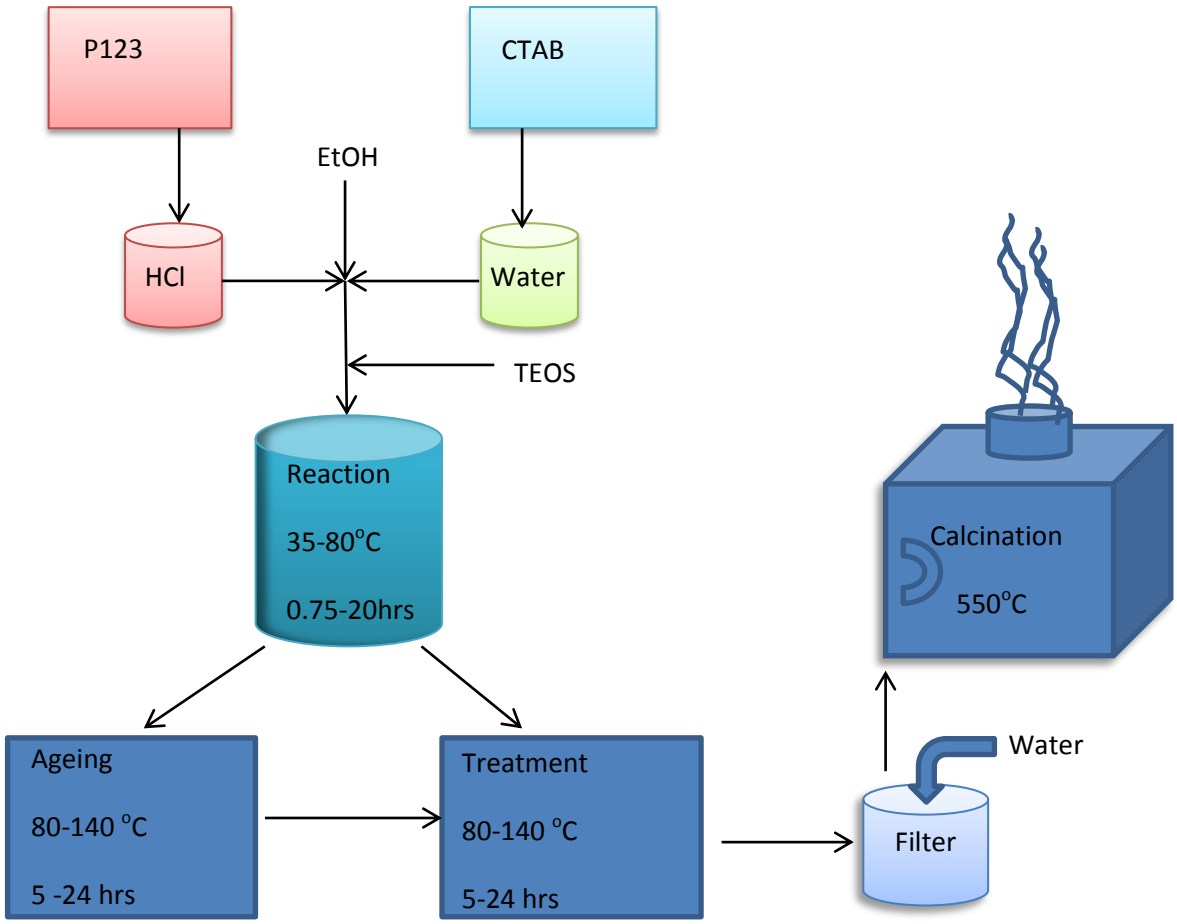

Figure 10. Synthesis Scheme showing the general flow of the procedure. Adjustments to temperature and duration of reaction, ageing, and treatment steps can be made (with best results from staying within the limits presented, especially within the reaction step). The reaction can be followed by both ageing and treatment, or just treatment.

hours. Once the reaction was complete, the modified silica was washed on a glass filter with ~100 mL of toluene, followed by 100 mL of acetone and 100 mL of a water/acetone mixture. After a final filtering with more acetone, the modified silica was dried at 90^{o}C for 4 hours.

3.3 Methods of Characterization

Modified and unmodified spherical SBA-15 silicas were characterized by low temperature nitrogen adsorption (LTNA), thermogravimetric analysis, elemental analysis and optical microscopy.

3.3.1 Equipment

3.3.1.1 Low temperature nitrogen adsorption

Nitrogen adsorption measurements were performed on an Omnisorb model 100CX (Omnisorb, NJ,US) using the static adsorption mode with full equilibration of each adsorption point, measuring both the adsorption and desorption isotherms. Raw data from the adsorption system were transferred into Mathcad 14.0 software utilizing a homemade template was used for the calculation of the adsorbent pore volume, surface area, BET C constant, and pore size distribution (an example of the Mathcad template can be seen in the appendices).

3.3.1.2 Thermogravimetric analysis

Thermogravimetric analysis was performed using a TA 2950 thermogravimetric analyzer (TA Instruments Inc., New Castle, Delaware) operated between room temperature and 800^{o}C in air with a heating rate of 10^{o}C per min. Analysis of the data was carried out on TA instrument software for the calculations of % weight loss.

3.3.1.3 Elemental analysis

Elemental analysis (C,H) of the spherical SBA-15 silicas was performed by Schwarzkopf Microanalytical Lab, NY, on a Perkin Elmer 2400 CHN Analyzer using the ASTM method. Bonding densities were calculated using Eq. (1).

3.4 Materials

Materials used in the synthesis of spherical SBA-15 include Pluronics P123 (Sigma-Aldrich Co., St. Louis, MO), cetyltrimethylammonium bromide (CTAB) (Fischer Scientific, Fair Lawn, NJ), concentrated hydrochloric acid (Fisher Scientific), and ethanol (Pharmco, Brookfield, CT). Purified water was supplied by an in-laboratory Milli-Q purified water system (Millipore, El Paso Texas). Aminosilanes for C1, C8 and C18 were purchased from Gelest (Morrisville, PA).

IV. Results and Discussion

4.1 Synthesis of Spherical SBA-15

The synthetic procedure detailed in section III was carried out with modifications to the ageing and hydrothermal treatment steps in order to ascertain the effect of heating temperature and time on the synthesis of spherical SBA-15. According to the literature [3-4, 12-13] changes to both the temperature and duration of reaction/ageing should produce structural changes to the synthesized material overall morphology as well as pore structure. The intention of adjusting the parameters of the synthesis was to gain an understanding of the critical parameters to both forming spherical particles as well as maintaining a well-ordered system. Initial attempts at synthesis of spherical SBA-15 included a confirmation of the above procedure along with several variations including a synthesis with only one aging at 80^0C and a synthesis with ageing at 75^0C for 5 hours and 10 hours respectively. This was performed primarily to see the effect of a single aging scheme since the original procedure of Zhao et. al. [3,4] consisted of a reaction time followed by a single aging. Results confirmed that indeed two aging temperatures were necessary (at least at 75-80^0C) to successfully synthesize spherical SBA-15. However, although spherical particles were obtained with a single aging scheme, low temperature nitrogen adsorption (LTNA) results indicated that the batches synthesized at 80^0C and at 75^0C were mainly microporous in nature and showed a low level of ordered pore structure as compared to adsorption isotherms of fibrous SBA-15.

Table II shows the results of varying temperature of the first ageing stage as well as the hydrothermal treatment (herein, called 'treatment'). Figures 11-14 show the adsorption isotherms of the samples listed in Table II. Varying the ageing temperature to 75^oC had a

Table II. Synthesis Results: Effect of temperature

Sample	Ageing	Treatment	S_{BET} m^2/g	V_{pore} mL/g	R_{pore} Å
SBA-S1-10	80°C, 5 hr	140°C, 12 hr	707	1.39	38.9
SBA-S1-3	80°C, 5 hr	120°C, 12 hr	750	1.39	32.5
SBA-S1-9	75°C, 5 hr	120°C, 12 hr	885	1.07	23.0
SBA-S1-30	90°C, 5 hr	120°C, 12 hr	822	1.13	24.7

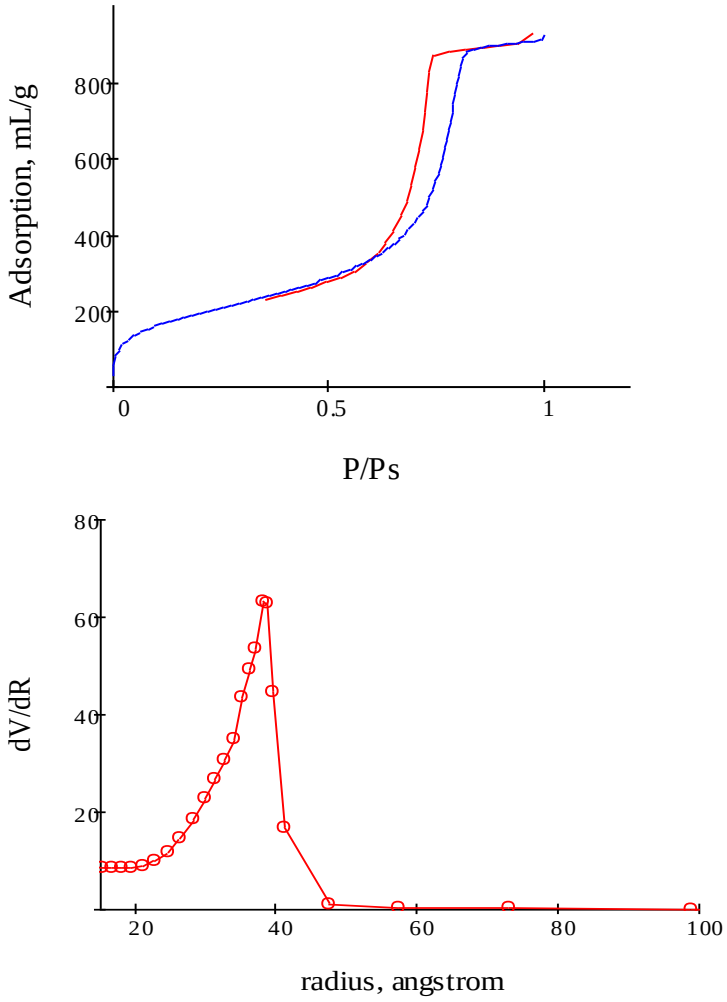

Figure 11. S-1-10 nitrogen adsorption isotherm (top) and pore size distribution.

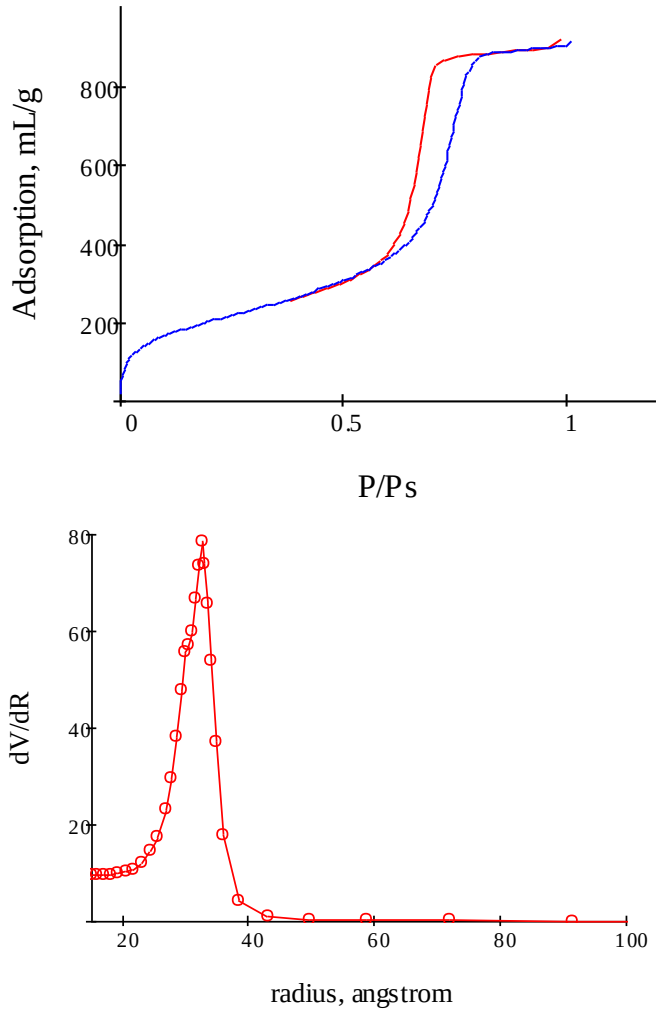

Figure 12. S-1-3 adsorption isotherm (top) and pore size distribution (bottom)

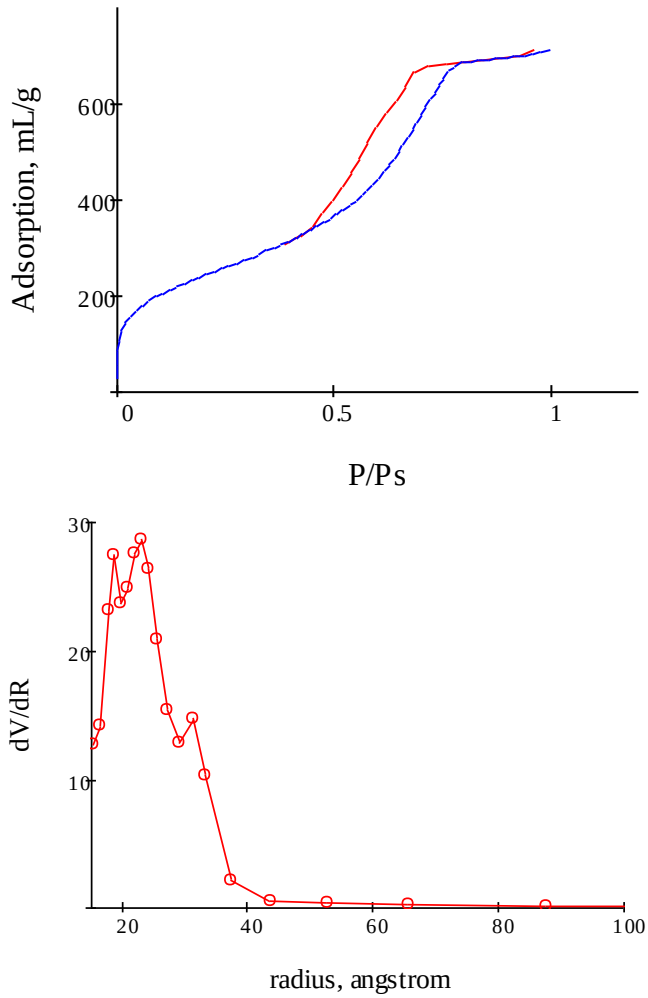

Figure 13. Nitrogen adsorption isotherm (top) and pore size distribution for S-1-9.

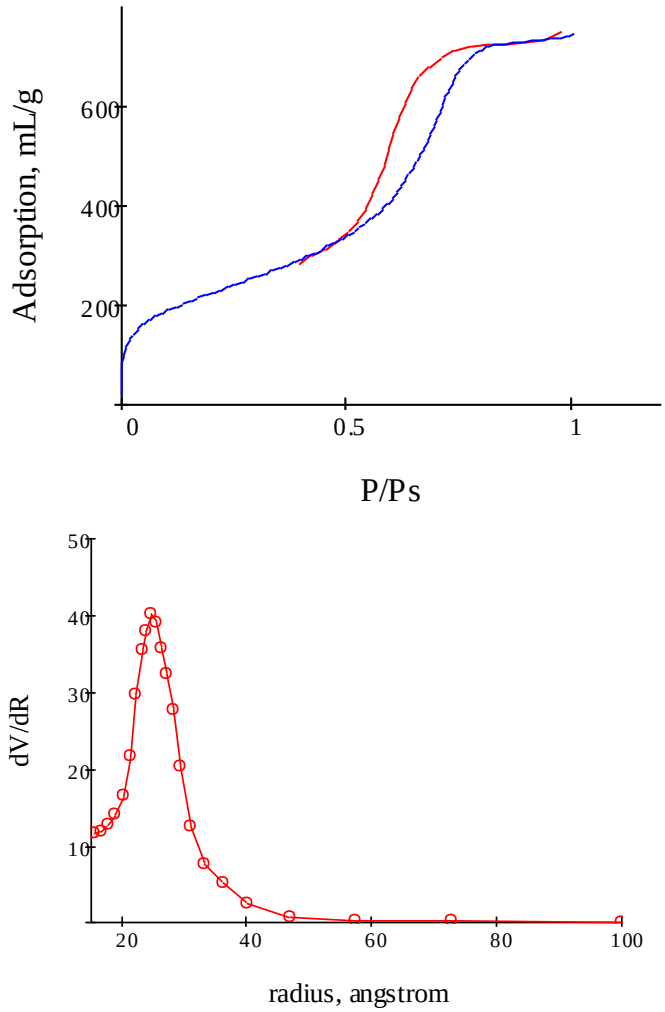

Figure 14. Nitrogen adsorption isotherm (top) and pore size distribution (bottom) for S-1-30.

negative effect on the porous structure as is evident by the broad pore size distribution. On the other hand, raising the temperature of the treatment step has increased the pore size without significantly increasing the pore size distribution. Even the increase of the ageing step to 90^{o}C did not produce a significant increase to pore size distribution, but it was not an improvement over the ageing at 80^{o}C either.

Table III shows the results of the variation made to the ageing and treatment step time. It is interesting that the increase in the ageing step at 80^{o}C from 5 hours to 12 and 24 hours resulted in a drastic drop of the pore size. Since the pore size has been reduced by almost a half, the desorption curve of the isotherm is close to the closure point, around 0.4 P/P^0 (Figures 15 and 16). Although the isotherms for the two silicas synthesized with increased ageing times might indicate a loss of pore structure, the pore size distributions show that although the pores are getting small in these samples, they are not necessarily disordered. The shape of this isotherm is more a product of approaching the lower closure point than it is the result of disordered pores. Also, the increase in the treatment step had no significant effect on the pore size or surface area or pore size distribution. It could be concluded that while an increase in the hydrothermal treatment will increase the pore size, as was expected [3,4] the increase in ageing or treatment time resulted in the reverse of what was expected.

Table IV shows the result for the single ageing schemes, in which the synthesis goes straight from the reaction at 45^{o}C to the oven at 120^{oC} or 130^{o}C for 12-24 hours. The results from the single ageing step is much different when the temperature is 100^{o}C or over. For the single ageing scheme, the longer duration as well as the higher temperature produced larger pore sizes, as is expected. There is a slight broadening of the pore size distribution from the synthesis at 120^{o}C to 130^{o}C (Figure 17). However, under the microscope, the samples synthesized with a

Table III. Synthesis results: Effect of heating time.

Sample	Ageing	Treatment	S_{BET} m^2/g	V_{pore} mL/g	R_{pore} Å
SBA-S1-3	80°C, 5 hr	120°C, 12 hr	750	1.39	32.5
SBA-S1-17	80°C, 12 hr	120°C, 12 hr	880	0.803	18.4
SBA-S1-19	80°C, 24 hr	120°C, 12 hr	924	0.813	18.3
SBA-S1-21	80°C, 5 hr	120°C, 24 hr	750	1.02	29.7

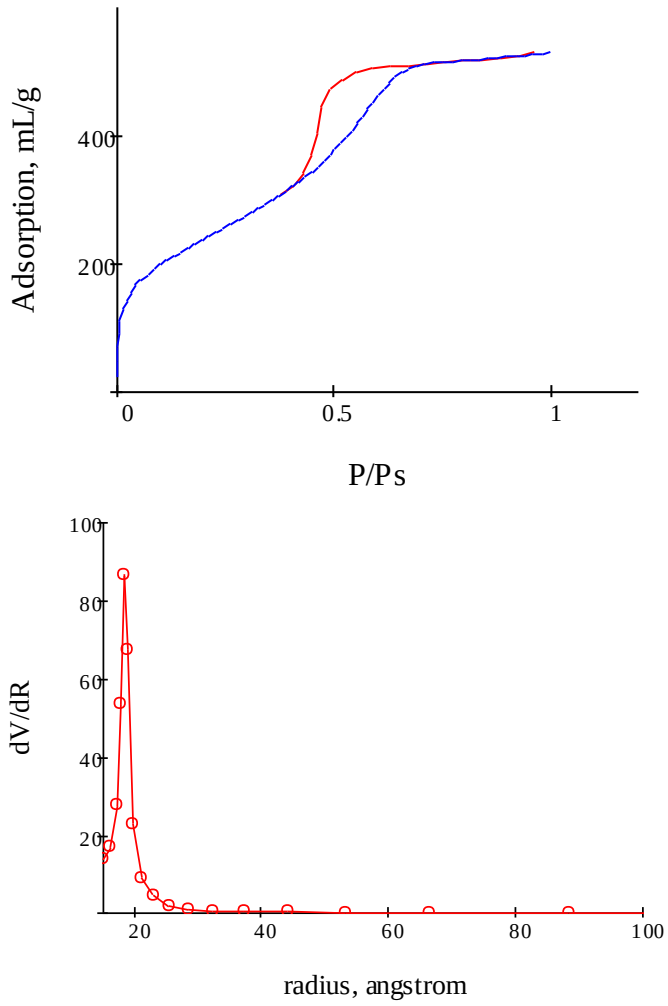

Figure 15. Nitrogen adsorption isotherm and pore size distribution for S-1-17

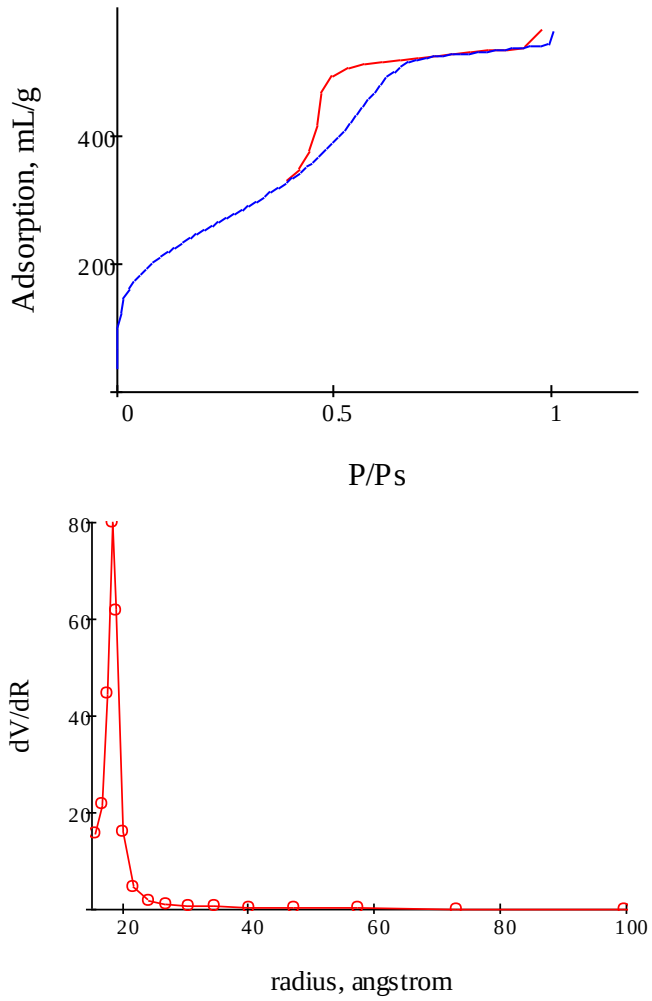

Figure 16. Nitrogen adsorption isotherm and pore size distribution for S-1-19

Table IV. Synthesis results. Single Ageing time and temperature

Sample	**Ageing**	**S_{BET} m^2/g**	**V_{pore} mL/g**	**R_{pore} Å**
SBA-S1-4	120°C, 12 hr	783	0.95	25.6
SBA-S1-20	130°C, 12 hr	713	0.95	29.0
SBA-S1-22	130°C, 24 hr	649	1.24	36.7

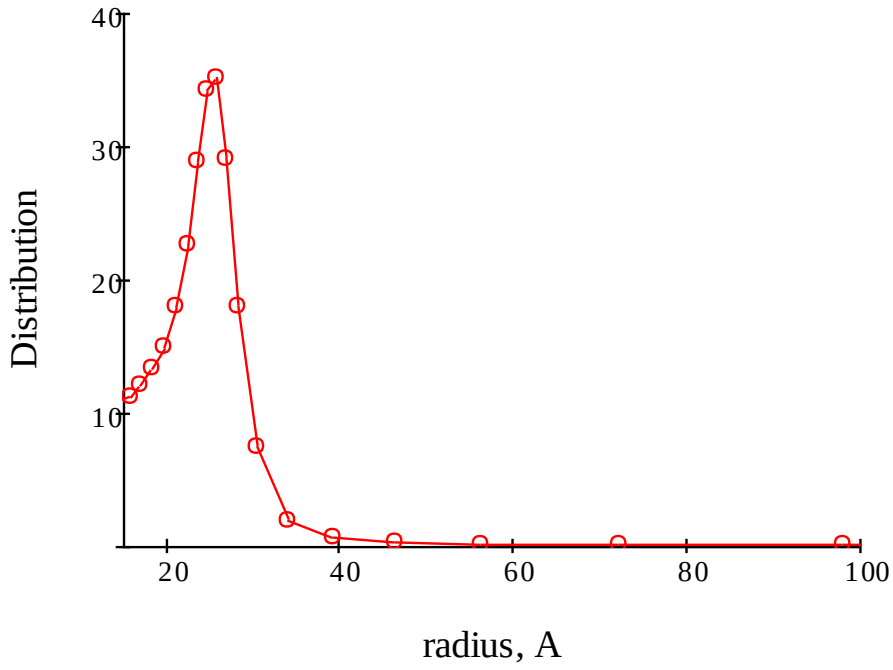

Figure 17. Pore size distribution for S-1-4 (120^{o}C 12 hours)

single ageing at 120^{o}C to 130^{o}C contained only very small irregular particles, perhaps 1 μm or smaller in size. It is apparent from this information as well as the initial syntheses carried out at 80^{o}C for 5 hours, that in the two-step synthesis, the initial step is crucial for forming the spherical particle, while the second higher temperature, hydrothermal treatment, is responsible for the further ordering and ripening of the porous system. As we discussed in the introduction, the cross-linking process is continues as silica condensation continues through the ageing and treatment steps. It seems likely that during the initial ageing stage at 80-90^{o}C, the loose crosslinking between the micelles allows for the co-surfactant and co-solvent to influence the energy of curvature of the surface. However, once the hydrothermal treatment begins and the temperature is raised to 120^{o}C to 140^{o}C, the crosslinking takes a much stronger role and the system beings to further condense and polymerize around the core ordered structure. The initial ageing is more of a setting phase, where the forces controlling particle morphology can take precedence while the second treatment phase is where the hardening of the structure and ordering takes place.

Apart from the increase in temperature during the treatment step of the synthesis, changes made to the temperature and time had little or no positive effect on the synthesis of spherical SBA-15. Optical microscopy of batches synthesized under the dual ageing scheme all exhibited sphered of roughly 15-20 um size by counting method, which is admittedly limited. However, for purposes of morphology identification, optical microscopy is sufficient. Since, as we saw above, the single ageing procedure yielded irregular particle morphologies, it was decided to continue using the two step procedure. As the goal is to synthesize spherical SBA-15 exhibiting porous structure similar to fibrous SBA-15, the effect of adjusting co-surfactant and pH was investigated. We hypothesized that since CTAB is used to create the curved morphologies

absent in fibrous SBA-15, a reduction of its concentration in the synthesis should help produce spherical SBA with a more ordered porous structure resembling fibrous SBA. The original molar ratio of CTAB to TEOS was 0.037:1, and 1:5 to P123. Therefore, we attempted syntheses with 10:1 and 20:1 P123 to CTAB ratios (dropping it down to 0.009 moles per mole of TEOS). All other parameters of the original synthesis were left unchanged. In Table V, spherical silica S-1-26 was synthesized with a 20:1 ratio to P123. The nitrogen adsorption isotherm showed extreme promise as the branches of adsorption and desorption were almost completely parallel to each other, indicating pores of a very similar size, and hence a narrow pore size distribution as fibrous SBA-15 exhibits (Figure18).

Alongside the changes to the concentration of co-surfactant, changes to the pH were also carried out. Since it was clear that in order to obtain a more well-ordered system, a sacrifice to particle morphology would need to be made, it was believed that by increasing the concentration of HCl in the synthesis mixture, we would be able to quicken the pace of condensation and polymerization in the reaction mixture at 45^{o}C. If we could get the condensing silica to surround and interact with the micelles at a quicker pace, we could essentially reduce the forces fighting to curve the morphology, just enough to allow the spherical particle to take shape – but just barely. We could minimize the contributions to curvature, by enabling the silicate-copolymer assembly to interact faster and become ordered faster.

Results for the attempts to increase pore structure can be seen in Table V. Sample S-2-31 is from a procedure outlined in ref [12] where Zhao et al. discuss a procedure for synthesizing spherical SBA-15, however, the resulting material, although showing excellent porous structure, was not spherical (irregular 1 μm particles). The culmination of the synthetic trial and errors are the synthesis of batches S-1-29 and S-2-36 which have the closest match to fibrous SBA – both

Table V. Final synthesis results

Sample	Reaction	**Ageing**	**Treatment**	S_{BET} m^2/g	V_{pore} mL/g	R_{pore} Å
SBA-S1-26	45°C, 45 min	80°C, 5 hr	140°C, 12 hr	744	1.63	39.5
SBA-S1-29	45°C, 45 min	80°C, 5 hr	120°C, 12 hr	630	1.2	34.2
SBA-S2-31	80°C, 20 hr	100°C, 24 hr		939	1.16	26.3
SBA-S2-36	45°C, 5 hr	80°C, 5 hr	120°C, 12 hr	752	1.21	29.1

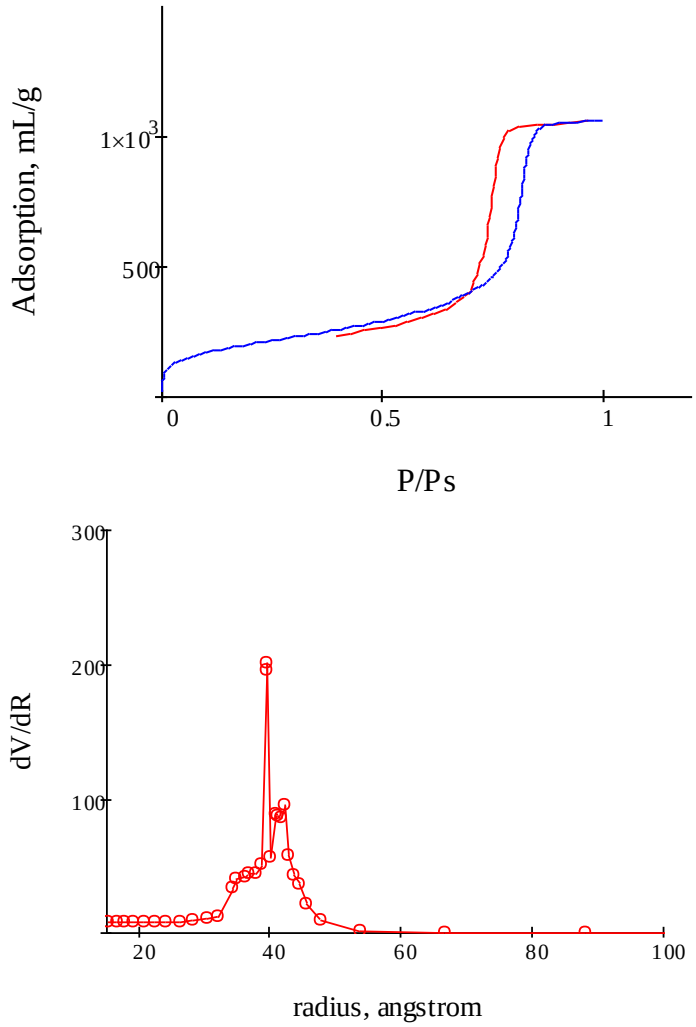

Figure 18. Nitrogen adsorption isotherm and pore size distribution for S-1-26

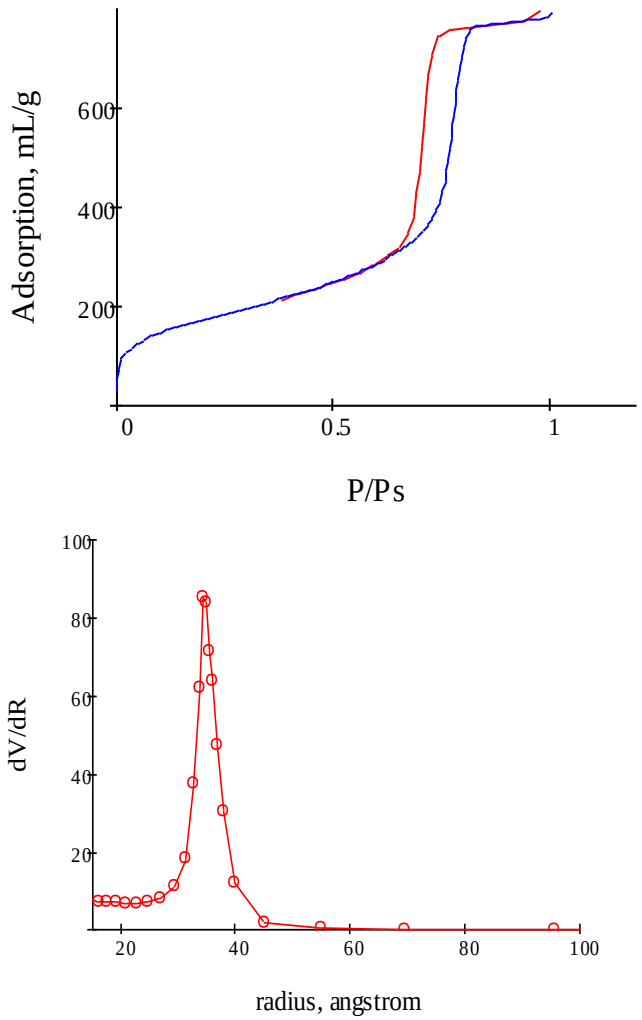

Figure 19. S-1-29 Nitrogen adsorption isotherm and pore size distribution

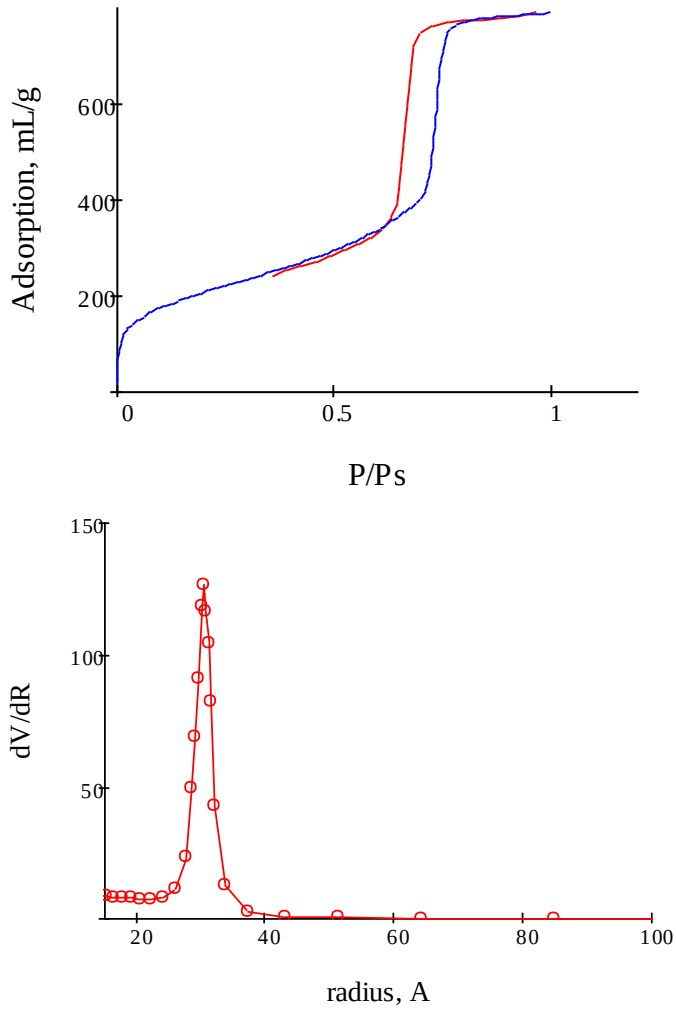

Figure 20. Nitrogen adsorption isotherm and pore size distribution for S-2-36

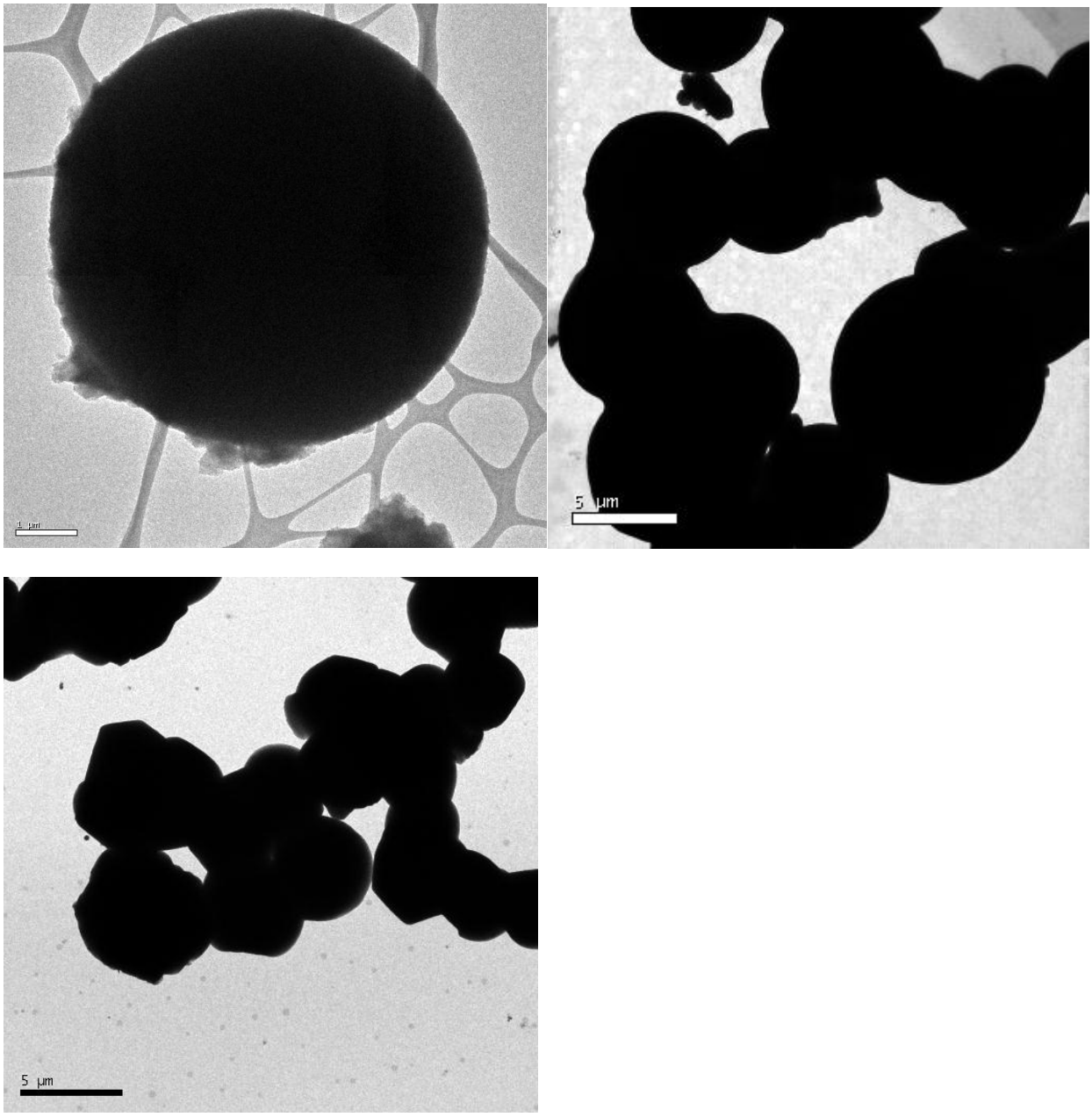

Figure 21. TEM of S-1-10 C8 (left) and S-1-29 (right) and SBA-2-36 (bottom)

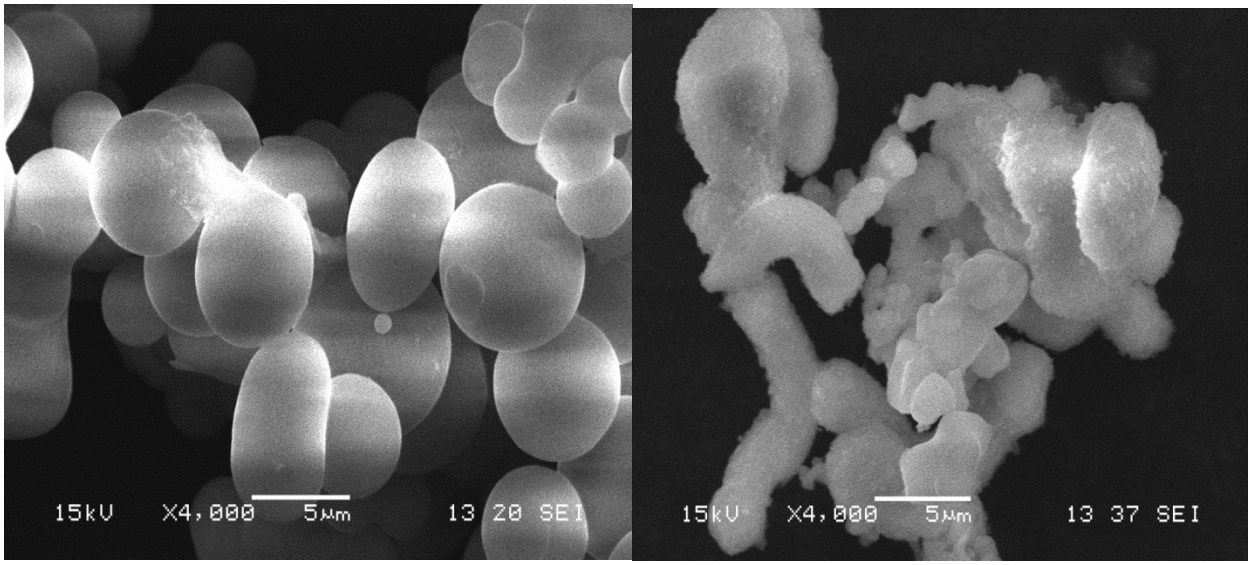

Figure 22. SEM of S-1-2 (75^{o}C, 10 hours) with CTAB (Left) and (right) without CTAB

in the nitrogen adsorption isotherm as well as the pore size distribution. Batch S-1-29 was the the result of synthesis method 1 (Table I) in which we increased the concentration of HCl to match closely to the fibrous method, as well as decreased the CTAB concentration to 0.009 moles per mole of TEOS. Sample S-2-36, however, was synthesized using synthesis 2 (Table I) in which we adjusted the synthesis procedure listed in ref [12] to include ethanol and a different ageing and treatment scheme. Whereas the authors in ref [12] performed a reaction of the P123-silicate solution at 40^{o}C for 20 hours followed by 100^{o}C for 24 hours, we used a reaction time of 5 hours, followed by a two-stage ageing at 80^{o}C for 5 hours, followed by 120^{o}C for 12 hours.

As can be seen in Figure 21, the S-2-36 material exhibited some slight edges and would be more accurately described as having a spheroid shape. However, the S-1-29 batch was more spherical. Figures 21 and 22 show SEM/TEM images of several batches. Figure 22 shows the results of synthesis with and without CTAB illuminating the importance the co-surfactant has on influencing spherical morphology.

4.2 The C constant and cross-sectional area of nitrogen

In order to accurately characterize bonding density an accurate value of the surface area of the bare silica needs to be made. By convention, the use of 13.5 Å^2 or 16.2Å^2 for the cross-sectional area of nitrogen was being used to calculate the surface area on the polar, bare silica surface. However, in order to calculate the surface area of a modified hydrophobic silica surface, a value of 20.5 Å^2 or 21 Å^2 has been suggested [26,29,33]. However, an interesting occurrence was observed during the characterization of these SBA-15 materials. While it is admitted that these spherical SBA-15 silicas do not exhibit the same strict ordered pores as do fibrous SBA-15

silicas, never the less, they still do show a high degree of ordered structure and it cannot be denied that the pores show characteristics of cylindrical pores. For cylindrical pores, the relation of $R/2 = V/S$, should hold. Meaning, that a comparison of the pore radius from the desorption curve by way of the kelvin equation should equal $2V/S$. However, it was clear that most, if not all of the SBA silicas characterized, mainly bare silica, were failing to satisfy this relationship. For instance, Table VI shows sample S-1-3 which showed a -36% difference between the two values for pore radius! Moreover, a fibrous SBA sample (24/80) which had been measured on by LTNA twice over two years apart showed an 11-12% difference each time analyzed. The fact that this is silica is specifically known to exhibit cylindrical pores, makes the possibility very high that there is an error of some sort with the measurement, and not the actual physical characteristics of the silica. For instance, when the silica mentioned above with -36% error in the measurement was modified and run on LTNA, the difference was only 1% for the C8 modified sample. Therefore, this issue is more about the energy of the surface and the value for the cross-sectional area of nitrogen (ω) used than anything with the silica. Table VI shows the original value of ω and then the value needed in order to bring the % error to zero. Interestingly enough, the values of ω range from 11.8 to 18.2 and correlate well with the value of the C constant. The higher the value of C, the lower the value of ω needs to be. Although this is a limited dataset, this is an area of study that should be developed further. Instead of using set values for the cross-sectional area of nitrogen – a model should be proposed in which a value depending on the energy of the surface as evaluated by the C constant will be used.

Table VI. Correction for cross-sectional area of nitrogen based on correlation of C constant to geometric relationships in cylindrical pores.

Sample	C	ω_{N2}	S_{BET} m2/g	V_p mL/g	R_{pore} Å	2V/S Å	% diff	$\omega_{\%0}$	2V/S Å
S1-3	54	13.5	629	1.39	32.5	44.1	-36	18.2	32.7
S1-3C8	16	21	578	0.71	24.9	24.5	1.9		
S1-10(1)	69	13.5	589	1.39	38.0	47.3	-24	16.8	38.0
S1-10(2)	87	13.5	629	1.44	38.9	46.5	-19.6	16.2	38.8
S-24/80(1)	163	13.5	961	1.19	28.3	24.8	12.3	11.8	28.4
S-24/80(2)	209	13.5	858	1.09	28.7	25.5	11	12	28.7
S-1-26	78	16.2	744	1.63	39.5	43.9	-11	18	39.5

4.3 Characterization of Modified Silicas

Table VII shows the calculated bonding densities for three batches of spherical SBA-15 silica (S-1-25, S-1-29, and S-2-36) each modified with C1, C8, and C18. Also shown on the table are the bonding density calculations for three additional spherical silicas which were packed into stainless steel columns for the chromatographic evaluation in Part II (S-1-3 C8, S-1-10C8, and S-1-26 C8). The batches selected for modification were chosen as a result of their exhibiting narrow pore size distributions in combination with pore sizes large enough to allow modification with the long C18 group. Calculated bonding densities for all 6 batches of spherical SBA-15 are within close agreement to each other. As expected, the value for bonding density declines as the size of the grafting molecule increases. For instance, on sample S-2-36, the calculated bonding densities decrease from 2.00 groups/nm^2 for C18 to 1.47 for the C1 modified material. As described earlier, a theoretical value for maximum bonding density can be calculated based on the geometry of a cylindrical pore with relation to the C18 bonded ligand length and distance between anchoring groups as p= 0.217D when the bonded layer thickness is assumed to be at a value of (h= D/6) [36]. The theoretical value for bonding density for C18 on silica with a pore diameter of 72Å is 1.56 groups/nm^2, while the value for silica with a diameter of 62Å is 1.35 groups/nm^2. The bonding density of C18 on spherical SBA-15 sample S-1-29, with a diameter of 72Å was 1.87 groups/nm^2, which is slightly higher than the theoretical value fo 1.56 groups/nm^2. Spherical SBA-15 silicas S-1-25 and S-2-36, both with diameters of 62Å showed bonding densities of 1.57 and 1.47 groups/nm^2 respectively, which compare closely to the

Table VII. Calculation bonding densities for modified spherical SBA-15 silicas

Batch	Bonded Ligand	S_{BET} (m^2/g)	n_c	FW (g/mol)	%C	ρ (group/nm^2)	ρ (μmole/m^2)	f corr. Factor
S-1-25	trimethyl	789	3	73.2	7.64	1.91	3.17	0.845
S-1-25	octyl	789	10	171.38	18.65	1.61	2.68	0.734
S-1-25	octadcyl	789	20	311.65	30.18	1.57	2.61	0.609
S-1-29	trimethyl	700	3	73.2	7.95	2.26	3.75	0.839
S-1-29	octyl	700	10	171.38	19.14	1.88	3.13	0.727
S-1-29	octadcyl	700	20	311.65	31.15	1.87	3.10	0.596
S-2-36	trimethyl	798	3	73.2	8	2.00	3.31	0.838
S-2-36	octyl	798	10	171.38	19.1	1.65	2.73	0.728
S-2-36	octadcyl	798	20	311.65	29.2	1.47	2.45	0.622
S-1-3	octyl	750	10	171.38	19.5	1.80	2.99	0.722
S-1-26	octyl	826	10	171.38	20.09	1.71	2.83	0.714
S-1-10	octyl	742	10	171.38	19.85	1.87	3.10	0.717

Table VIII. Calculation of bonded layer thickness and molecular volume of ligand

Characteristics of unmodified and modified Spherical SBA-15 Silicas										
	$S_{(BET)}$	R_{pore}	C const	V_p	V_p corr	V_{BL}	*h*	V_{MOL}	$V_{ligand\ ACD}$	$R_{pore\ calculated}$
Silica	m^2/g	Å		mL/g	mL/g	mL/g $_{Si}$	Å	$Å^3$	$Å^3$	Å
S-1-25	789	31.0	88	1.247	1.247	0.000	n/a	n/a	n/a	
S-1-25 C1	752	27.1	14	0.866	1.025	0.222	2.8	202.0	184.9	28.2
S-1-25 C8	486	22.5	16	0.575	0.783	0.464	5.9	500.0	376.8	25.1
S-1-25 C18	254	19.4	18	0.273	0.448	0.799	10.1	881.7	651.0	20.9
S-1-29	700	36.3	107	1.340	1.340	0.000	n/a	n/a	n/a	
S-1-29 C1	642	32.9	14	0.984	1.173	0.167	2.4	128.3	184.9	33.9
S-1-29 C8	481	27.3	16	0.676	0.929	0.411	5.9	378.8	376.8	30.4
S-1-29 C18	271	19.2	19	0.324	0.543	0.797	11.4	740.3	651.0	24.9
S-2-36	798	31.0	99	1.073	1.073	0.000	n/a	n/a	n/a	
S-2-36 C1	578	27.6	14	0.710	0.847	0.226	2.8	141.6	184.9	28.2
S-2-36 C8	415	22.2	17	0.457	0.628	0.445	5.6	339.0	376.8	25.4
S-2-36 C18	176	18.2	18	0.160	0.257	0.816	10.2	693.6	651.0	20.8
S-1-3	750	32.5	57	1.380	1.380	0.000	n/a	n/a		
S1-3 C8		24.2	16	0.710	0.983	0.397	5.3	293.7	376.8	27.2
S-1-26	826	38.4	150	1.303	1.303	0.000	n/a	n/a		
S-1-26 C8	478	29.7	16	0.610	0.854627	0.448	5.4	318.3	376.8	33.0

theoretical value of 1.35 groups/nm^2. The fact that these silicas saw bonding densities slightly higher than the theoretical maximum is evidence for the rigid conformation the bonded ligand must be in on the silica surface. On a side note, it is interesting that before correcting the bare silica surface areas according to the C constant as discussed above, the bonding densities for C18 ranged from 2.01 to 2.36 groups/nm^2 for all three silicas, which is significantly higher than the maximum value these pore sizes.

For each of the modified silicas, the value of specific pore volume, before and after modification, was used in the determination of the bonded layer volume. Table VIII shows the correction of the modified pore volume to one gram of silica with the use of Eq. (4). The thickness of the bonded layer is given as the volume of the bonded layer across the entire surface area of the bare silica material (Eq. 3). Values for the thickness of the bonded layer agree well with previously calculated values by Rustomov et al. were it was shown that the thickness of the bonded layer is an indication of the arrangement of alkyl chains on the surface of the silica. Since the average length of a C18 ligand is approximately 25Å long, the height of the bonded layer for the C18 grafted silicas shows that the conformation of the C18 chain must be in a dense, "liquid-like" state [28]. This is also confirmed by comparison to the theoretical determination of the bonded layer height based on the maximum bonding density in a cylindrical pore [36], which can be calculated as D/6 for the C18 bonded ligand. The calculated value for S-1-29 (pore diameter 72Å) according to this method yields a bonded layer thickness of 12Å, while the experimental value found the thickness to be 11.4Å. Likewise, the theoretical values for S-1-25 and S-2-36, both with 62Å diameter pores was 10.3Å while the experimentally determined value was 10.1Å and 10.2Å respectively. Both latter samples show remarkable comparison to the theoretical value, and interestingly enough, the S-1-29 sample showed a thickness significantly larger which

seems to correlate well with the larger pore size of this silica. These results confirm that the bonded ligands are in a rigid conformation on the surface of the silica. A plot of the experimentally calculated bonded layer height or thickness versus the theoretical height for the same length alkyl chains illustrates the arrangement of the C8 and C18 chains on the surface (figure 23) as compared to the theoretical values of the different bonded group heights. Also, very interesting is the fact that the calculated value for the molecular volume for both samples S-1-29 and S-2-36(C1 through C18) shows extremely close values to the molecular volumes given by ACD software (ACD Labs, Toronto Canada).

Table X shows the results of thermogravimetric analysis of modified spherical SBA-15 silicas. The weight loss plotted against the % Carbon from elemental analysis shows a straight line with the slope equal to the mass fraction of carbon in the ligand cleaved from the surface during heating (Figure 24). Table IX shows a comparison of bonding densities as calculated from the % Carbon and from the % weight loss from TGA. Sample S-2-36 shows close comparison in the C18 bonding density between both calculations with a 1.43 groups/nm^2 from the % weight loss data and 1.47 from the % carbon. Although not quite as close, both samples S-1-29 and S-1-25 show bonding densities calculated by % carbon roughly 0.2 groups/nm^2 higher than the value calculated using % weight loss. This discrepancy increases as the bonded ligands reduce in size and mass from C8 to C1. The reason for this is most likely associated with uncertainties of the weight loss for due to the trimethyl silyl group and possible errors in the weight loss calculation due to decomposition assumptions. Also, with C8 and even more so C18, the greater number of easily cleaved and accounted for methylene groups makes the % weight loss more accurate. At the low weights associated with C1 in combination with uncertainties due to the cleavage of the C1 group, the difference in bonding densities at the low level is understandable.

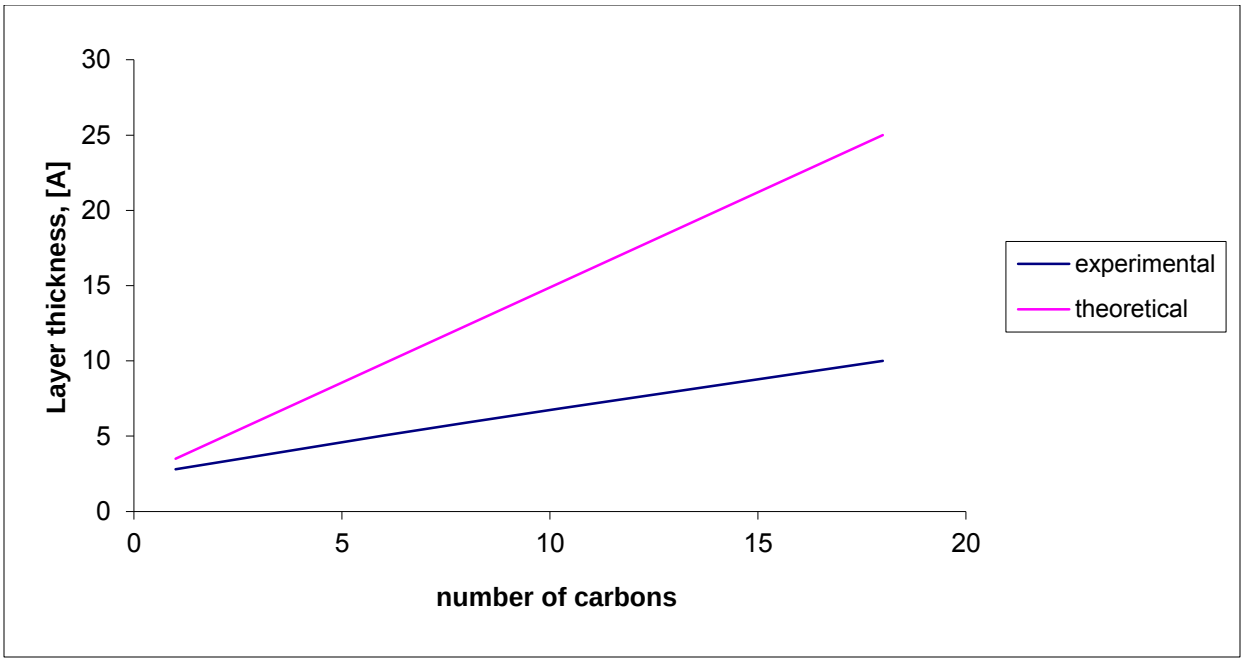

Figure 23. Plot of experimentally determined modified layer height versus theoretical

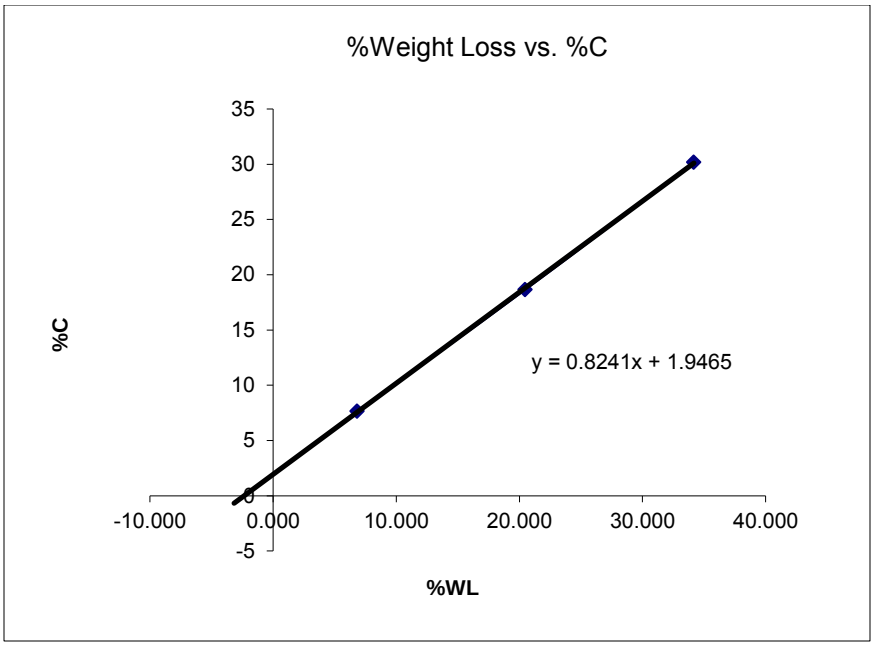

Figure 24. Plot of % Carbon versus %WL. The slope is equal to the fraction of carbon in the cleaved group. (theoretical is 0.85 for C8 and C18)

Table XI. Comparison of bonding densities from % carbon and % weight loss

Grafting density comparison		
silica	by %WL	by %C
S-1-25 C1	1.24	1.91
S-1-25 C8	1.37	1.61
S-1-25 C18	1.40	1.57
S-1-29 C1	1.55	2.26
S-1-29 C8	1.51	1.88
S-1-29 C18	1.68	1.87
S-2-36 C1	1.47	2.00
S-2-36 C8	1.44	1.65
S-2-36 C18	1.43	1.47

Table XII. TGA data

TGA DATA	Grafted Group	Weight C + H (g)	Carbon Weight (g)	weight frac carbon	TGA sample weight (mg)	Weight Loss (mg)	Weight loss due to C (mg)	% Loss	% Loss C due to C
S-1-25 C1	O-Si (CH3)3	45.11	36.03	0.80	9.105	0.621	0.496	6.818	5.446
S-1-25 C8	O-Si (CH3)2-C8H17	113.25	96.08	0.85	11.574	2.367	2.008	20.450	17.350
S-1-25 C18	O-Si (CH3)2-C18H37	253.55	216.18	0.85	12.343	4.218	3.596	34.170	29.137
S-1-29 C1	O-Si (CH3)3	45.11	36.03	0.80	7.771	0.586	0.468	7.540	6.022
S-1-29 C8	O-Si (CH3)2-C8H17	113.25	96.08	0.85	6.809	1.369	1.161	20.100	17.057
S-1-29 C18	O-Si (CH3)2-C18H37	253.55	216.18	0.85	9.197	3.280	2.797	35.670	30.407
S-2-36 C1	O-Si (CH3)3	45.11	36.03	0.80	13.622	1.105	0.883	8.109	6.479
S-2-36 C8	O-Si (CH3)2-C8H17	113.25	96.08	0.85	22.630	4.871	4.133	21.490	18.261
S-2-36 C18	O-Si (CH3)2-C18H37	253.55	216.18	0.85	24.159	8.451	7.205	34.980	29.825

4.4 Pore structure and Tortuosity

Upon modification of the spherical SBA-15 silicas with C1, C8, and C18, a significant deformation of the adsorption/desorption curves and shift of the hysteresis point to the potential blockage or variation in in radius of the pore after modification. However, this notion of uneven modified layer heights, or pore blockages is confusing since the results of the calculations for bonded layer thickness and molecular volume of the grafter ligand, and the good agreement across different samples, makes this a difficult question to answer. Figure 25 shows an overlay of the nitrogen isotherms for S-1-29 C1 through C18. From the shift in the hysteresis, determination of r_m over the P/Po of 0.6 to .45 by the Kelvin equation gives a change in radius from 25Å to 12Å. This roughly translates (without accounting for the thickness of the adsorbed nitrogen monolayer) to bonded layer heights ranging from 5Å to 12Å. Therefore it is reasonable that the modified layer shows variation in height, an effect that could be compounded in the presence of pore tortuosity. Possible evidence of this effect was observed in the thermogravimetric analysis of as-synthesized spherical SBA-15 (still with P123 in the porous space). The TGA profile for uncalcined samples show a strange dual processes for the loss of mass as the P123 and CTAB are burned off, as if one set of pores is easily accessible, followed by another set of pores slightly more difficult to access (figure 26). With a study of these materials in chromatography, this will be investigated in more depth as the ability of analytes and mobile phase to enter into the porous space can be measured.

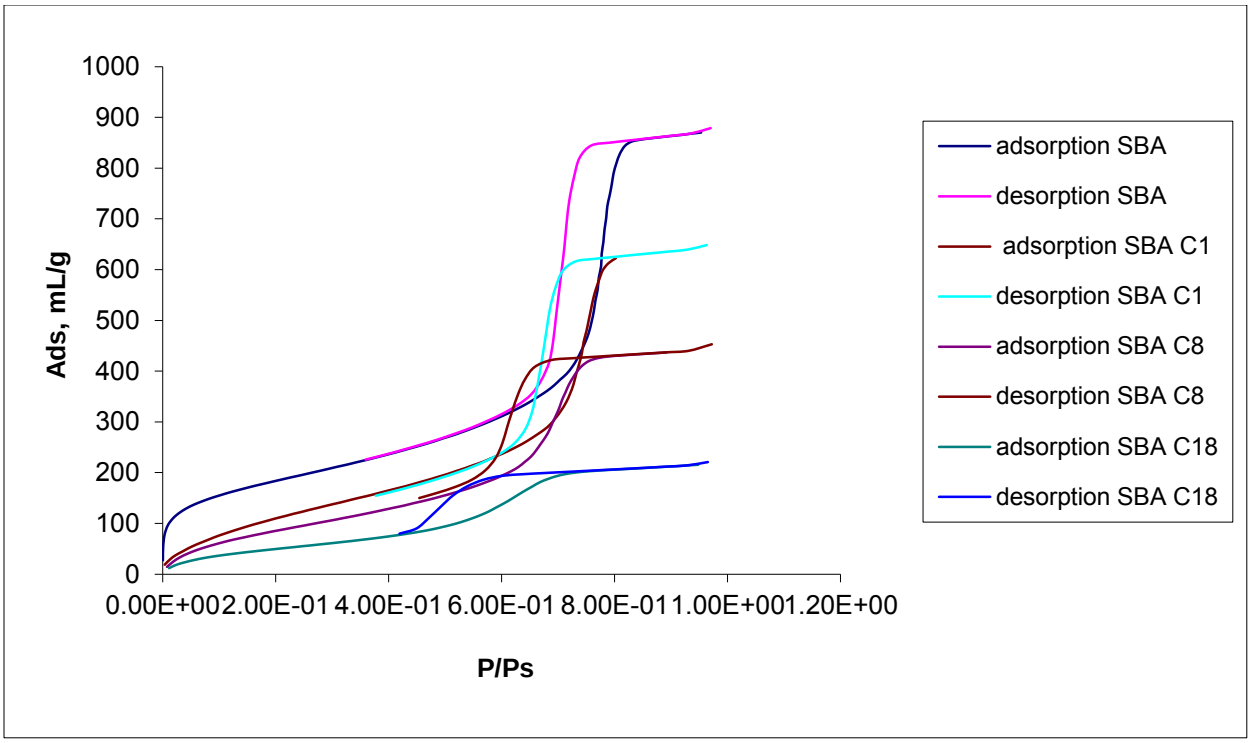

Figure 25. Overlay of nitrogen adsorption isotherms for S-1-29 (bare, C1-C18). Ideally, the hysteresis should get thinner and move slightly to the left, but it should not completely change shape. This is an indication there may be some sort of blockages inside the modified pores.

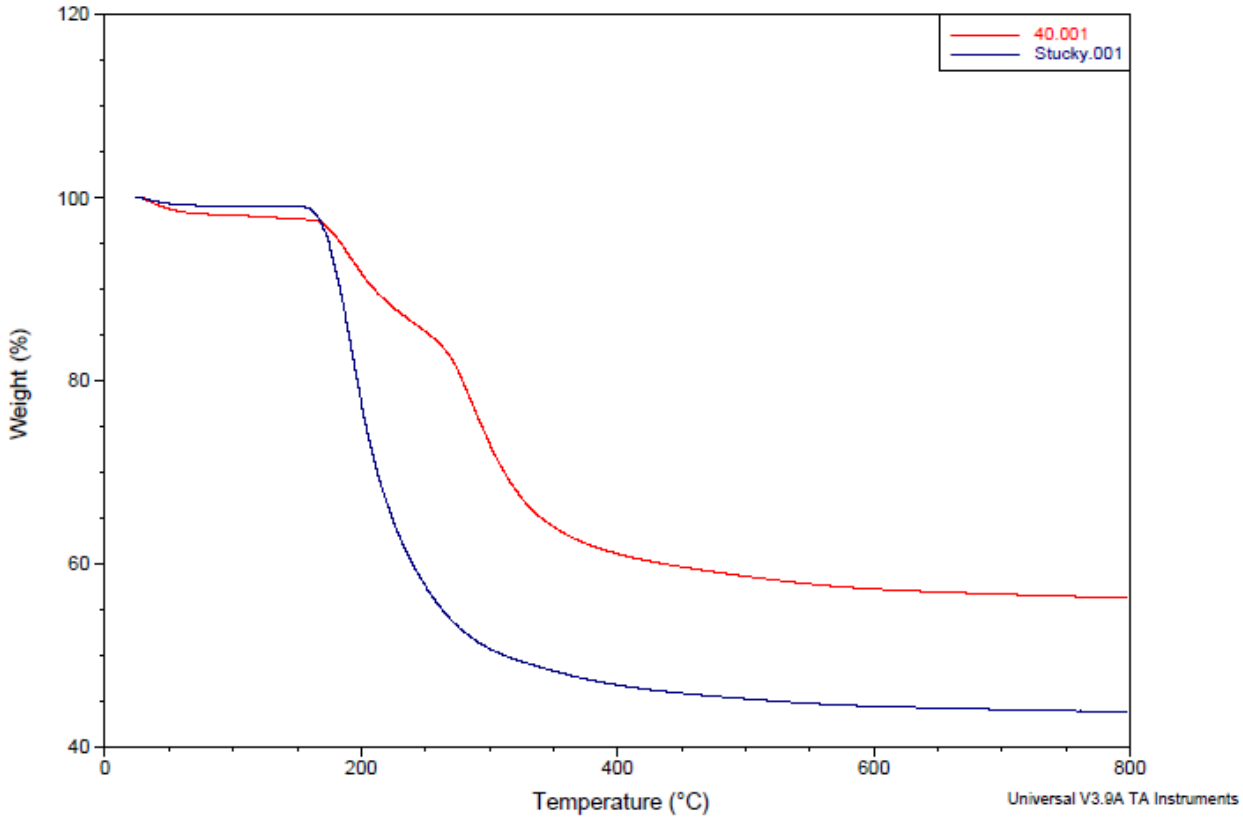

Figure 26. Comparison of TGA decomposition of P123 surfactant from the pores of spherical SBA-15 (red) and fibrous SBA-15 (blue). The weight loss curve for spherical SBA-15 shows a two-step process requiring greater energy for the decomposition of the surfactant from the pores. This comparison demonstrates the possible effect spherical morphology can have on the obstruction of the porous space in spherical SBA-15.

V. Conclusions

1. In the synthesis of spherical SBA-15 silicas, the effect of changing the initial ageing time was shown to decrease the size of the pores, as well as the pore size distribution, while increases to the duration of hydrothermal treatment produced a wider pore size distribution, but no significant change in pore size. In single ageing schemes, however, a change in the duration of ageing resulted in an increase in pore size.
2. Increases to the hydrothermal treatment temperatures produced increases in pore size and corresponding decreases in surface area. Conversely, any change to the initial ageing temperature resulted in a decrease in pore size and a loss of order as seen in the nitrogen isotherm.
3. The first ageing step has been shown +to be crucial for the synthesis of silica spheres while the hydrothermal treatment has been shown to be critical to the development of long range order in the pores.
4. An increase in pH was shown to increase the condensation rates of the silica species and allow for the synthesis to be tailored to produce spherical/spheroid particles with long range order.
5. As CTAB has been shown to be necessary for the formation of spherical particles, a decrease in the concentration of CTAB produced silicas exhibiting a greater extent of long range order.
6. The island-type coverage observed by modification with alkyl(dimethyl amino) silanes was confirmed with the near maximum bonding densities calculated for spherical SBA-15 silicas.

7. Calculations of the bonded layer thickness for modified silicas showed close comparison to theoretical predictions based on the assumption of uniform cylindrical pores and confirmed that the bonded layer exists in a rigid, liquid-like state on the surface of the silica.
8. Deformation of the hysteresis loop for modified spherical SBA-15 silicas in low temperature nitrogen adsorption, in combination with weight loss profile from thermogravimetric analysis of uncalcined silicas refers to cause by the presence of either pore obstruction or tortuosity.

6. References

1. C.T. Kresge, M.E. Leonowics, W.J. Poth, J.C. Vortulli, J.S Beck, Nature 359 (1992) 710.
2. T.C. Shen et al. Science 268 1590 (1995)
3. D. Zhao, Q. Huo, J. Feng, B. F. Chemelka, G. Stucky, J. Am. Chem. Soc. 1998, 120, 6024-6036.
4. D. Zhao et al. Science 279, 548 (1998)
5. M. Bruzzoniti, R. DeCarlo, S. Fiorilli, B. Onida, C. Sarzanini, J. Chrom A 1216 (2009) 5540-5547.
6. H. Wan, L. Liu, C. Li, X. Xue, X. Liang, J. Coll. Inter. Sci. 337 (2009) 420-426.
7. X. Liu, L. Li, Y. Du, Z. Gao, T. Ong, Y. Chen, S. Ng, Y. Yang, J Chrom A 1216 (2009) 7767-7773.
8. T. Yasmin, K. Muller, J Chrom A 1218 (2011) 6464-6475.
9. R. Tian et al., Electrophoresis 2006, 27, 742-748.
10. Y. Ma, L. Qi, J. Ma, Y. Wu, O. Liu, H. Cheng, Colloids and Surfaces A: Phys. Chem Eng. Aspects 229 (2003) 1-8.
11. J. Zhao, F. Gao, Y. Fu, W. Jin, P. Yang, D. Zhao, Chem Comm. 18 March 2002.
12. D. Zhao, J. Sun, Q. Li, G. Stucky, Chem. Mater. 2000, 12, 275-279.
13. A. Katiyar, S. Yadav, P.G. Smirniotis, N.G. Pinto, J Chrom A 1122 (2006)13-20.
14. J.D. Wright, N.A.J.M. Sommerdijk, Sol Gel Materials: Chemistry and Applications. CRC Press, FL 2001.
15. R. K. Iler. Chemistry of Silica. Wiley-Interscience. NY, 1979. Chp 3.
16. U. Brinkman, M. Ettlinger, D. Kerner, and R. Schmoll in Colloidal Silica Fundamentals and Principles. Synthetic Amorphous Silica. CRC Press, FL, 2006. Chp 43.

17. R. K. Iler. Chemistry of Silica. Wiley-Interscience. NY, 1979. Chp 5.

18. J. Rouquerol et al. Pure and Appl. Chem.,Vol.66, No. 8,pp. 1739-1758,1994.

19. P. Petrov et al. J. Phys. Chem. B 2008, 112, 8879-8883.

20. M. Monzen, T. Kawakatsu, M. Doi, R. Haseqawa. Computational and Theoretical Polymer Science 10 (2000) 275-280.

21. V. L. Zholobenko, A.Y.Khodakov, M.I.Clerc,D. Durand, I. Grillo, Adv. in Coll. Int. Sci.142 (2008) 67-74.

22. H.B. Chan, P.M. Budd, T. Naylor, J. Mater. Chem.,2001, 11, 951-957.

23. Z. Jin, X. Wang, X. Cui, Colloids and Surfaces A: Phys. Eng. Aspects 316 (2008) 27-36.

24. W.H. Zhang, L. Zhang, J. Xia, Z. Shen, Y. Li, P. Ying, C Li, Micropor. Mesopor Mater. 89 (2006) 179-186.

25. A.Y. Fadeev. Hydrophobic Monolayer Surfaces: Synthesis and Wettability. Encyc. of Surfaces and Colloid Sci. 2006

26. Y.V. Kazakevich, R. LoBrutto, HPLC for Pharmaceutical Scientists, Wiley-Interscience, NJ, 2007

27. S.M. Staroverov, A.Y. Fadeev. J. Chromatography 544 (1991) 77-98.

28. I. Rustamov, T. Farcas, F. Ahmed, F. Chan, R. LoBrutto, H.M. McNair, Y.V. Kazakevich, J Chrom A 913 (2001) 49-63

29. A.W. Adamson, A.P. Gast. Physical Chemistry of Surfaces. Wiley-Interscience, NY. 1997. chp. 17.

30. S.J. Gregg, K.S.W. Sing, Adsorption, Surface Area and Porosity. Academic Press, NY. 1982.

31. Y.V. Kazakevich, A.Y. Fadeev. Langmuir 2002, 18, 3117-3122.

32. A. Giaquinto, Z. Liu, A. Bach, Y.V. Kazakevich, Anal. Chem 2008 80 6358-6364

33. D. Amati, E. Kovats, Langmuir,3, 687 (1987).

34. D. Amati, E. Kovats, Langmuir 4, 329 (1988).

35. J. McElwee, R. Helmy, A. Y. Fadeev. J Colloid Int. Sci. 285 (2005) 551-556.

36. A.Y. Fadeev, S.M. Staroverov, J. Chromatography, 447 (1998) 103-166

PART II

Evaluation of Spherical SBA-15 in High Performance Liquid Chromatography:

Accessible Surface Area and Effects Pore Structure

1. Introduction

For more than thirty years there has been debate over the definitive mechanism and theoretical description of analyte retention in Reversed Phase HPLC [1]. It is commonly accepted, however, that retention should be due to adsorption of the analyte onto the stationary phase surface or to partitioning of the analyte between the layer of mobile phase and stationary phase, or a combination of both [2]. Whether adopting a model for the description of analyte retention as proportional to the stationary phase volume (partitioning) or adsorbent surface (adsorption), there is one constant: the characteristics and geometry of the stationary phase [1,3].

In modern liquid chromatography, porous silica particles are most commonly used as they possess large surface area with the ability to provide hydrophobic surfaces through chemical modification [4] and can be manufactured reproducibly with narrow particle size and pore size distributions [5,6]. As early as 1970, Kiselev wrote of the importance and relationship of the adsorbent geometry to retention and efficiency, and over the years the manufacture of silica has evolved to address the ever growing demand for chromatography to become more efficient, have faster analysis times, and have the ability to separate large complex biomolecules [7,8,9]. Thus, soon after the discovery of ordered mesoporous silicas in the early 1990's attention has been given to the ability of large pore (SBA-type) ordered silicas to act as an adsorbent in HPLC. Ordered silicas demonstrate the ability to possess large pore volume while maintaining high surface area and thus the ability to maintain significant separating power while the potential to reduce band broadening effects and increase efficiency with increased through flow [10,11]. The purpose of this study is to investigate the use of spherical SBA-15 type ordered mesoporous silica as a stationary phase in HPLC as well as to investigate the correlation between adsorbent geometry of ordered pores and their influence the retention process.

1.1 Chromatographic Theory

In order to discuss the evaluation of spherical SBA-type silica as a stationary phase in HPLC, it would be worthwhile to first briefly explore the theory behind chromatographic separation and the key descriptors we shall use to describe its phenomena.

Chromatographic separations are based on a forced transport of the liquid mobile phase which carries an analyte mixture through the stationary phase and the differences in analyte interactions with the surface of the stationary phase gives rise to different migration times [6]. The differences in migration times for each analyte can be plotted on the HPLC output chromatogram in the form of peaks. In the absence of strong analyte interactions with the stationary phase and while injected at low concentrations, the analyte peaks can be expected to be rather symmetrical and take on a normal, Gaussian, distribution [6]. The distance from the time of injection to the peak maximum, in units of time, is called the retention time ($\boldsymbol{t_R}$)[6]. The retention time is dependent on the mobile phase volumetric flow rate, as well as the pump stability, therefore to avoid these dependencies as well as to provide a more universal descriptor, we can define the retention volume, V_R, as the product of the flow rate, F, and retention time:

$$V_R = t_R \cdot \mathrm{F} \qquad (1)$$

The retention volume is the amount of mobile phase, in mL, that is required to pass through the column before the elution of the analyte [6].

Assuming there are no interactions of the analyte with the stationary phase, a certain amount of time must still pass before the analyte reaches the detector. This amount of time is known as the dead time and it is the amount of time it takes an unretained component to get from the injector to the detector. The dead time can be related to volume by:

$$V_O = t_O \cdot \mathrm{F} \qquad (2)$$

where V_0 is the void volume. There has been considerable debate [12] over the correct definition and procedure to determine the void volume, however for the purpose of this study we shall define the void volume as the volume of liquid phase present in the column as measured by the injections of a deuterated component of the eluent.

Analyte retention consists of the analyte's time traveling through the column in the mobile phase plus the time it spends retained on the stationary phase surface [6]. The ratio of the difference between the total retention time and the dead time (known as the reduced retention time) to the dead time is a dimensionless parameter known as the retention factor.

$$k = \frac{V_R - V_O}{V_O} = \frac{t_R - t_O}{t_O} \qquad (3)$$

The retention factor describes the ratio of the time the analyte spends on the surface to the time spent in the mobile phase. The retention factor is a routinely used, convenient parameter for comparing properties of different columns [13] and as such is traditionally used to represent retention in HPLC [14].

Chromatography basically involves separation due to differences in the equilibrium distribution of sample components between the stationary and mobile phases [15]. As a rough approximation, the equilibrium constant of the process is proportional to the analyte retention factor [6].

$$K \propto k \qquad (4)$$

Thermodynamically, the equilibrium constant can be described as the exponent of the Gibbs free energy of the analyte's competitive interactions with the stationary phase [15]. In liquid

chromatography, the analyte competes with the eluent for a place on the stationary phase surface and as such the resulting analyte retention can be described as the difference between the analyte and eluent interactions with the stationary phase [6].

$$K = \exp\left(\frac{\Delta G_{analyte} - \Delta G_{eluent}}{RT}\right) \qquad (5)$$

With higher concentrations of organic modifier in the mobile phase the stronger the interactions of the eluent with the stationary phase which leads to a lower difference in Gibbs free energies and a lower analyte retention [6].

Selectivity is defined as the ratio of the retention factors of two analytes and describes the ability of the chromatographic system to discriminate between them [6].

$$\alpha = \frac{k_2}{k_1} = \frac{t_{R2} - t_O}{t_{R1} - t_O} \qquad (6)$$

Fundamentally, selectivity is equal to the ratio of equilibrium distribution coefficients for two components and, in effect, is a measure of the thermodynamic differences in their distribution [15]. By applying equations (4) and (5) to equation (6):

$$\alpha = \exp\left(\frac{\Delta G_{analyte,2} - \Delta G_{analyte,1}}{RT}\right) \qquad (7)$$

The selectivity relates to the differences in the interactions of the two components [15] and, ideally, is independent of the eluent interactions with the stationary phase [6].

Thus far, the chromatographic phenomena described have been concerned primarily with thermodynamic aspects i.e., retention time, retention factor, and the ratio of retention factors as well as the relation of the retention factor to the thermodynamic equilibrium constant. However, to provide a complete picture of the chromatographic process, a description of the kinetic aspect

should be described. As an injection of sample travels through the column, the interactions of the sample with the stationary phase is determined by the thermodynamic factors while kinetic factors, such as diffusion, are responsible for band broadening [16]. For example, to look at a peak on a chromatogram, the retention time and peak position is a function of thermodynamic factors, while the width of the peak is more a function of the kinetic aspect [6]. In order to understand and quantify the processes of equilibria as an analyte travels through the column, early chromatographers described them as a discontinuous string of plates on which these equilibria took place [16]. The efficiency of a column arises from this concept and can be described as the number of plates (N) a column possess. The classical equation

$$N = 16\left(\frac{t_R}{\omega}\right)^2 \qquad (8)$$

which, assuming a Gaussian peak distribution, relates the retention of a peak to its width at the baseline [17] (Figure 27). The peak variance, σ, is proportional to the diffusion coefficient [18]:

$$D = \frac{\sigma^2}{2t} \qquad (9)$$

While relating the peak width to the kinetic aspect of diffusion, it is interesting to this study to review a description of the relation of pore structure and particle size given by Guiochon in ref [16]. The plate number, N, is considered the ratio of the retention time and the time needed to achieve one equilibrium (τ_e).

$$N = \frac{t_R}{\tau_e} \qquad (10)$$

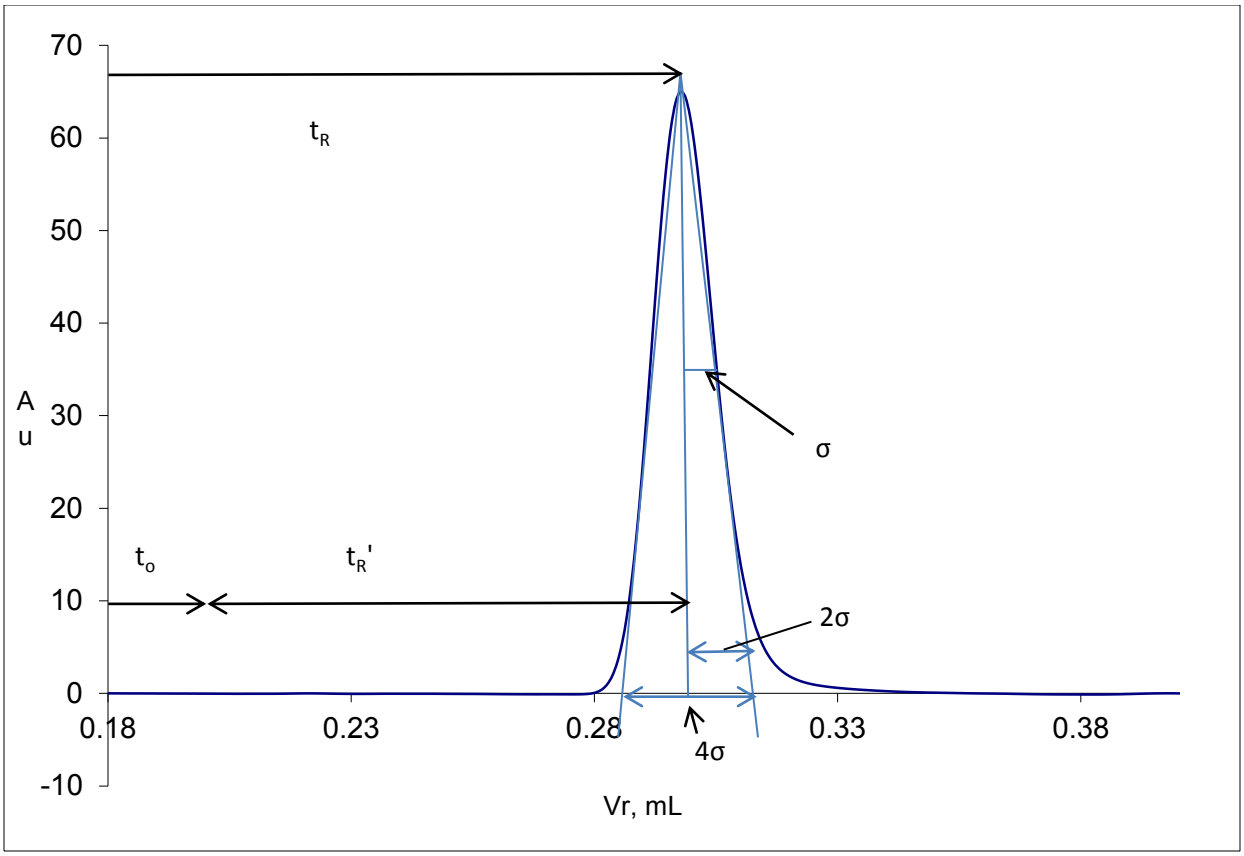

Figure 27. Chromatogram displaying retention time t_R, dead time t_o, reduced retention time t_R' And the peak variance, σ.

The problem, however, is defining and calculating τ_e. An estimate can be defined from Fick's law which states that the time to achieve equilibrium between the center of a sphere and the solution surrounding it is proportional to d_p^2/D_m. Combining with equation (10):

$$N \propto \frac{D_p}{d_p^2} t_R \qquad (11)$$

D_p is the pore diffusion coefficient which includes the contributions of the diffusion coefficients in the mobile phase and inside the particles, the hindrance coefficients due to tortuosity and the constriction of the pore network and surface diffusion. Improving the pore structure and pore network inside the particles can lead to increased column efficiency [16].

In chromatography, column efficiency is traditionally measured by the plate height as well as the dimensionless plate number [18]. The plate height, H, can be defined as the variance per unit length (σ^2 = HL) [19]. There have been many equations introduced which relate the height of each plate to column properties and operational variables [19] and all are based on the additive incremental variances arising from various contributions to band spreading:

$$H = A + \frac{B}{u} + Cu \qquad (12)$$

The simplified Van Deemter equation relating the contributions to the plate height arising from 1) maldistribution of flow in the packed column (term A), 2) band spreading due to diffusion of the sample component (B term) and 3) the resistance to mass transfer (C term). In columns packed with porous particles, the C term is largely determined by the slowness of intraparticle mass transfer[19]. A plot of *H* versus *u* is often referred to as a Van Deemter plot, in which each of the three terms above represents a contribution to the broadening of a peak.

The A term is independent of the mobile phase linear velocity and describes the broadening that occurs due to the multiple possible paths of flow in the column bed [6]. Since the paths are of different lengths, analyte molecules will travel different distances depending on the paths they take through the column, ultimately leading to an increase of the peak width. The A term is proportional to the particle diameter and its magnitude is directly proportional to the packing structure of the column ($A=\lambda d_p$) [6].

The B term is related to the diffusion of the analyte in the mobile phase and describes the broadening due to axial molecular diffusion and is inversely proportional to the linear velocity [26]. It is also related to the tortuosity of the packing material which accounts for the obstruction the packing presents to diffusion ($B=2\gamma D_m$) [15].

Finally, the C term represents the resistance to mass transfer and is an agglomeration of all broadening that becomes greater with increasing flows. Generally speaking, the C term is related to the diffusion coefficient of the analyte in the medium through which mass transfer is taking place and is directly proportional to the distance over which diffusion is occurring ($C \propto d^2/D$) [6].

1.2 Retention Mechanism and Surface Specific Retention Factor

Representation of HPLC retention is traditionally based on the retention factor [14] which can be equated to the thermodynamic equilibrium constant [6]. Retention factor is routinely used to compare retention properties between different columns [13]. However, the relation of the equilibrium constant to the retention factor is dependent on the model that is selected to describe the retention process [20]. As this research pertains primarily to porous silica chemically modified with aminoalkylsilanes, the following discussion is devised keeping in mind the nature of the stationary phase as seen in reversed phase HPLC.

There have been numerous publications that investigate the inherent difference between adopting either a partitioning or adsorption model of the retention mechanism [1-2,5,21-22]. In the partition model, the analyte distribution takes place into the stationary phase volume [8,21]. However, in the adsorption model, the analyte interacts with the surface of the bonded layer, which is considered to be rigid and not penetrable by the analyte molecule [5]. Mathematically, both models describe analyte retention in a very similar form [1]:

$$V_R = V_m + V_s \frac{dc_s(c)}{dc} \quad \text{partitioning (13)}$$

$$V_R = V_O + S \frac{d\Gamma(c)}{dc} \quad \text{adsorption (14)}$$

where V_m is the volume of the mobile phase, V_s is the volume of the stationary phase, V_o is the volume of the liquid inside the column and S is the total surface area in the column. Equation (13) states that the reduced retention is proportional to the volume of the stationary phase, while the equation (14) indicates that the reduced retention is proportional to the adsorbent surface area [20]. The partitioning view requires a view of the stationary phase that views the modified alkyl

layer as penetrable and solvated by organic eluent [5,8,21-22] and the void volume will ultimately include the volume of the stationary phase [5,21]. On the other hand, the adsorption model view of HPLC retention mechanism allows a view of the column void volume as the total volume of liquid inside the column as well as requires the use of surface specific retention factors [6].

The idea of using surface specific retention was introduced by Kiselev [7] and later advocated by Kovats [24]. As seen in equation (14), the reduced retention is proportional to the adsorbent surface area, therefore using surface specific retention factors provides a more meaningful parameter by which to compare different columns with similar surface chemistry [20]. The surface specific retention factor can be calculated by:

$$k_s = \frac{V_R - V_O}{S_{tot}} \qquad (15)$$

where V_R is the analyte retention volume, V_0 is the column void volume, and S_{tot} is the total surface area of the adsorbent in the column. Thus, the use of surface specific retention factor requires the mass of adsorbent inside the column as well as the specific surface area of the adsorbent. A more detailed discussion of the methods used to determine the mass of adsorbent inside the column as well as its surface area will be given in Chapter 3 Experimental Methods of Characterization.

1.3 Porous Silica In HPLC

Since its inception, the development of HPLC goes hand-in-hand with the ever present drive to create more efficient stationary phases. In fact, the decision of Horvath to use porous layer beads in order to facilitate better mass transfer of molecules in liquid chromatography necessitated the need to create a system able to produce the required pressures dictated by the new stationary phase, and High Pressure or High Performance Liquid Chromatography was born [6]. Since then an orchestrated dance between column manufacturers and HPLC system manufactures has played out as each one works to develop more efficient ways to perform chromatography. In an attempt to answer industry demands forced upon them from regulatory and economic origins to produce better and faster separations, researchers are constantly trying to produce new strategies in chromatography – one of these being the advancement of stationary phases to increase efficiency and separation by tailoring its physical and or chemical aspects [9,24-26].

Porous silica has remained one of the most widely used stationary phase for over 30 years, in addition to its chromatographic friendly physio-chemical characteristics, precisely because it has been studied for over two centuries and its synthesis is fairly well understood and reproducible [6,27]. The ability to be synthesized in particles of a wide variety of sizes and shapes with different configurations of pore structures is an inherent advantage of silica as a column packing [25]. In addition to this, the ability to easily chemically modify the silica surface with a variety of stable organic bonded phases has been a key factor in the development of silica as a stationary phase [28]. Although there are many important characteristics of silica that are noteworthy for any description of its use as a stationary phase, for the purposes of this study we shall focus on the importance of the geometric characteristics of HPLC silica and it influence to retention and the retention process.

1.3.1 Geometry

In order to evaluate the influence of silica surface area and pore structure on the thermodynamic and kinetic aspects of the retention process, we will briefly examine the geometric relationship between surface area, pore volume and pore size. We will then examine pertinent research on the influence of stationary pore structure on the retention process as this will provide the basis of comparison to the evaluation of the ordered porous silica performance. First, however we will look at the effects particle size and shape can have on the performance of an HPLC column.

1.3.1.1 Particle Morphology and Size

The first silicas used in liquid chromatography were made prom large particles, milled to size from tech-grade xero-gels to obtain 5-10 µm particles which were irregular in shape. From the sides of these irregular particles, "fines" would be attached and eventually dislodge during use in the analytical column, eventually clogging the frit and producing larger than expected back pressure [26]. From this time attention has been put into making particles without milling techniques and in the late 60's into the 70's the development of spherical silicas of about 5-10 µm were being developed [29]. Although the debate between the use irregular and spherical particles still exists today, spherical particles from about 3-5µm are the most common used today [9]. The use of spherical particles has been shown to increase efficiency [6]. Most critical is the absence of fine particle ($\leq$ 0.5µm) which will clog the frit of the column [6,26].

The size of the particle has been shown to have an effect on the pressure drop along the column with smaller particles producing higher back-pressures [6]. The distribution of particle will not affect the chemical behavior of the stationary phase [6], and although a correlation between particle size and quality of packing has been shown [31], the efficiency of the column is not affected by a wide particle size distribution so long as the optimum flow rate is being used [32]. Particle roughness, though, can be a factor to column efficiency as it has been shown that the external roughness of the particles can contribute to a increased resistance to mass transfer [33].

1.3.1.2 Surface Area

Surface area is directly proportional to the surface area as can be seen with a variation of equation 14:

$$V_R = V_0 + SK_H \qquad (16)$$

where K_H is the henry adsorption constant. Although the surface area of a adsorbent is the most important characteristic in the retention of a compound, it is practically ignored in the everyday use of chromatography [6]. In fact, it has been shown that minor fluctuations in the physical characteristics of the base silica can have an effect on the performance of the material as a stationary phase [34].

As a high surface are is desirable for a stationary phase, it is the porous nature of most silica adsorbents which gives it its high surface area. Therefore, it is necessary to consider the size and structure of the pores and their geometric relation to surface area. Assuming cylindrical pores

and using the formulas for the surface of a cylinder ($S = 2\pi RL$) and the volume of a cylinder ($V = \pi R^2 L$), the following geometric relationship can be obtained:

$$\frac{S}{V} = \frac{2}{R} \qquad (17)$$

The surface are is inversely proportional to pore size and pore volume while pore size and pore volume are directly proportional. So, in porous silica a very high surface area is usually associated with a small pore diameter and by increasing pore diameter, a sacrifice to the surface area must be made. Hence, in HPLC, the pore size becomes a critical parameter to the accessible surface area that can be seen by the analyte molecule [6,35]. This fact brings up the issue of determining the surface area. Since surface area is determined by Low Temperature Nitrogen Adsorption (LTNA) in which the probe molecule is the very small N_2 molecule, the actual surface that can be seen by a much larger analyte molecule may be significantly smaller [6,35]. See Figure 28 for an example of how surface area, pore volume and pore size is determined through LTNA. A detailed description of the methods involving porous silica characterization by LTNA is given in the Part 1 of this thesis: *Synthesis and Characterization of spherical mesoporous SBA-type Ordered Silica*.

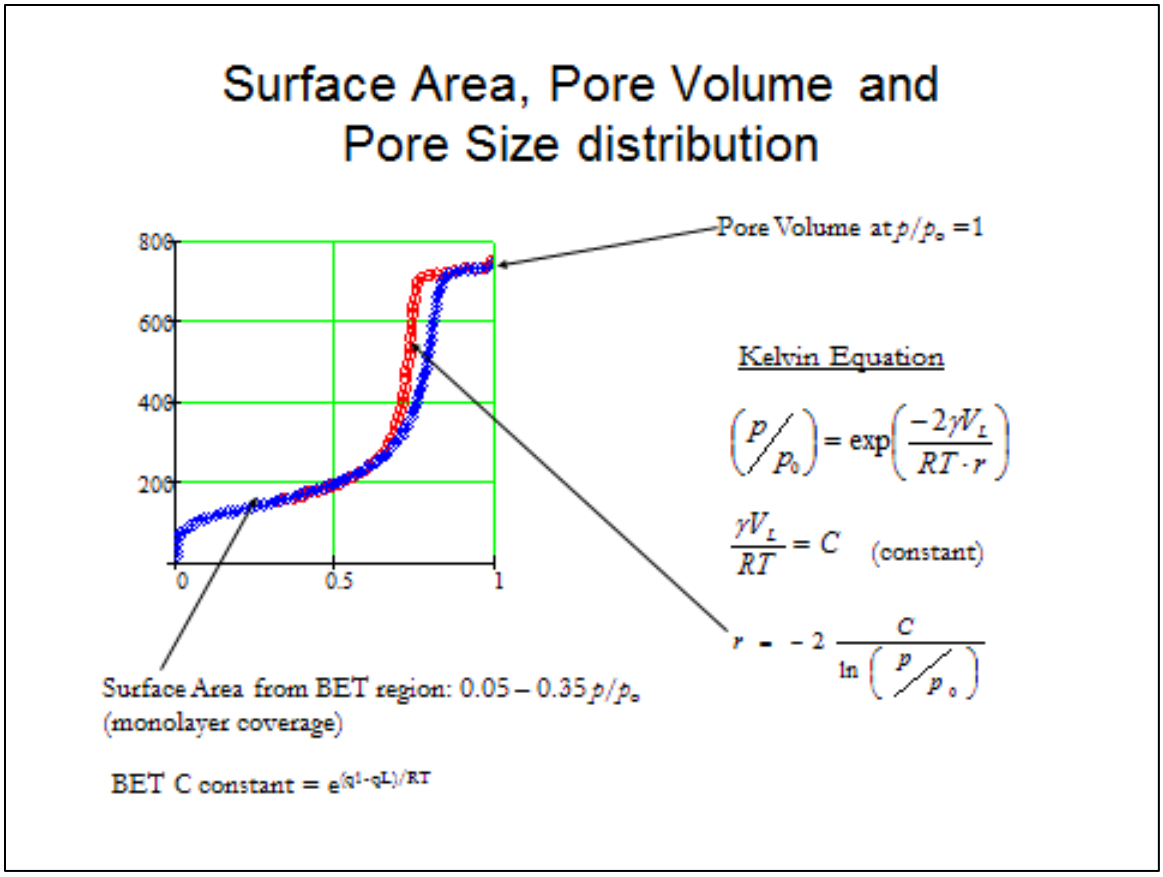

Figure 28. Low Temperature Adsorption Nitrogen Isotherm of a porous silica sample and description of the how pore volume, pore size and BET surface area are calculated

1.3.1.3 Pore Structure

Pore structure is characterized by pore size, pore size distribution, pore connectivity and the degree of randomness of the spatial distribution of the pores [42]. As stated above, the size of the pore will have an effect on the surface area available depending on the size of the analyte molecule [6,35]. Also, the presence of micropores can result in a large discrepancy between the surface area as determined by nitrogen adsorption versus that as seen by an analyte in HPLC [6]. Generally speaking, to be suitable as a stationary phase in HPLC, an adsorbent should have an average pore size of around 50Å [6].

As previously discussed, pore structure can have an effect on analyte retention through relationship of pore size to surface area. In addition to this, pore structure can also have an effect on kinetic aspects of the retention process. The volume of liquid inside the analytical column consists of both the volume of the liquid inside the porous particles (pore volume, v_p) and the volume of liquid in the interparticle space in between silica particles (interparticle volume, v_{ip}) (Figure 29).

$$V_0 = V_p + V_{ip} \qquad (18)$$

It is widely believed that the liquid/mobile phase inside the pores (v_p) is stagnant and that there is no active flow inside the pores and migration of an analyte molecule through the pores is only achieved by way of diffusion [15,36-39]. The diffusion of an analyte molecule through the porous network inside the silica particle is described by the diffusion coefficient. The diffusion coefficient of a mobile phase traveling in an open tube depends on the solvent, temperature and analyte properties [39]. For an analyte traveling through a column packed with porous non-

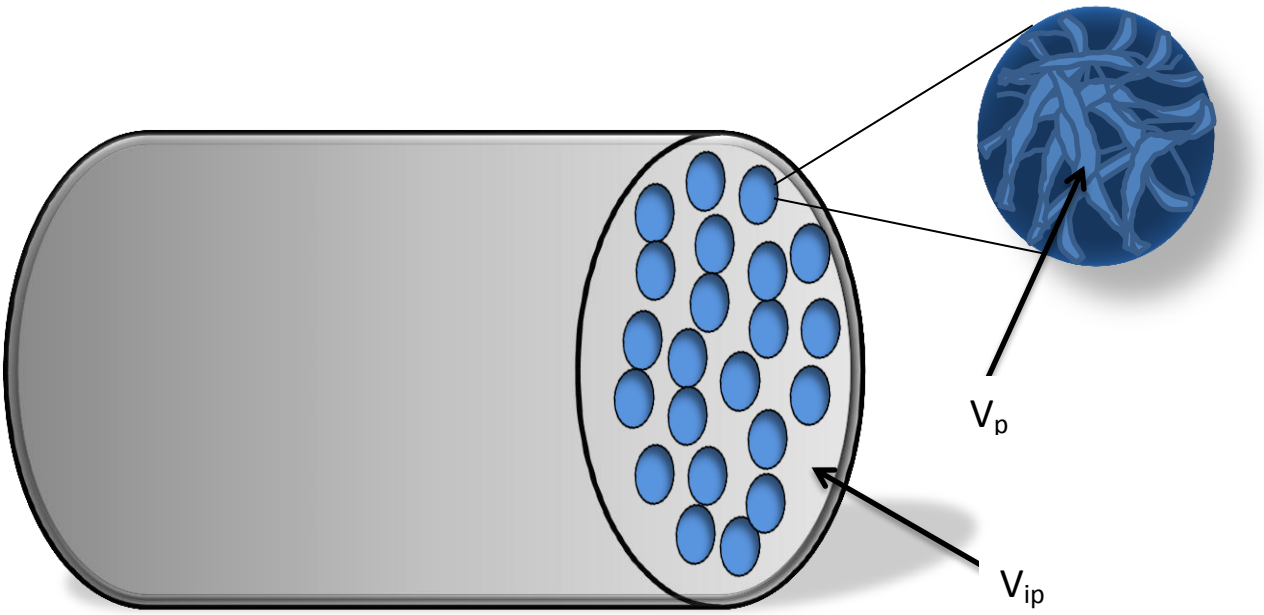

Figure 29. Cross section of an analytical column portraying the pore volume arising from interconnected, intraparticle pores within the particles (V_p) as well as the interparticle pore volume (V_{ip}) from the spaces in-between the particles columns inside the column.

interacting particles, both tortuosity and constriction cause the diffusion coefficient to appear smaller [39]. The obstruction parameter is defined as the ratio of the coefficients of the effective diffusion in the porous medium to the diffusion of the molecule in the solvent and is a measure of the tortuosity of the packed column:

$$\gamma = \frac{D_{eff}}{D_m} \qquad (20)$$

The main sources of mass transfer resistance arise from 1) radial and eddy diffusion, 2) external film mass transfer, 3) intraparticle diffusion, and 4) kinetics of adsorption/desorption [36]. Of these, the first two are fairly well understood and the fourth is "fast" and considered negligible [36]. Intraparticle diffusion itself is due to a combination of pore diffusion in the stagnant solution filling the pores and possible surface diffusion or diffusion in the adsorbed layer on the surface [36]. However, according to Miyabe et. al, it is difficult to measure the exact effects of pore tortuosity versus pore connectivity, especially in the more exotic silica substrates such as silica monoliths, and many must rely on computer modeling to define the effects of pore structure on diffusion [40]. Gritti and Guichon define pore connectivity as that which describes the average number of possible paths for a molecule to move from one side of a particle to the other [41]. Tortuosity, on the other hand, is defined as the ratio between the average length of the path of a fluid that percolates through the porous medium to the length of the imaginary straight path [41]. They also explain that there is external and internal tortuosity relating to the paths through the column and those through the particle [41]. Further, they explain that although surface diffusion was recognized by Giddings, it remains ignored by chromatographers today and that tortuosity and constriction of the pores in silica may effect and inhibit surface diffusion [49].

Pore interconnectivity and tortuosity are elusive parameters, not readily measured and so simulations are usually employed to quantify their effect [40,41]. For example, Liapis et al have conducted many simulation employing Monte Carlo simulations on the measurement and effect of pore connectivity on analyte diffusion and column efficiency [42-47]. Generally speaking, they have found that with an increase on pore interconnectivity the intraparticle diffusion coefficient will increase and resistance to mass transfer decrease. Therefore it is desirable to have a stationary phase with high interconnectivity [42].

Many studies have been undertaken to measure the effective diffusion of an analyte through porous media and its influence on mass transfer [48-56]. Miyabe and Guichon have shown that the effective diffusion coefficient can be directly measured by relating the peak variance, σ, to the time in peak parking experiments. By stopping the flow for given amounts of time and plotting the peak variance as a function of parking time the effective diffusion is obtainable[53,55]:

$$\sigma_x^2 = 2D_{eff} \cdot t_{park} \qquad (21)$$

The effective diffusion coefficient has been shown to be directly proportional to the size of the pores in a porous stationary phase, increasing with increasing pores size, and similarly decreasing as the molecules size approaches that of the pore [54]. Although computer simulations have reported on the effect of interconnectivity on the diffusion of analytes through porous media, it is still a difficult relationship to define as the interconnectivity and tortuosity are parameters usually unknown and practically impossible to anticipate [41,56].

1.4 Ordered Silica in High Performance Liquid Chromatography

Over the last decade and a half, ordered mesoporous silicates have gathered much attention for their potential uses in the fields of drug delivery, adsorption and separation [59]. Discovered in 1992, Mobile Oil introduced surfactant template silica in the form of MCM-41 [57]. MCM-41 ordered silica is characterized by a very high surface area (roughly 1000 m^2/g) and highly ordered pores. Much effort was made to use MCM-41 in chromatography with hopes to utilize the very high surface area [10], however due to their small pore size and pore walls MCM-41 was found to be unsuitable as a packing material for HPLC [26]. Throughout the next decade a broad spectrum of other mesoporous material was discovered and in 1998, Stucky and Zhao reported on the synthesis of SBA-15 mesoporous silica using tri-block copolymers as a structure directing agent with the ability to exhibit large pore sizes (in the hundreds of angstroms) while maintaining pore wall thickness [58].

In 2002, Zhao et al. reported on the use of large pore SBA-15 as a stationary phase in biomolecule separations [10]. With its tunable pore size (up to 50nm) and high surface area, they concluded SBA-15 synthesized with 80Å pores and modified with octyldecyl organosilanes made a promising chromatographic substrate for protein/peptide separation. The following year, Y. Ma et al. reported on the synthesis of large pore SBA-15, with 5µm particles and 80Å pores, and evaluation in HPLC with the separation of naphthalene, biphenyl, and diphenanthrene [58].

The next three years saw resurgence in the attempts at using MCM-41 type silica in chromatography, this time utilizing pseudomorphic synthesis techniques in which pre-existing porous spheres are partly dissolved and preformed into mesostructured materials. These studies reported questionable gains in the thermodynamic performance of the substrates (greater

retention) as well as apparent reductions in the resistance to mass transfer [59-61]. In 2006, submicrometer SBA-15 spheres with 120Å pores were used in capillary electrophoresis chromatography with the high speed separation of neutral compounds [62]. However, an unexpected high resistance to mass transfer observed in the evaluation was attributed to the existence of pore structure [62]. Also in 2006, phenyltrimethoxysilane co-condensed SBA-15 type silica spheres with 40Å diameter pores and stability to high pH was shown to have comparable chromatography with commercial columns of similar phase [63].

The next few years saw little activity in the investigation of ordered silica spheres in HPLC. In 2009, Bruzzoniti et al. produced a study of SBA-15 mesoporous silica for use in ion chromatography in the separation of alkali, alkali earths, ammonium, and transition metal ions [64]. Spherical SBA-15 was also synthesized with roughly 200Å pores for the separation of large biomolecules [65] as well as small sub-micrometer particles for use in µHPLC [66]. Most recently in 2011, spherical SBA-15 was synthesized with roughly 2µm particles and 90Å pores for use in HPLC in which various alkyl chain lengths with and without endcapping were assessed [67]. Finally, a study on a spray drying technique for the synthesis of MCM-41 type ordered silica boasted the doubling of retention as compared to commercial HPLC silica columns [68].

In conclusion, the studies so far, especially on SBA-15 materials in HPLC have not had a rigorous evaluation in HPLC and have not attempted to relate the unique pore structure of SBA-15 to the retention process. Several references have related observed results in terms of mass transfer hindrance and greater retention to the physical properties of SBA-15, however, in the case of retention, most if not all, of their hypotheses are based on erroneous uses of comparing retention.

II. Scope of Research

SBA-15 ordered mesoporous silica offers some interesting possibilities for the study of analyte retention in high performance liquid chromatography. SBA-15 exhibits a unique pore arrangement of hexagonally non-intersecting parallel pores with a 1000:1 aspect ratio of pore length to pore diameter. In addition to this characteristic, SBA-15 silicas possess large surface areas typically ranging from 500 to 800 m^2/g. Whereas most silicas displaying large pore size typically show a low surface area, an attractive feature of SBA ordered silicas to chromatographers is the ability to tune pore size while maintaining a high surface area as compared to most HPLC silica gels. This makes SBA-15 a good candidate for the separation of large peptide and biomolecules. However, in the decade since its inception however, chromatographic studies on the practical use of SBA-15 as a stationary phase have failed to convincingly show the benefits of using SBA-15 over available commercial silicas [63-67]. In the author's opinion, many of these studies lack rigorous evaluation of SBA-15's performance in terms of increased retention or other kinetic benefits. In this work, we attempt to provide an unbiased and rigorous study of the performance of SBA-15 providing comparison with commercial silica gels on the basis of an evaluation of surface specific retention.

Moreover, the main objective of this study was not to provide practical applications for the use of SBA-15 as a stationary phase, but rather to evaluate the overall effect the unique pore structure has on the retention process. The pore structure of SBA-15 offers several interesting possibilities for the study of retention. Primarily, the correlation of any retention parameter to the structure of the porous silica employed is usually accompanied with the necessary assumption that the pores are cylindrical. With SBA-15, we now have a stationary phase that

exhibits the cylindrical pores structure that so many assumptions are based off. With a comparison to commercial silica stationary phases (silica gel) we have the opportunity to investigate how the structure of the stationary phase will affect the retention process and specifically what role the porous structure may play. At the heart of this is the question of pore flow. According to theory, the mobile phase inside the pore volume is stagnant and analyte migration in the pores is solely regulated by diffusional effects. However, there is no direct evidence that there is no flow inside of the pores.

In this study we will attempt to investigate the role of pore structure and geometry as it relates to chromatographic behavior. Columns packed with spherical SBA-15 silica were fully characterized for physical properties such as void volume and interparticle volume. The effect of flow rate on retention (down to 2-5 μL/min) will be assessed to investigate diffusional effects and the possible presence of convective mobile phase inside of the pores. Retention will also be compared against commercial silica gel by evaluating the hydrophobic selectivity across the range of mobile phase organic modifier. By using the calculated and or determined mass of the absorbent in the columns, we will calculate surface specific retention factors for the basis of comparisons across columns. Using this method and knowing the physical characteristics of the SBA-15 silica from nitrogen adsorption data, we will be able to calculate the accessible surface area.

III. Experimental

3.1 Experimental Design

To investigate the effect of the porous structure of spherical SBA-15 silica on the retention process we will be investigating the effect of flow rate on retention and peak shape, the hydrophobic selectivity compared to commercial silica as well as the comparison of surface specific retention factors. These analyses required complete characterization of SBA-15 packed HPLC columns and of the SBA-15 materials themselves as well as the commercial silica gel being used for comparison.

A. The following adsorbent properties were measured:

    1. Surface area

    2. Pore size and Pore size distribution

    3. Particle size

B. SBA-15 with and without C8 modification were packed into stainless steel columns following sedimentation to remove fine particles.

C. Columns packed with adsorbents were characterized for the following properties:

    1. Column void volume

    2. Column interparticle volume

    3. Mass of adsorbent inside the column

D. The effect of analyte retention as a function of flow rate was measured on columns packed with SBA-15 material. SBA-15 adsorbents with and without modification with C8 as well as a commercially available silica gel were analyzed.

E. The Hydrophobic selectivties of SBA-15 silicas modified with C8 were compared to a commercially available silica gel. Hydrophibic or methylene selectivity was performed by measuring the retention of a series of alkylbenzenes using mobile phases from 100% to 0% acetonitrile in water as well as 100% to 0% methanol in water.

The methodology and data obtained as described in part A. above (low temperature nitrogen adsorption) were discussed in detail in the first part of this dissertation: *Synthesis and Modification of Spherical SBA-15 Ordered Mesoporous Silica*. A description of the method utilized in packing the adsorbents into columns, the method to determine methylene selectivity as well as the methods used in column characterization: void volume by deuterated component and SEC chromatography will be discussed below.

3.2 HPLC

3.2.1 Systems

Chromatographic retention of probe analytes were performed on an Agilent model 1100 system (Agilent, New Castle, DE) with a diode array detector. Determinations of interparticle volume by size exclusion chromatography were performed on a Agilent model 1050 system with UV detection. Column void volumes were measured on an Agilent model 1050 system equipped

with a 3900E analog interface, and a PE LC-30 refractive index detector (Perkin Elmer, Wellesley, MA) . All three systems utilized chemstation software.

The dead volume of all three systems was evaluated by removing any column and connecting lines with a zero volume connector and measuring the retention volume of the analyte being used.

The 1100 Agilent system was checked for pump stability and accuracy by pumping 1.0mL/min and 0.1mL/min for 50 and 50 minutes respectively with water and measuring the weight of delivered liquid to determine volume delivered.

3.2.2 Methodology

All runs were performed in isocratic mode. Analyses were carried out with analyte concentrations producing a signal to noise ratio from roughly 10 to 30 signal to noise untis. Columns were cleaned after each set of measurements by cyclic flushes of water and acetonitrile for 1 minute each and 10 min equilibration at the next eluent composition.

3.2.3 Experimental Conditions

In the flow rate study, retention was measured on packed SBA-15 columns along with a commercially available column using Acetonitrile/water (60:40 v/v) or Methanol/Water (70:30 v/v) at varying flow rates from 2.0 mL/min to 0.002 mL/min.

Methylene selectivity was measured using a flow rate of 1.0 mL/min. Mobile phase organic modifier was varied from 100% to 0% in 10% increments for both acetonitrile and Methanol.

3.2.4 Analytes

For flow rate experiments benzene was used with detection at 254 nm. For Methylene selectivity experiments, the series: benzene, toluene, ethylbenzene, propylbenzene, butylbenzene, and amylbenzene were used as analytes.

For flow rate experiments, benzene was chosen as it is a neutral molecule that exhibits some retention in reverse phase chromatography.

3.3 Sedimentation and Slurry Packing method

Sedimentation was performed on SBA-15 silicas prior to column packing. A suspension of silica was prepared in roughly 200 mL of methanol. The solution is sonicated gently and poured into a large graduated cylinder. Sedimentation was allowed to take place for an hour. The cloudy supernatant containing the fine particles was decanted and discarded. The remaining silica was re-sonicated and the process repeated for the same time until the solution was clear after one hour.

The remaining silica (roughly one to two gram) was then diluted in with methanol to produce a light suspension. The solution was added to the reservoir of an ISCO pump (Teledyne-Isco, Lincoln, NE) and an empty column was tightly connected to the outlet of the pump. A constant pressure method was used to pump the silica suspension through the column which had a frit on one end to catch the silica. An initial pressure of around 200 bar which was ramped up to 500 bar and left to pump through for several minutes. When complete, the column was disconnected from the pump and any excess material wiped off before placing the frit and end connector onto the column. According to Kirkland, low viscosity methods of column packing were used when sizing of particles during packing was not an issue due to narrow particle size distributions [29].

Table I. Packing Densities for Slurry packed columns

Column	Dimensions, cm	V_{col}, mL	V_{pack}, mL	% Density
SBA10	10 x 0.3	0.707	0.386	54.7
SBA3	5 x 0.3	0.353	0.200	56.7
SBA26	5 x 0.3	0.353	0.172	48.8
SBA36	5 x 0.21	0.173	0.065	37.8
SBA29	5 x 0.3	0.353	0.200	56.7
GeminiC18	10 x 0.3	0.707	0.434	61.5

In addition, the low viscosity slurry method was identified as superior over high density techniques for packing silica microspheres, and the constant pressure packing technique was determined as favorable to constant flow methods [10].

3.4 Column Characterization

Methods to determine the column volume, interparticle volume and the mass inside the column were performed as described by Rustamov et al. [4]. The retention of deuterated acetonitrile using pure acetonitrile as the mobile phase has been shown to correspond to the column void volume. The values obtained for void volume by this method have compared to the minor disturbance method as well as pyncometry [4]. Deuterated acetonitrile retention was measured by refractive index detector.

The interparticle volume was determined by injecting a series of polystyrene polymers eluted in tetrahydrofuran (THF). . Polystyrene standards with low polydispersity and molecular weights from 87,000 to 1,850,000 were used in this study with detection at 254nm. Solutions were prepared at 0.1% for each molecular weight of polystyrene injected. The interparticle volume is defined as the volume of space in between the spherical particles packed into the column. By using large polymers, we can measure the exclusion of these polymers from interparticle space. The use of large polymers ensures there is no penetration into the porous space as the polymer molecules are too large. Due to their own significant volume, the polymer molecules cannot get close to the adsorbent surface and are excluded from the column space based on their radius of gyration which is proportional to the cubic root of the molecular weight. There is a linear relationship between the measured retention time and the cubic root of the molecular weight.

We can correct for the exclusion volume of the actual polymer by measuring the retention times for a range of weights and extrapolate to a zero point mass, leaving only the volume of the space in between the column particles. An example of this can be seen in Figure 30.

The mass of adsorbent inside the column can be calculated from the interparticle volume, void volume and specific pore volume of the material from LTNA [4].

$$m_{ads} = \frac{V_0 - V_{ip}}{V_{pore}} \qquad (22)$$

where V_0 and V_{ip} are the column void and interparticle volume respectively and V_{pore} is the specific pore volume in mL/g of the absorbent. F. Chan et al. [3] were able to show by using this relationship that calculated masses of several absorbents compared favorably with the actual weights measured from emptying the analytical columns. It should be noted that this equation will work if the specific pore volume of the *absorbent* is known. Many column manufacturers will supply pore volume and surface areas for the base silica material. If the absorbent is chemically modified, then the volume of the modified layer must be taken into account. A correction factor, which is described in refs [3] and [4], must be applied in these situations. Fortunately, the silicas used in this study have been measured by nitrogen adsorption before and after surface modification.

3.5 Methylene Selectivity

Selectivity, α, as we have discussed earlier reflects the ratio of retention factors between two analytes. If the same eluent is used for tow analytes, as we saw with equation (7), the contributions of the eluent cancel out leaving only the analytes interactions with the surface.

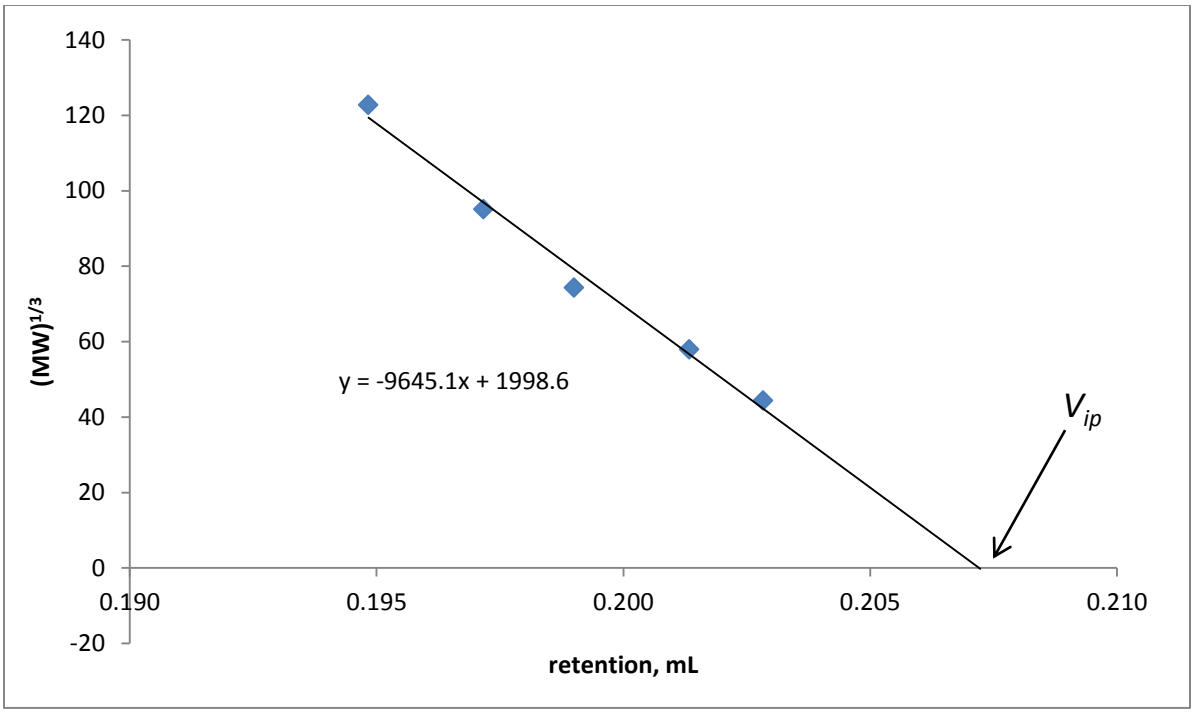

Figure 30. Example of the extrapolation of V_R vs $MW^{1/3}$ for polystyrene standards to zero in the determination of V_{ip}.

Assuming secondary effects are negligible, any differences in the selectivity should only be due to the interaction of the analyte with the surface [69,70].

In this experiment, we will be measuring the relative retention based on adjacent members of the alkylbenzene series which differ by one CH2 group from one to the next. Classically, methylene selectivity is given as the ratio of $k_{ethylbenzene}$ to $k_{toluene}$ or $\alpha_{EB/T}$ or as the slope of ln k against the number of methylene groups. According to Engelhardt and Jungheim, methylene selectivity is linear function of the % carbon load of a column up until about 12%, above which the correlation is less pronounced [71]. Since we are comparing SBA-15 columns modified with C8 to a Gemini-C18 column, being that the carbon % for a C8 bonded silica is roughly 17%, we should not see a large effect due to the difference in chain length. However, other studies have concluded that bonded chain length does play a role in increased selectivity [69,70].

3.6 Materials

The effect of flow rate and eluent composition on the retention of several alkylbenzenes was studied. Benzene, toluene, ethylbenzene, propylbenzene, butylbenzene, and amylbenzene chemicals were purchased from Fluka (Castle Hills, South Wales).

The Gemini base 5µ base silica, coated silica, and C18 modified were all donated by Phenomenex, along with the empty stainless steel columns (100 x 3.0mm; 50 x 3.0mm).

All solvents used (acetonitrile and methanol) are HPLC grade purchased from Pharmco (Phillipsburg, PA). Water purified using a Milli-Q system (Millipore, El Paso, TX).

4. Results and Discussion

4.1 Adsorbent Characterization

In order to evaluate the effect of the ordered porous structure of SBA-15 on the retention process it is necessary to have a complete evaluation of the physical properties of both the absorbent and the column. All adsorbents used in the chromatographic study were characterized for surface area, pore volume, pore size and pore size distribution by low temperature nitrogen adsorption prior to packing into analytical columns. Table II lists the adsorbent values for the silicas packed into the stainless steel columns.

Although it is necessary to discuss the characterization results in order to properly evaluate the other properties of the column, it should be noted that this is not how the story of this research unfolded historically. As the synthesis of spherical SBA-15 was evolving based on the findings through characterization and chromatography, new batches were being produced and new columns being packed. For the purposes of this section we will concentrate on a "time-independent" discussion of this research.

In determining the surface area of the adsorbents used in this study, it should be noted that we are using the surface areas of the modified silicas. It has been discussed previously [20] that there is some debate over the correct value to use for the cross sectional area of nitrogen in the surface area calculation. It is believed that nitrogen occupies a larger space on hydrophobic surfaces, and thus, an increase in the nitrogen molecule area is used as a correction for the less energetic surface. It has been shown [20] that applying a larger value of 20.5Å for the cross sectional area of nitrogen corrects for the hydrophobic surface. As can be seen in table II, the C constant is approximated as $= exp\frac{\Delta G_{ads}-L}{RT}$, where L is the heat of adsorbate condensation.

Table II. Adsorbent Geometry

ADSORBENT GEOMETRY					
Adsorbant	S m^2/g	$V_{pore(LTNA)}$ mL/g	Radius A	Radius 2V/S	C const.
Gemini-C18	244	0.555	42.1	45.6	21.3
SBA-3C8	579	0.71	24.2	24.7	15.6
SBA-10C8	512	0.7	30.6	27.3	16.2
SBA-26C8	479	0.61	29.7	25	16
SBA-29C8	481	0.676	27.3	27.8	16
SBA-36	711	1.09	28.9	30.6	86.6

Essentially, the C constant is related the heat of adsorption and provides a description of the overall energy of the surface. High values for the C constant, such as 80-200 are generally seen for bare silica surfaces, which under normal conditions are very similar to a surface covered with water. The energy of these surfaces are relatively high. On the other hand, a surface that has been dehydroxylated through heat, or that has been chemically modified, exhibits a much lower C constant. For example, a silica surface chemically modified with C8 or C18 will have a C constant of roughly 20, while the dehydroxylated bare silica may have a C constant between 50 and 70. In the first part of this thesis we argue that the C value may provide a more accurate way of assigning the proper value of the cross sectional area of nitrogen when calculating surface area.

From looking at Table II, it is evident that the last adsorbent (SBA batch 36) has a high C constant as compared to the other adsorbents. This SBA sample, batch SBA-36, was packed as bare silica to evaluate the effects, if any, of using an unmodified silica as a stationary phase as opposed to all of the other C8 modified SBA silicas packed into columns. In Table II, the calculation of the pore radius from the surface area is provided as a check for the surface area value as measured by nitrogen adsorption. Theoretically, we can relate the surface area to the pore radius by assuming that the pores have a cylindrical shape. Interestingly enough, SBA silica is known to possess very long cylindrical pores, therefore it is expected that the radius from desorption compares closely to the radius as calculated from the surface for SBA silicas. Batches SBA29 and SBA36 both show very good correlation between the measured and calculated values. However, the remaining batches show similar correlation to the Gemini C18. There is most definitely a trade-off between the morphology of the SBA versus the pore structure as we saw in discussing the synthesis of these SBA materials. Also, as stated above, the value

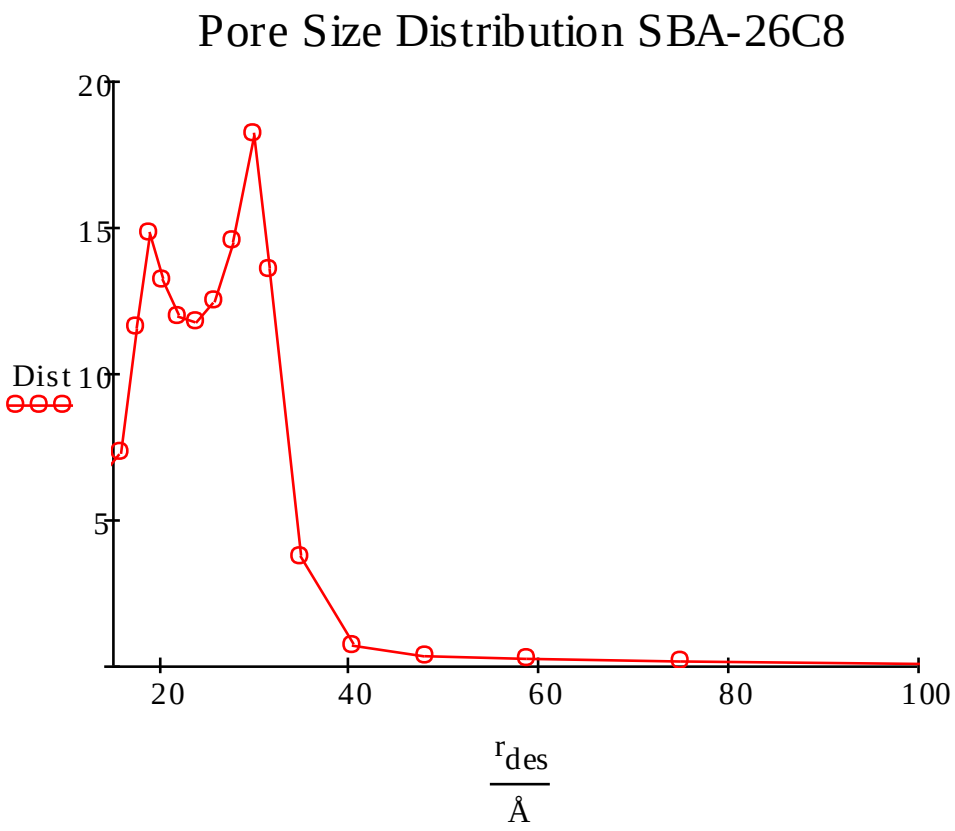

Figure 31. Pore size distribution for SBA-16 modified with C8

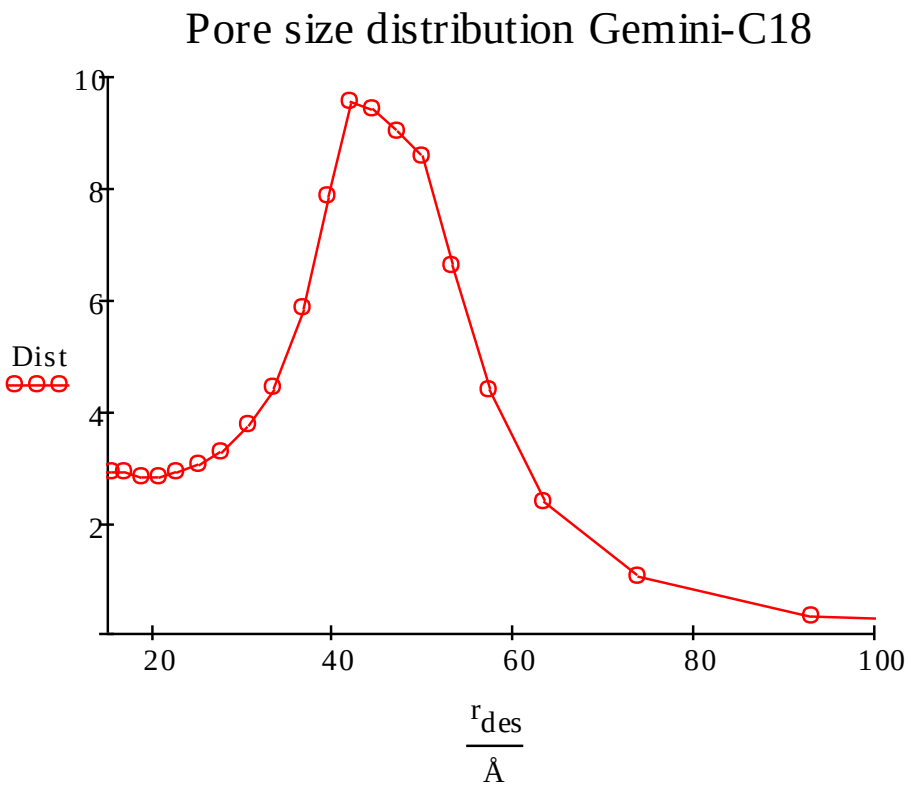

Figure 32. Pore size distribution of Gemini C18.

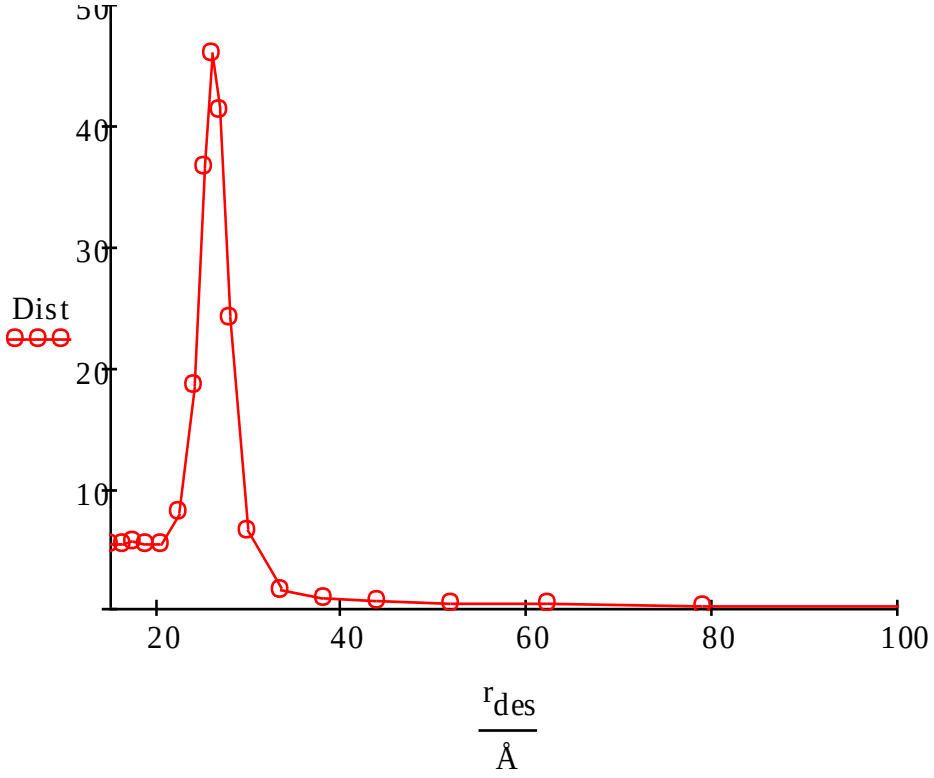

Figure 33. Pore size distribution of fibrous SBA-15

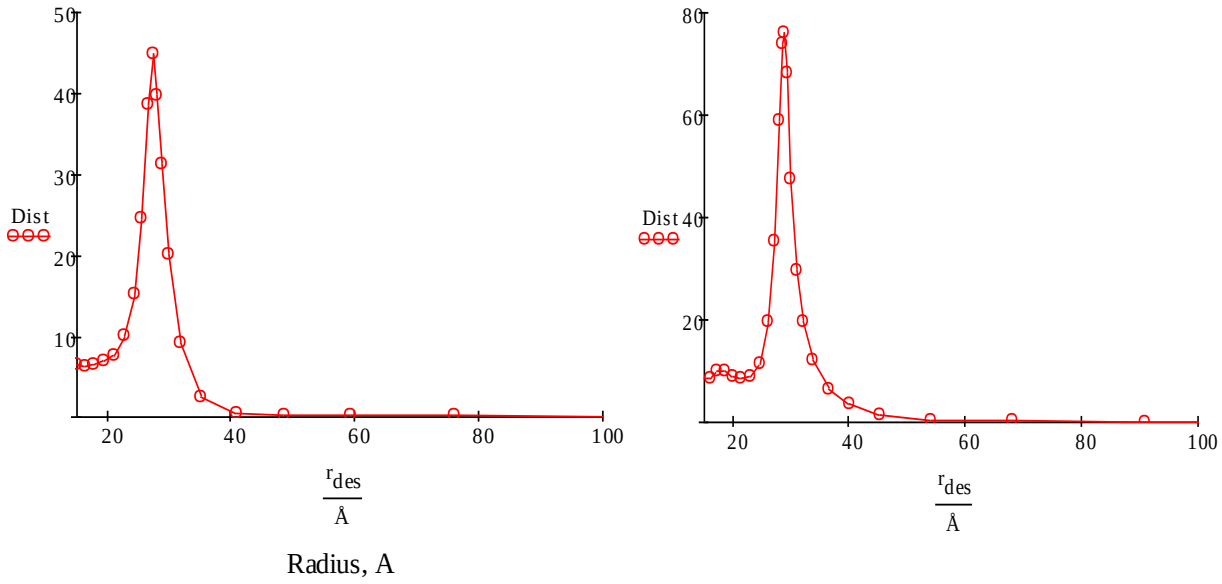

Figure 34. Pore size distributions of SBA-29C8 (left) and SBA 36 (right)

used for the cross-sectional area of nitrogen can greatly affect the calculated value of the surface area, however, the pore size determination is dependent on the analysis of the desorption curve and does not take into account the cross sectional area of nitrogen used. Therefore, the difference in radius as calculated from the surface area versus the value obtained from the desorption curve could have origins either in the morphology affecting the pore structure as well as the determination of the surface area. Figures 31, 32 and 33 show the differences in the pore size distributions of spherical SBA batch 26 and Gemini C18 as compared to the pore size distribution of fibrous SBA-15. However, it should be noted that both SBA36 and SBA29 exhibit pore size distributions very similar to fibrous SBA-15 (Figure 34).

Once packed into stainless steel column the materials were characterized for void volume and interparticle volume. As discussed above, the void volume was determined by the injection of deuterated acetonitrile and the interparticle volume was determined by the exclusion volumes of several polystyrene standards. For the bare silica batch, we also determined the void volume by continuing the range of polystyrene standards to low molecular weights and a large range of alkyl benzenes which are small enough to penetrate the pores.

The measured values for the void volumes of all 6 columns are listed in Table III. The determination of the void volume and interparticle volume allow for the calculation of the column pore volume for each column based on the relationships given in Eq (18). From the specific pore volume measured by LTNA, the mass of adsorbent in each column was calculated by Eq (22). It should be noted that for the three C8 modified spherical SBA silicas (batches 3, 26, and 29), very different masses were obtained. The low packing density of batch 26 could partly explain for the low calculated mass, which is echoed in the high value for interparticle volume measured (0.181 mL). It is curious that batches 26 and 29 which are both packed into 50

Table III. Column Geometry

COLUMN GEOMETRY							
	S	Vo	Vip	Vp	Vpore(LTNA)	mads	Stotal
Adsorbant	m2/g	mL	mL	mL	mL/g	calc.	g
Gemini-C1	244	0.463	0.272	0.191	0.555	0.344	83.94
SBA-3C8	579	0.25	0.153	0.097	0.71	0.137	79.32
SBA-10C8	512	0.494	0.32	0.174	0.7	0.248	126.98
SBA-26C8	479	0.229	0.181	0.048	0.61	0.0791	37.89
SBA-29C8	481	0.21	0.153	0.057	0.676	0.0844	40.60
SBA-36	711	0.151	0.085	0.066	1.09	0.0604	42.94

x 3.0 mm columns exhibit similar values for calculated adsorbent mass with batch 36 which has been packed into a 50 x 2.1mm column, which has considerably less empty volume as compared to the 50 x 3.0mm column. When comparing all three batches of C8 SBA, batches 29 and 3 have the exact same interparticle volumes, packing densities and very similar specific pore volumes. However, there is a large difference in the measured void volumes between the two. While batch 26 shows a slightly higher measured void volume as compared to batch 29, the larger interparticle volume yields a similar column pore volume as per Eq. (18). Being that the pore diameters of all these materials are above 50Å and that the t-plots (figure 35) for all three indicated the absence of micropores, it is difficult to explain the low void volume and calculated mass values. Unfortunately, Batch 3 was unpacked early in this study and no longer exist. Further, it was unpacked before we had the notion of actually weighing the material to determine the mass by weight. We will discuss the issue of calculated mass inside the columns later in the discussion.

The initial interparticle volume and void volume determined for the SBA36 column was confirmed by the extended polystyrene/alkylbenzene size exclusion data (Figure 36). The curve of retention volume to the cubic root of molecular weight is divided into two branches. The polystyrene standards are excluded from the column space and their retention volumes are extrapolated to zero mass to give the interparticle volume. The retention volumes corresponding to the alkylbenzenes are related to the volume inside the pores and extrapolating the upper curve to zero gives the void volume. Both values are given by the y-intercept for the respective linear regression curve. The retention volumes were corrected for column and system void volume prior to graphing.

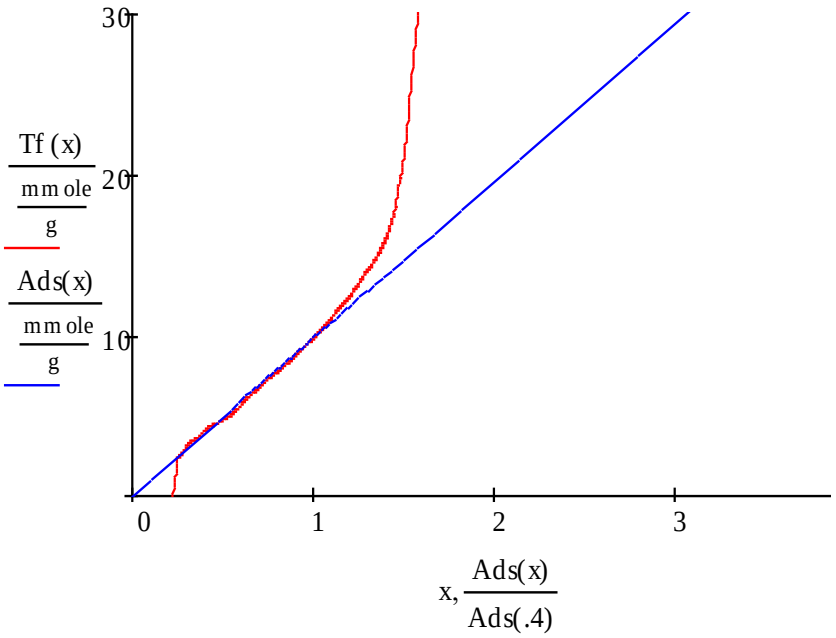

Figure 35. t-plot for spherical SBA batch 29 showing the absence of micropores

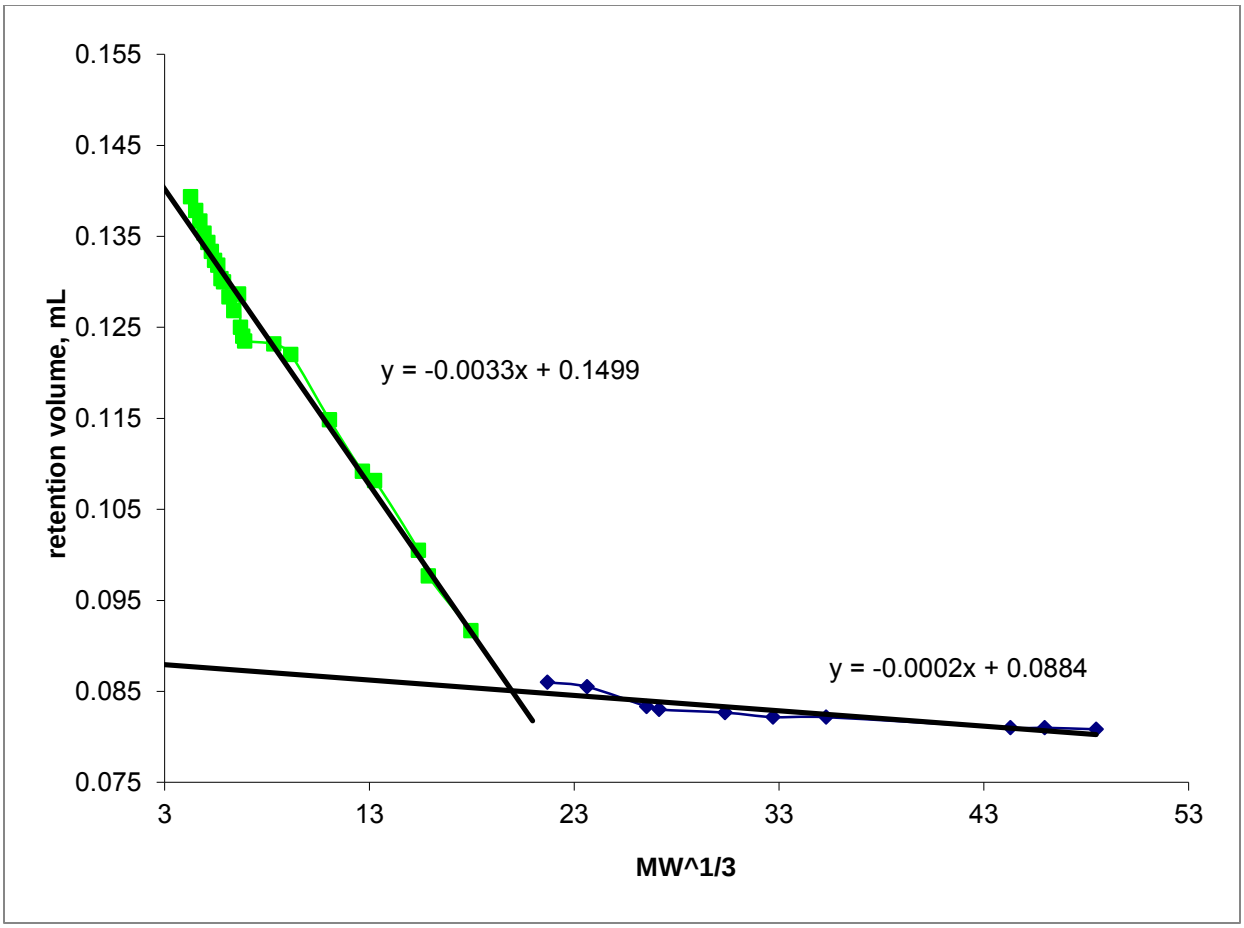

Figure 36. Interparticle and void volume as determined on SBA batch 36

4.2 Flow rate studies

When initially beginning this study, our original idea was to evaluate the effect of slowing down the flow to the point where the flow rate would approach the diffusional rates of the analyte. The hypothesis was that a significant increase in the retention volume at the slower flow rates might be an indication that migration of the analyte through the pores was not only determined by diffusion, but that perhaps there was also an element of convective flow. Whereas diffusion in gaseous media is on the level of 10^{-1} cm^2/s. the diffusion coefficients in liquid media are on the level of 10^{-5} cm^2/s. By lowering the large difference between the convective flow moving around the particles and the diffusional migration believed to take place in the stagnant liquid in the pores, we believed that greater retention might occur due to the higher concentration of analytes which could migrate into the porous space without being forced through the column by the percolating mobile phase.

The first batches of spherical SBA modified with C8 were batches 3 and 10. These two batches exhibited the narrowest pores size distributions as compared to the other batches synthesized at that point. The flow rate was slowed down to values on the order of 5 to 3 µL/min in to evaluate any changes in retention. After confirming the proper operation of the pumps by evaluating flow accuracy, C8 modified batch 3and 10 were analyzed with varying flow rates. Benzene was injected at a concentration adequate to reach 10 signal-to-noise units, but not to go beyond 25 to 30 S/N units so as to minimize analyte-analyte and analyte-eluent interactions. The chromatograms were digitally exported to a Microsoft Excel Spreadsheet and the retention time profile was converted to a retention volume profile using the formula $V = F \times t$. This normalized the data over all flow rates so we could overlay the chromatograms and see any significant differences in retention. Although we did not see a drastic increase in retention, we did observe

some interesting effects of the flow rate on peak shape. As seen in Figure 37 and 38, the shape of the benzene peak at the fast flow rate (1.5mL/min) shows a large tail, which as the flow rate is reduced, turned into a hump on the backside of the peak. At the slowest flow rate (0.005 mL/min), the peak is symmetrical and the peak maximum matches closely to the retention volume corresponding to the hump on the preceding peaks. Since we are measuring the retention of benzene, which is a neutral molecule, and does not react with surface silanols, the presence of the tailing/hump can only be attributed either to mass transfer or "eddy diffusion" effects of the benzene travelling around the particles, which is more pronounced in fast flow rates, or to some effects involving diffusion in the pores.

In the first scenario, it is possible the benzene is encountering some resistance in its course down the column due to a range of particle size distribution of absorbent in the column. This material has a mean particle size roughly around 20μm. The distribution of the particle size is of a Gaussian form, however, it is possible that during the slurry packing procedure there could have been sizing of the particles before pressure was applied. This could result in the layering of the particles from biggest to smallest inside the packed column in the direction of the mobile phase flow (with the bigger particles toward the column outlet and smaller particles nearer to the inlet of the column). Thus, molecules of benzene could be reaching the end of the column and meet less resistance to mass transfer around the bigger particles, while the tag end of the sample band would be still struggling to find a path around the smaller, more tightly packed particles. The second possibility involves the migration of the benzene through the porous space. It is possible that a portion of the benzene is penetrating into the pores, while the mobile phase is quickly pushing the concentration of benzene in the interparticle space down the column at a faster velocity creating a tail. When the flow is slowed down to values of 5 μL/min, perhaps the

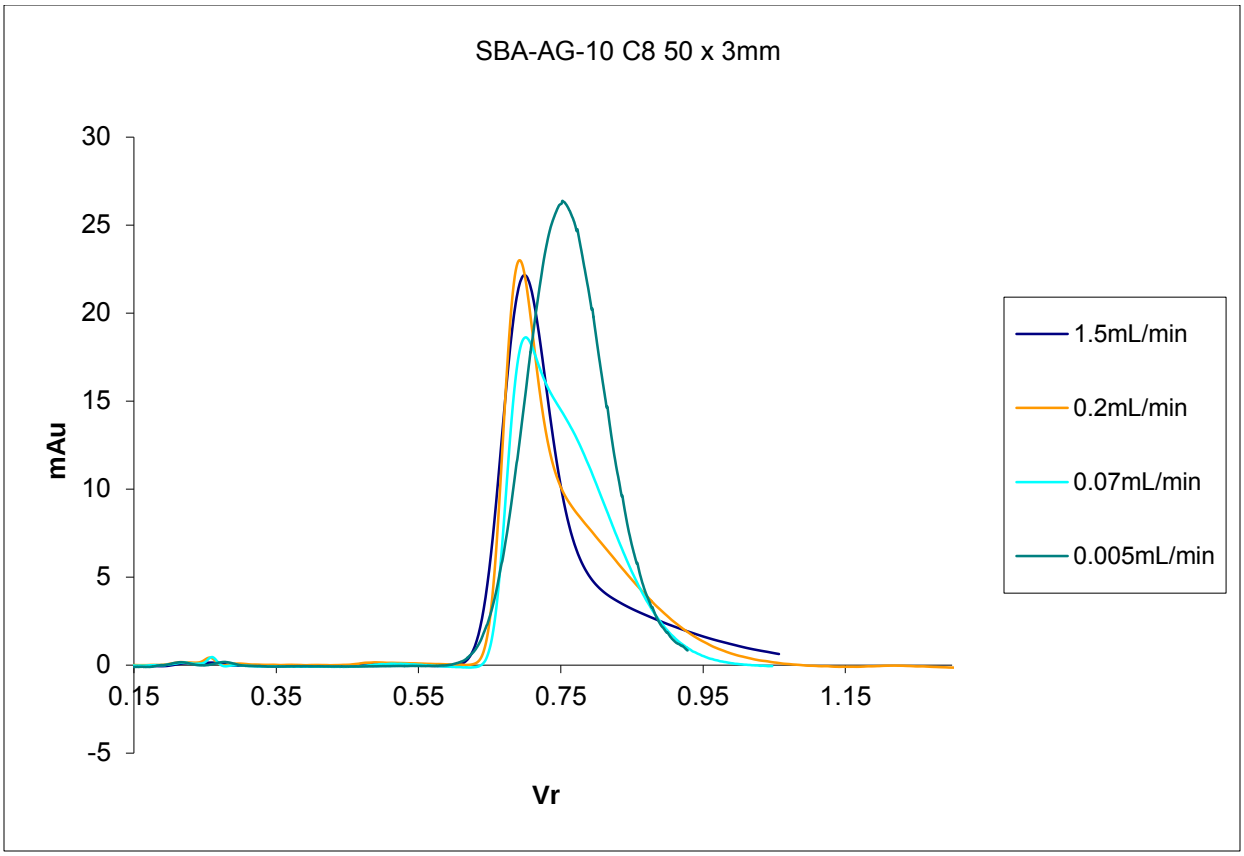

Figure 37. Effect of flow on peak shape and retention on C8 SBA batch 10.

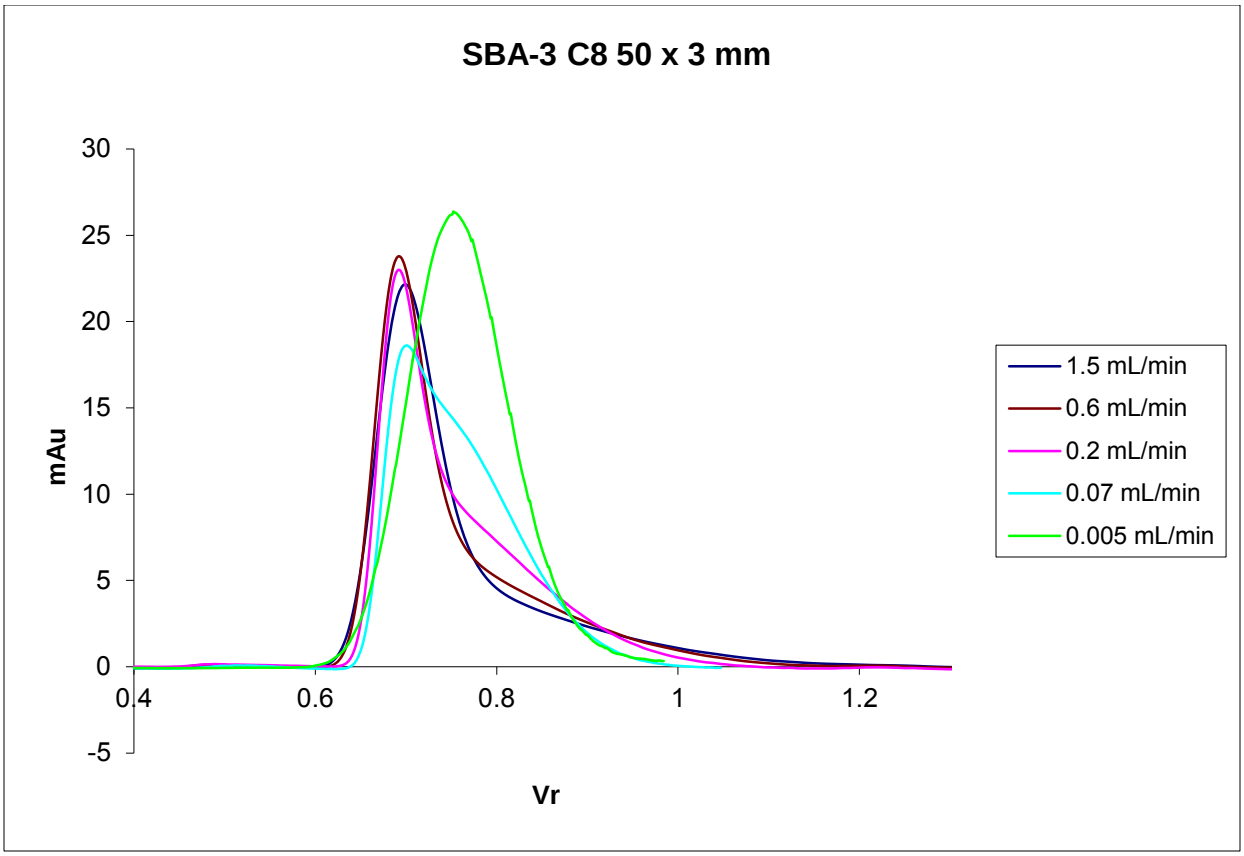

Figure 38. Retention of benzene at varying flows on SBA-3C8

percolating mobile phase does not have such an effect on the transfer of benzene from the surrounding area around the particles into the porous space where it interacts with the surface, allowing for a much more symmetrical peak, which elutes at the retention volume of the tail or "hump" on the peaks from the faster flow rates.

As more batches of SBA were synthesized, exhibiting better ordered pore structure these batches were modified and or packed into columns. Batch 26, 29 and 36 exhibited pore size distributions which correlated more closely to those observed for fibrous SBA-15. Batch 36 in particular was promising in not only the pore size distribution but the nitrogen isotherm as well was as much like fibrous SB-15 as any spherical batch synthesized seen in this study (Figure 39). The decision was made to keep batch 36 as bare silica and run under normal phase conditions and batch 26 and 29 were modified with octyldimethyl(dimethylamino)silane (C8).

Flow experiments performed on batch 29 modified with C8, although not showing any increase in retention with reduction of flow rate, did display similar peak shapes as was observed for modified batches 3 and 10. However, it should be noted that although the change in peak shape as the flow was reduced was observed, it was less pronounced with batch 29 (Figure 40). For comparison, a commercial silica gel column (Luna 5µ, C18(2) 50 x 2.00mm) was used for the flow rate experiments. The resulting chromatograms should peaks with normal Gaussian distribution shapes (Figure 41). It was also observed that the retention did not increase with a reduction of flow rate, and even though there was no significant increase in retention seen with the spherical SBA columns, it was observed that the SBA columns did show more retention increase than the commercial column, even if the increase was only minor.

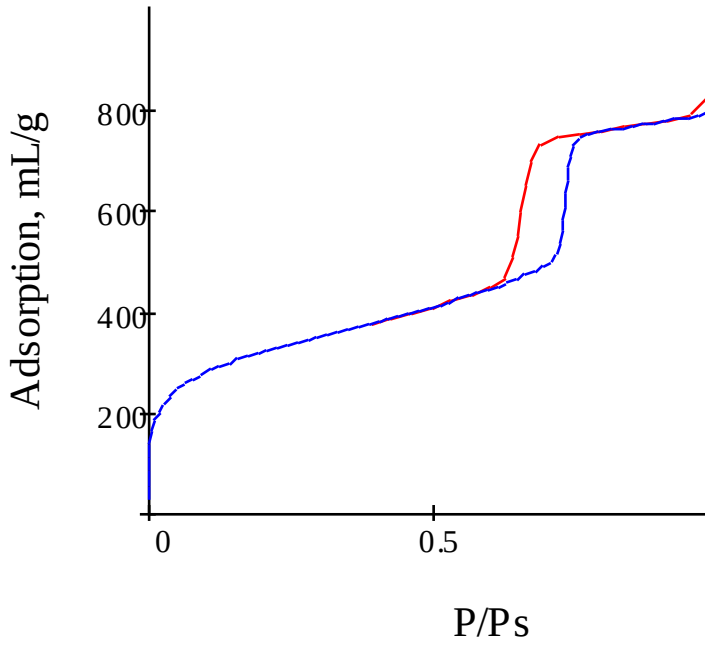

Figure 39. Nitrogen isotherm for SBA-36.

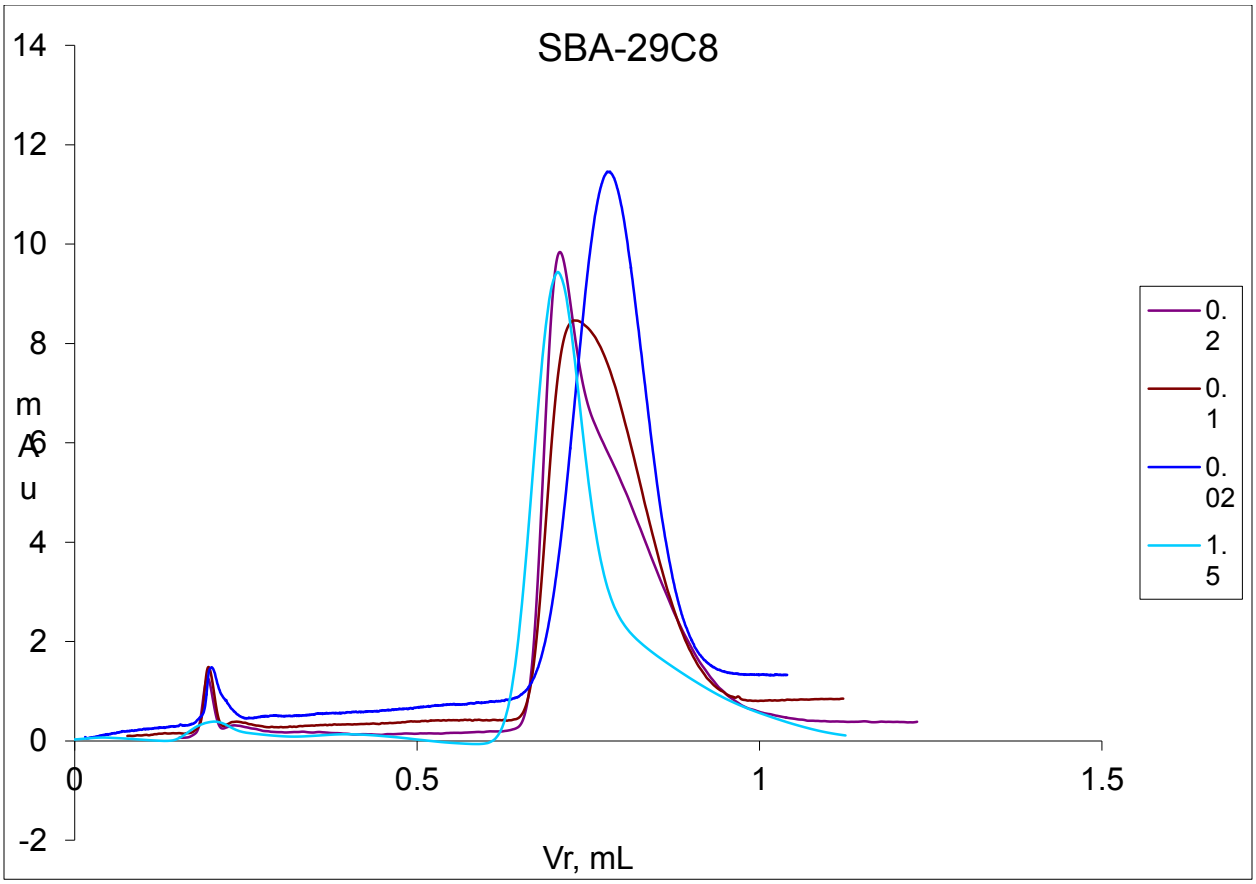

Figure 40. Effect of flow rate on retention and peak shape as seen using C8 modified batch 29.

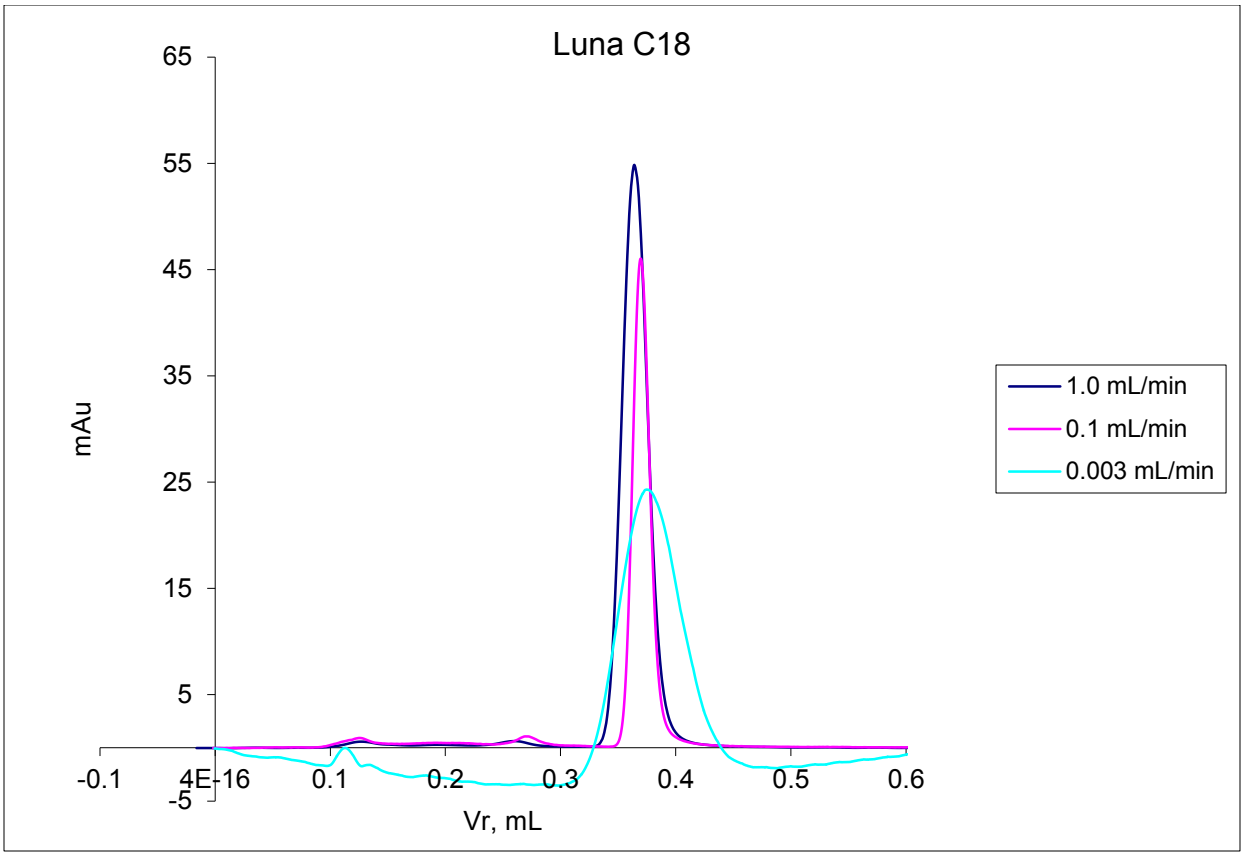

Figure 41. Flow studies as performed on the Luna C18 column 50 x 2.00mm.

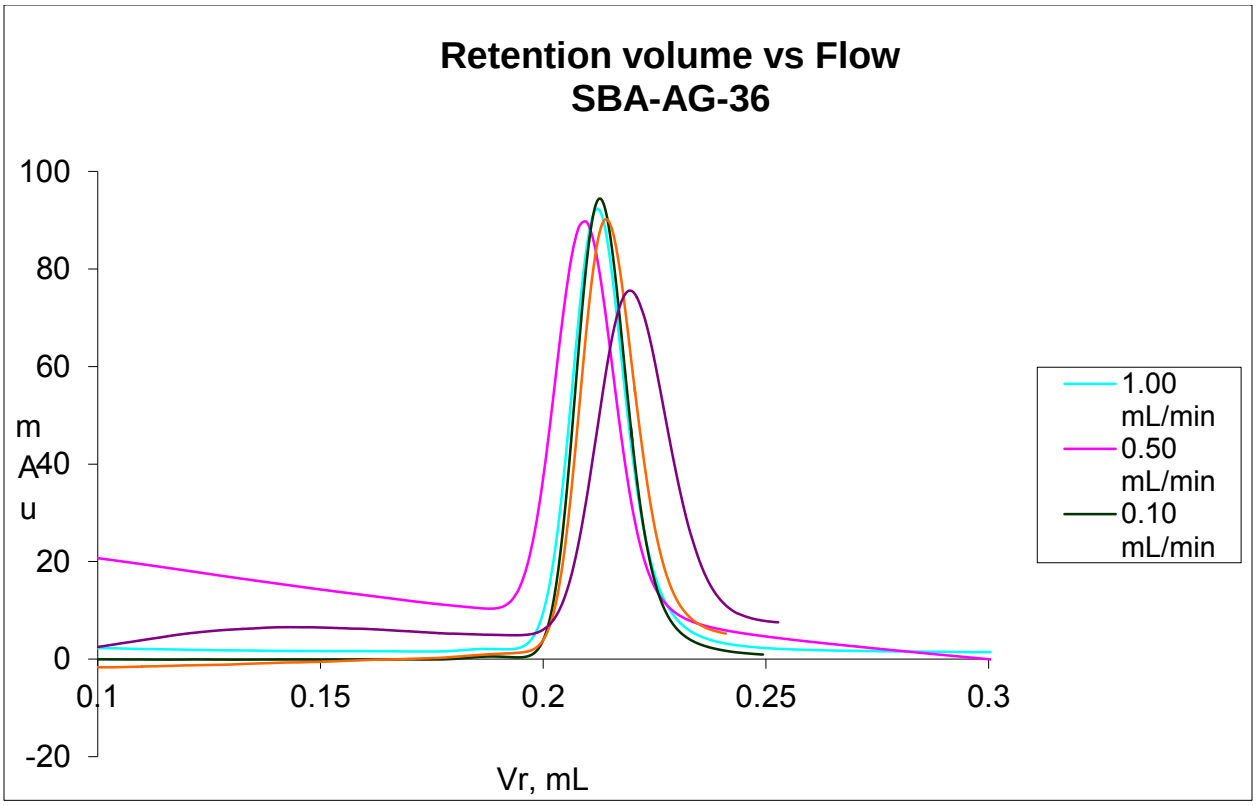

Figure 42. Effect of flow rate on bare silica SBA batch 36. Mobile phase used was hexane.

The effect of flow rate on retention and peak shape was run on the bare SBA spherical silica (batch 36) using hexane as a mobile phase eluent and benzene as an analyte (Figure 42). The injection of benzene at flow rates down to 0.002 mL/min did not produce any significant increases in retention. Also, the peak shapes for all chromatograms exhibited normal Gaussian type distributions, unlike the peak shapes observed for the modified batches. Since this material had roughly the same size particles as the other columns, and packed in the same manner, this result sheds some doubt on the hypothesis that the peak shape is the result of the multipath dispersion through the column. In addition to this, the fact that these runs were performed under normal phase conditions needs to be examined. Under normal phase conditions, benzene would show much less preference for the silica surface than it would for the C8 modified surface under reverse-phase conditions, especially with hexane as the eluent. With this in mind, it is conceivable that the benzene molecules were almost non-retained – therefore not interacting significantly with the stationary phase. If this is the case, then the irregular peak shapes seen with the modified batches should most likely be arising from some sort of interaction of the benzene analyte with the stationary phase. Since benzene is neutral and should not be affected by residual silanols, which is the usually the cause of tailing with ionizable compounds, the most reasonable possibility is that the irregular peak shape is arising from some kinetic aspect of the interactions between the analyte and the porous stationary phase which at faster flow rates results in unusual peak shapes, but as the flow slows, the resulting peaks becomes more Gaussian-like. The possible kinetic contributions possibly responsible will be discussed in the following section.

4.3 Kinetic Studies

The study of spherical SBA in HPLC was never intended be a rigorous kinetic study of efficiency. It was understood that these columns would not exhibit the qualities of what one would call an "efficient" column. In fact, it was understood that quite the opposite would be true. As pointed out in the introduction to this study, the evaluation of spherical SBA-15 would mainly revolve around the ability to assess the effect of the unique SBA-15 pore structure on retention. As such, this study originated as one that would be dominated by a thermodynamic-centric study or a study to evaluate how pore structure affected retention measured as the retention time or volume. However, it is evident that a complete assessment of the pore structure on the retention process must include a kinetic assessment. By kinetic, we mean a study of the processes which effects migration of the analyte through the mobile phase, through the stationary phase and the diffusional phenomena involved.

The Van Deemter equation, Eq (12), provides a simplified explanation of the plate height as it relates to mobile phase velocity. Although more detailed variations of this equation have been developed over time, the Van Deemter equation proves sufficient due to its simplicity for the cause at hand. By plotting the plate height ($H = \frac{L}{N}$) against the superficial mobile phase velocity, we can estimate the contributions of the A, B and C terms to band broadening. From the flow rate studies, the retention time and peak width (at half height) obtained from the Chemstation software were used to calculate the theoretical plates by

$$N = 5.545\left(\frac{t_R}{w_{1/2h}}\right)^2 \qquad (23)$$

The plate height is determined by the ratio of the column length in centimeters to the number of theoretical plates calculated using equation (23) and then converted to µm. The column mobile phase velocity was calculated as the superficial velocity using the column radius in centimeters and the volumetric flow by

$$u = \frac{F}{\pi \cdot r^2} \qquad (24)$$

Plots of H versus u were obtained for columns packed with spherical SBA batches 3C8, 10C8, 29C8, and 26C8 and 36 as well as two modified commercial silica gel columns (Luna, 5u C18 100 x 2.00mm and 50x 2.00cm) for comparison purposes.

The H/u plots for SBA batches 26C8 and 10C8 are overlaid with the curve obtained for the 50 x 2.00 cm Luna column. All three experiments were performed using mobile phases composed of mixtures of acetonitrile with water. The two spherical SBA batches were run with a mobile phase composition of 70% acetonitrile while the Luna column was run using 60% acetonitrile (Figure 16). The minimum plate heights achieved by both SBA columns are considerably larger than that of the commercial Luna column. Contributions from both the A term and B term influence the shape of the curve in the low velocity range. The A term can be described by dependence on the particle size:

$$A = 2\lambda d_p \qquad (25)$$

where λ is a geometrical variable related to the packing structure and d_p is the particle diameter. It is evident by Eq 25 that the A term is directly proportional to particle size. As was previously discussed in part 1 of this thesis, the average particle diameter for synthesized bathes of spherical

SBA ranged from 10 to 30μm. Since the Luna column is packed with 5 μm particles, this effect was expected. Similarly, the contribution of the B term can be described by

$$B = 2\frac{\gamma D_m}{v} \qquad (26)$$

where γ is a parameter relating to the obstruction or limiting of diffusion, D_m is the diffusion coefficient and v is the velocity. As the B term mainly describes axial dispersion in the column, since it is inversely proportional to velocity, its contributions are mainly seen at low velocities and as the flow speeds up the contributions from axial dispersion are negated.

From the description of the A and B term it is understandable that the SBA columns exhibit a much larger minimum (roughly 60 to 40 μm) plate height as compared to the Luna column (~20μm). The much larger particles of the SBA silica are the main cause to the increase in plate height from these two terms. In addition to this, the H/u curves for the SBA columns exhibit larger C term contributions as can be seen from the increased slope of the plot as the velocity increases. The C term, a complex term arising from multiple contributions itself [6], essentially relates to the analyte diffusion through the stationary phase medium and can be described by

$$C = \omega\frac{d_p^2}{D}\,v \qquad (27)$$

in which d_p refers to the diffusional distance (particle diameter), ω is a structural parameter relating to pore/particle size distribution, and *D* is the diffusion coefficient. Thus, the C term describes the resistance as it relates to the processes of analyte diffusion as it migrates through the column stationary and mobile phases [15]. Also, the C term is directly proportional to the mobile phase velocity and increases with increasing flow. For this reason, smaller particles are desirable for fast speed, efficient analyses, e.g. uPLC, where sub 5μm diameter particles are

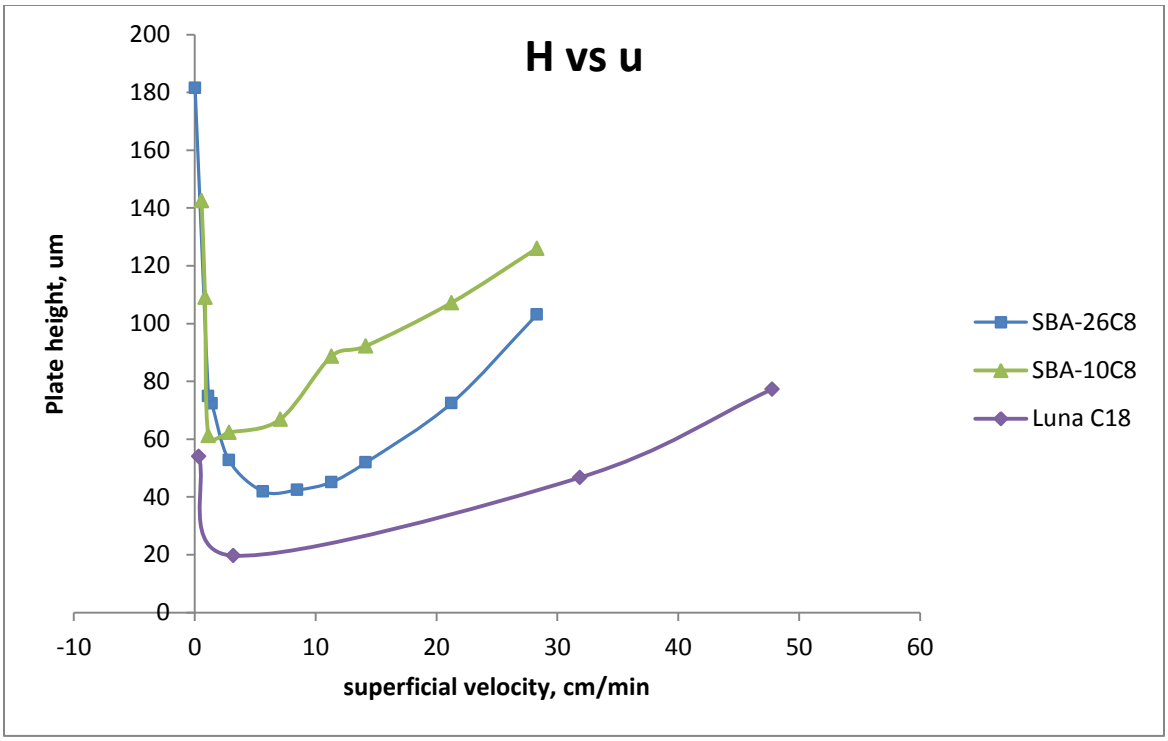

Figure 43. H/u curves for SBA-10C8, -26C8, and Luna C18

employed. The shorter distances of diffusion in the inter and intraparticle spaces allows for less resistance to mass transfer and less band broadening of the sample zone through the column.

As we can see with the plots for the SBA column, the increase of the H/u curve at the higher velocities exhibits a steeper slope as compared to the commercial column (Figure 43) . Keeping in mind the unique pore structure of SBA, this is not exactly unexpected. Although contributions to the C term undoubtedly arise from the large particle size, it is also reasonable to expect the long, narrow, non-interconnecting pores observed with SBA-15 could present a unique situation to the liquid system inside the particles dominated by diffusion. Whereas fibrous SBA-15 is characterized by the hexagonal array of parallel pores, the exact nature of the pore structure in the spherical SBA particles in not exactly understood. Understandably, long, straight non-interconnecting pores would be ideal for the diffusion of a molecule in liquid. However, in the spherical particles it is evident from the data presented in part I of this dissertation that there is a considerable loss of pore structure with the change of particle morphology. Depending how the pores are arranged within the spherical particle, it is possible that the parallel pore structure could present the diffusional system with a tortuous medium, increasing the distance needed to travel.

The SBA-26C8 column was assessed at varying flow rates using both 70/30 MeOH/water as well as 70/30 MeCN/water mobile phase systems. In a plot of H/u for both systems, the lines show comparable curves dominated by contributions from the A and B terms, however it is evident that a sharper increase is observed for the methanol system at high velocities (Figure 44). This corresponds well to the decreased diffusion coefficient as a result of the more viscous methanol. With higher viscosities, the diffusion of the analyte is hindered, thus increasing the resistance to mass transfer.

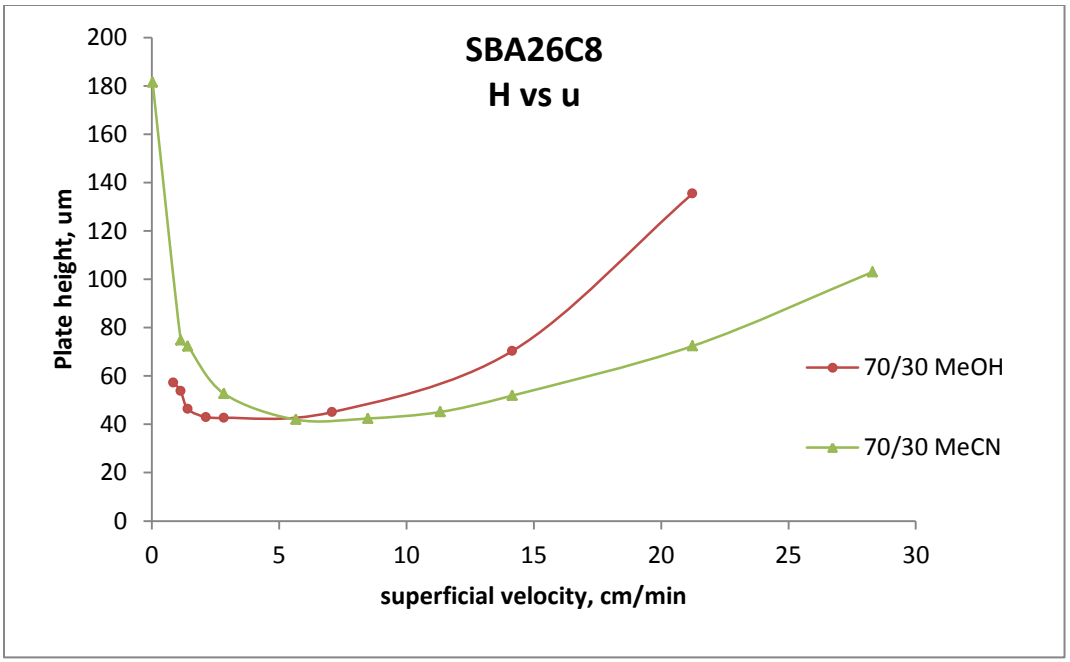

Figure 44. Comparison of H/u curves for 70/30 MeCN and MeOH on SBA-26C8.

Column SBA-29C8 was assessed in a mobile phase system of 100% acetonitrile. The Van Deemter plot shows extremely large plate heights, and as well as a steep increase from the C term contribution to mass transfer resistance (Figure 45). In an attempt to try and explain why such an increase to the mass transfer resistance would be present, an estimation of the diffusion coefficient was calculated. As seen in references [53] and [55], the diffusion coefficient of the analyte (benzene) can be measured through the broadening of the sample peak in peak parking experiments or in experiments in which the flow is adjusted to allow for long residence times. Thus, with the data collected at low velocities for the flow rate studies, the peak variance as a function of the residence time was used to calculate the effective diffusion coefficient of benzene inside the column. Modifying equation (21)

$$\sigma_x^2 = 2D_{eff} \cdot t_R \qquad (28)$$

we can plot the peak variance against the retention time of the injections at low velocities. The conversion of the peak variance from temporal units to spatial units is accomplished through

$$\sigma_x^2 = \frac{t_R^2}{N} \cdot u^2 \qquad (29)$$

Where u is the column velocity expressed in cm/s and t_R is the retention time in seconds. The plot of the square of the peak variance against retention time (Figure 46) for SBA-29C8 show a linear dependence with the slope being equal to $2 \cdot D_{eff}$. The effective or apparent diffusion coefficient for benzene was calculated as 9.4 x 10^{-6} cm^2/s. This coefficient describes the diffusion of benzene in the SBA-29C8 column and is a measure of the actual diffusion of the analyte molecule inside the column. The molecular diffusion coefficient for benzene in 100% acetonitrile was determined experimentally by the authors of reference [53] as 3.6 x 10^{-5} cm^2/s.

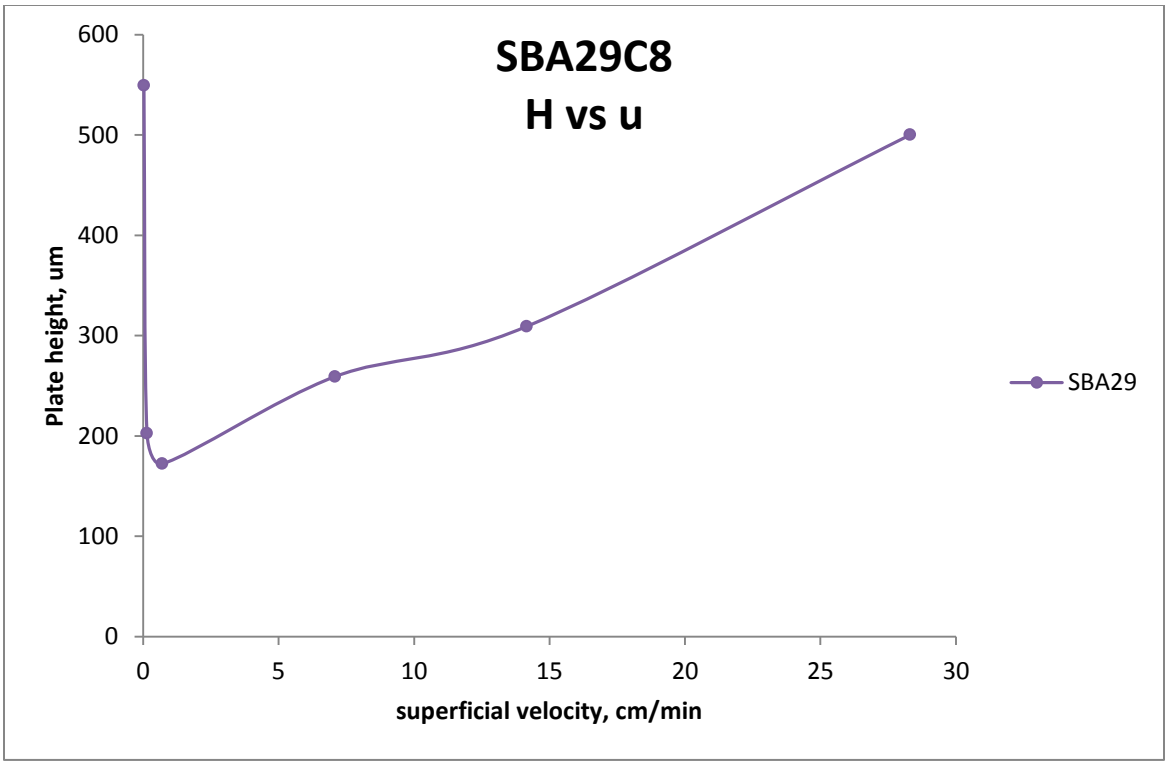

Figure 45. H/u curve for SBA-29C8

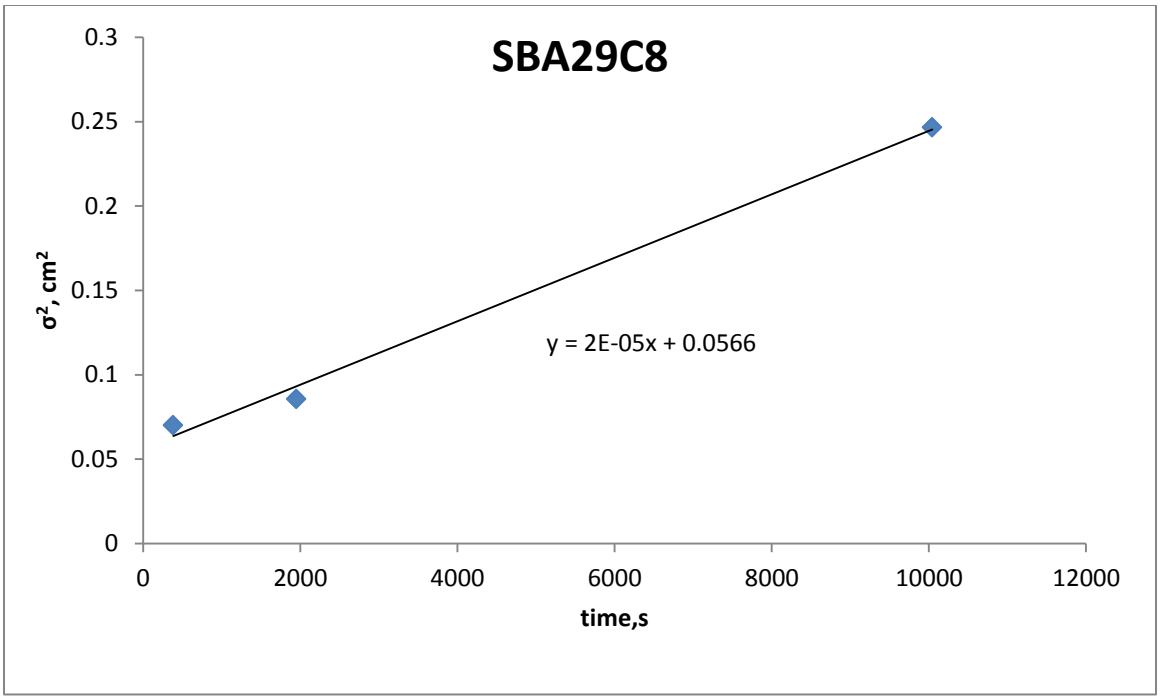

Figure 46. Plot of peak variance vs. retention time for SBA-29C8

This value corresponds well to the values determined by P.W. Carr [72] as well as the values calculated by the Wilkes-Chang equation:

$$D_{A,B} = 7.4 \times 10^{-8} \frac{\sqrt{\psi_B} MW_B T}{\eta_B V_A^{0.6}} \qquad (29)$$

where ψ is the association factor of the solvent, MW is the molecular weight of the solvent, and V is the molar volume of the solute at its boiling point, and η is the viscosity of the solvent.

Using the molecular diffusion coefficient for benzene in acetonitrile, the obstructive parameter, γ, can be calculated by Eq. (20) as the ratio of the coefficients for effective (D_{eff}) diffusion to molecular diffusion (D_m). The obstructive parameter is related to the physical structure of the stationary phase and describes the hindrances the stationary phase presents to the molecular diffusion coefficient. A value for γ of 0.25 was calculated for SBA-29C8. This value is far lower than typical values for packed columns (0.7-0.8)[53,55]. The lower the value of γ, the more obstruction/tortuosity presented by the stationary phase.

In order to provide comparison, the commercial Luna 100 x 2 column, which was also analyzed at varying flow rates in acetonitrile, was evaluated for D_{eff} and γ. From the plot of peak variance against time (Figure 47), the effective diffusion for the Luna column was calculated as 2.77×10^{-5} cm^2/s. Again, using the known molecular diffusion coefficient for benzene in acetonitrile, the obstructive parameter was calculated as γ= 0.77. This value is in good agreement with literature values and provides a picture of the C8 modified SBA columns as presenting obstruction to the diffusional paths of the analyte arising from interparticle tortuosity and/or intraparticle obstruction in the intraparticle space either through the low level of interconnectivity or long tortuous pores.

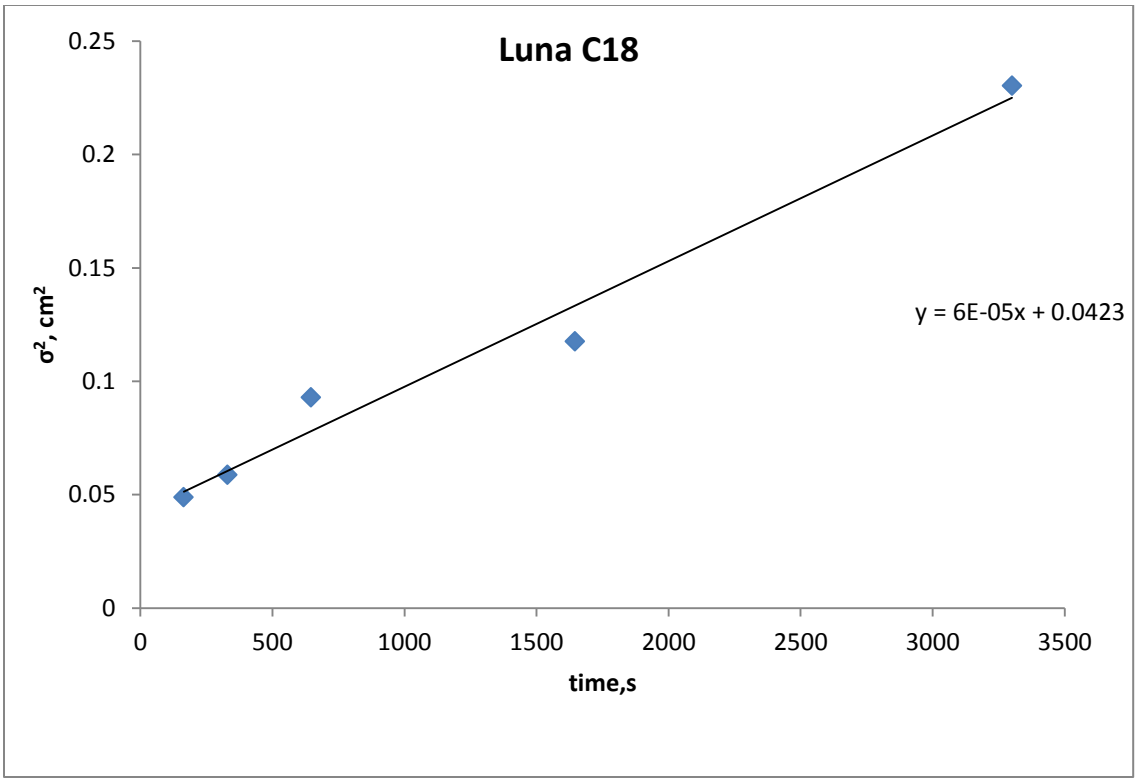

Figure 47. Plot of peak variance against retention time for Luna C18 column.

TABLE IV. Determination of Obstruction factor

Sample	Conditions	Deff cm^2/s	Dm cm^2/s	γ
SBA 29C8	100% MeCN	$9.4x10^{-6}$	$3.6x10^{-5}$	0.26
Luna C18	100% MeCN	$2.8x10^{-5}$	$3.6x10^{-5}$	0.77
SBA 10C8	70/30 MeCN	$2.2x10^{-6}$	$1.6x10^{-5}$	0.14
SBA 26C8	70/30 MeCN	$4.33x10^{-6}$	$1.6x10^{-5}$	0.27
SBA 3C8	7/30 MeOH	$5.6x10^{-6}$	$9.5x10^{-6}$	0.59
SBA 36	Hexane	$1.2x10^{-5}$		

Table IV shows the values of D_{eff} and γ for the other SBA columns. However, since the other columns were analyzed with mobile phase compositions consisting of aqueous mixtures of either acetonitrile or water at different concentrations, the value of D_m was estimated by using the Wilkes-Chang equation. Although values calculated by the Wilkes-Chang equation have been shown to be accurate within 10-20% [53,55,72] for such solvent mixtures, the data should be used as an estimation as the values could not be experimentally confirmed. It is interesting that the largest value (closest to D_m) for the effective diffusion was observed for the unmodified SBA-36 batch. However, without being able to calculate D_m for benzene in hexane, it is not possible to calculate γ. The increased diffusion and low plate height and H/u curve exhibited by batch 36 may be the result of being unmodified (Figure 48). It should be also noted that the H/u curve and γ measurement for SBA-3C8 are much closer to values seen with the commercial columns (Figure 49). Unfortunately, this column was unpacked to allow the packing of SBA-26C8 and no further studies are available on this column/batch. At this point it is difficult to explain the difference observed for the SBA-3C8 column as compared to the other modified SBA columns, especially without methylene selectivity and surface specific retention studies which were performed on the modified batches and discussed below.

4.4 Methylene Selectivity

Methylene selectivity, or hydrophobic selectivity as it is sometimes referred to, is a measure of the ability of the stationary phase to discriminate between adjacent members of a homologous series, in this case, alkylbenzenes. By measuring retention and calculating the relative retention of the adjacent members of the series, we are in essence measuring the differences in analyte

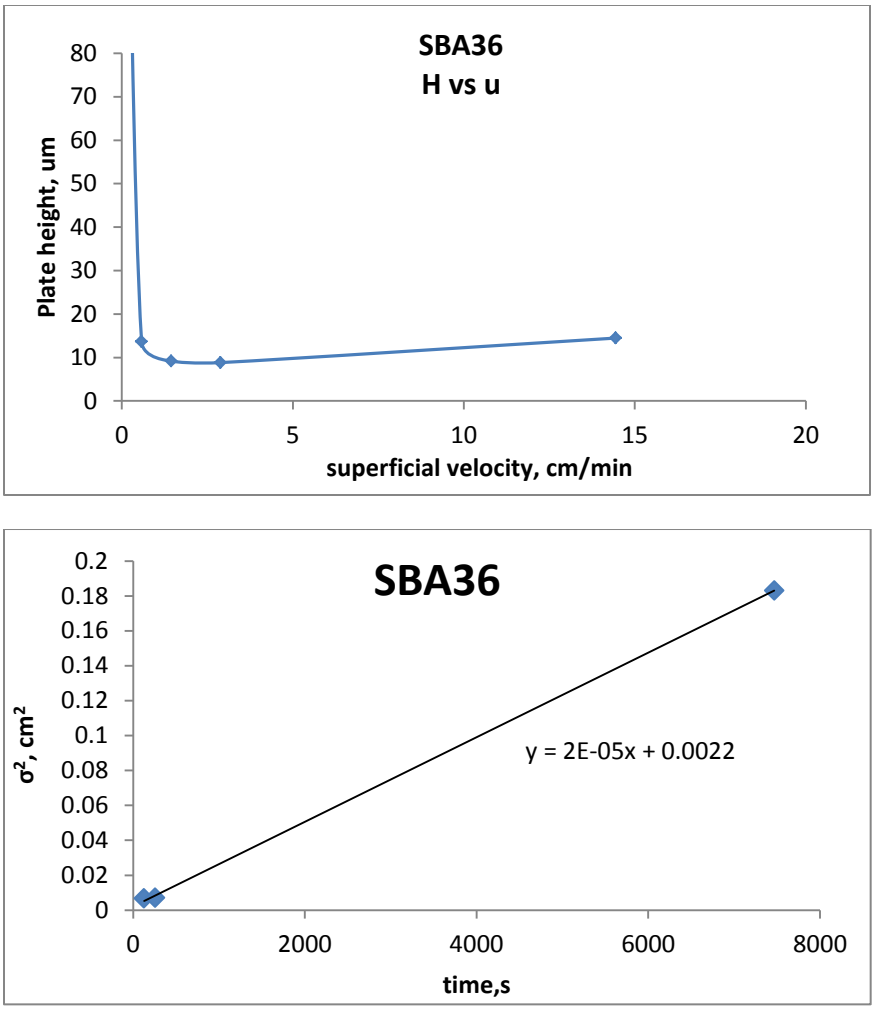

Figure 48. H/u (top) and Plot of peak variance vs. retention time (bottom) for SBA-36

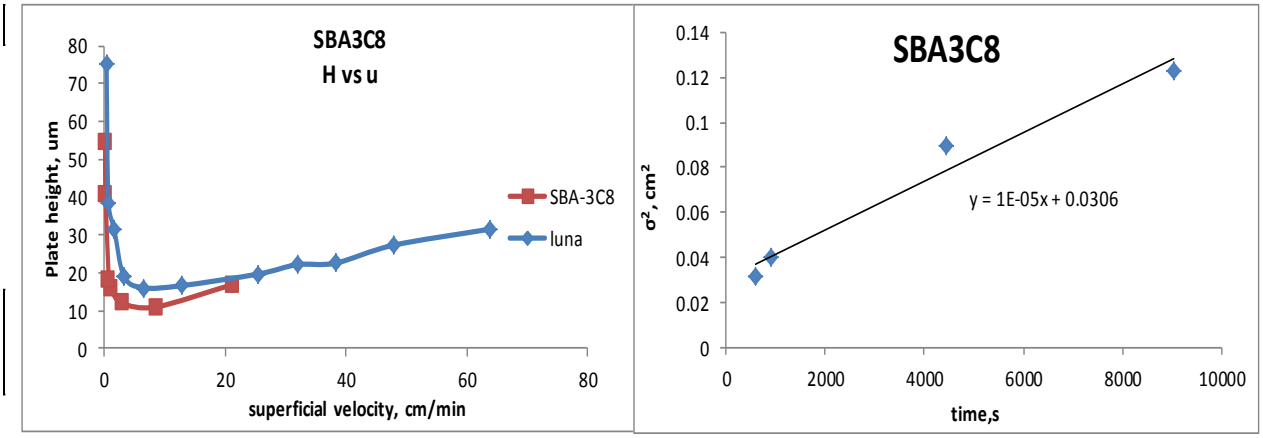

Figure 49. H/u (left) and plot of peak variance for SBA-3C8

interactions with the surface of the stationary phase. As it has been shown, being a ratio of retention factors, selectivity relates to the Gibbs free energy of the analyte interaction with the surface and with the eluent Gibbs free energy component being cancelled out in the ratio. For this study, Column SBA-10C8, 26C8, and 29C8 were evaluated. In injections of the series of benzene through amylbenzene were analyzed along mobile phase compositions of methanol from 100-0%. SBA-10C8 and 29C8 were also evaluated using an acetonitrile/water mobile phase system. The slurry packed Gemini C18 column was used as a comparator in both mobile phase systems (Figures 50-53).

Generally, the results of the evaluation of selectivity show very comparable results. Apart from some minor deviations at the extreme high and low methanol compositions in the mobile phase, the results from all SBA-C8 columns compare favorably with the Gemini C18 batch. As mentioned, column SBA-10C8 showed minor variability in the correlations of the natural log of the retention factor to both the mobile phase composition and the number of carbons in the alkylbenzene series when approaching the mobile phase composition of 100% methanol (Figure 50). SBA-26C8 (Figure 52) also showed some variability at the high aqueous concentration in the mobile phase, however, this was most likely due to stopping the flow in between measurements with high aqueous mobile phase concentrations, allowing for the exclusion of liquid from the porous space in between measurements and resulting in a loss of the available surface for retention [73].

The plot of the slope of the natural log of the retention factor versus the number of carbons in adjacent members of the series against the methanol composition of the mobile phase for all columns shows comparable results. There is slight variability approaching the high methanol content in the mobile phase (Figure 27). From the plot of ln k vs MeOH compositionin Figures

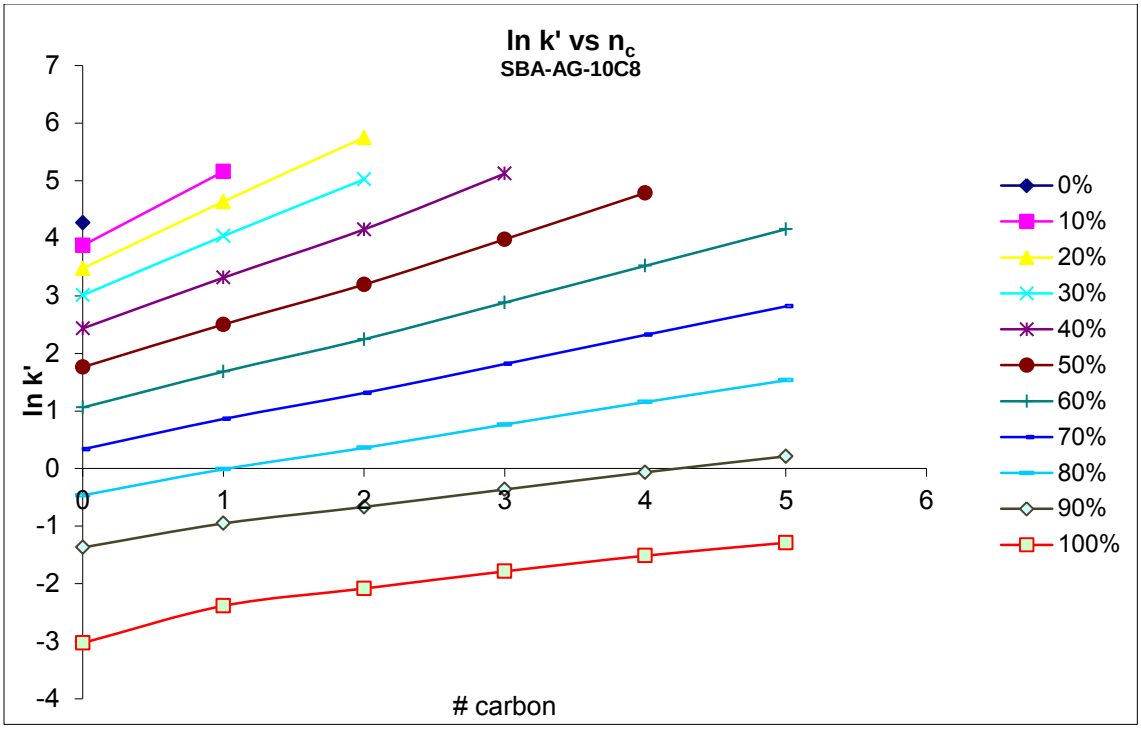

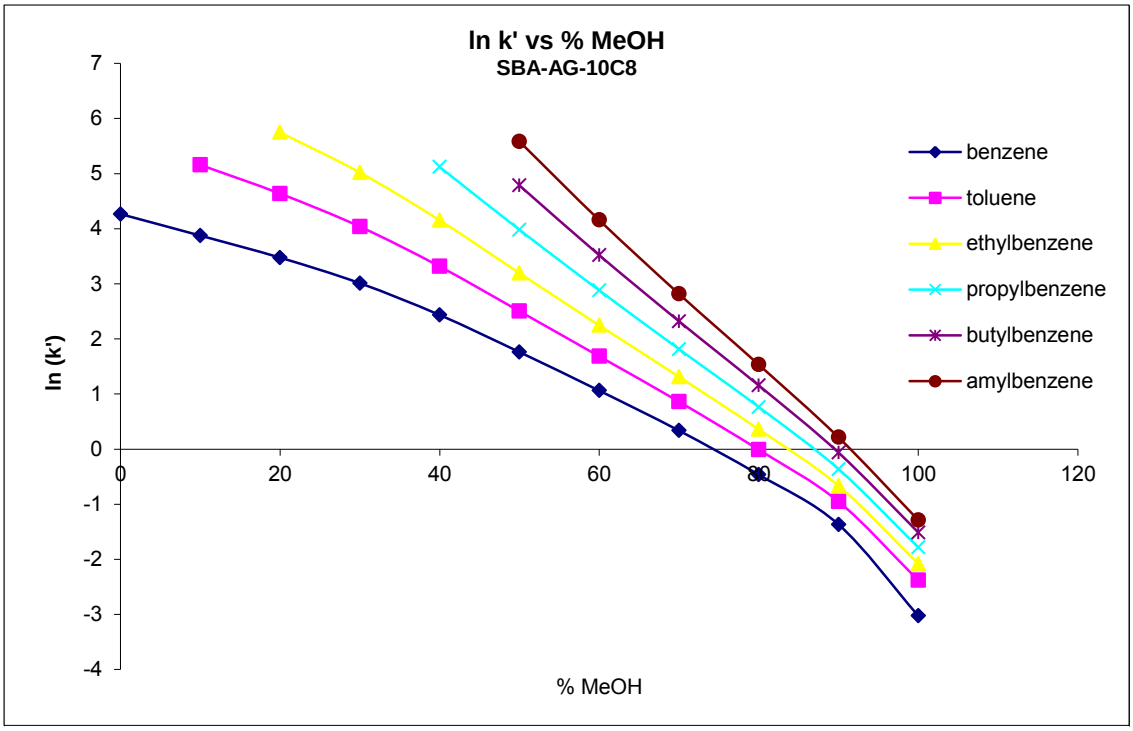

Figure 50. Methylene selectivity results for SBA-10C8

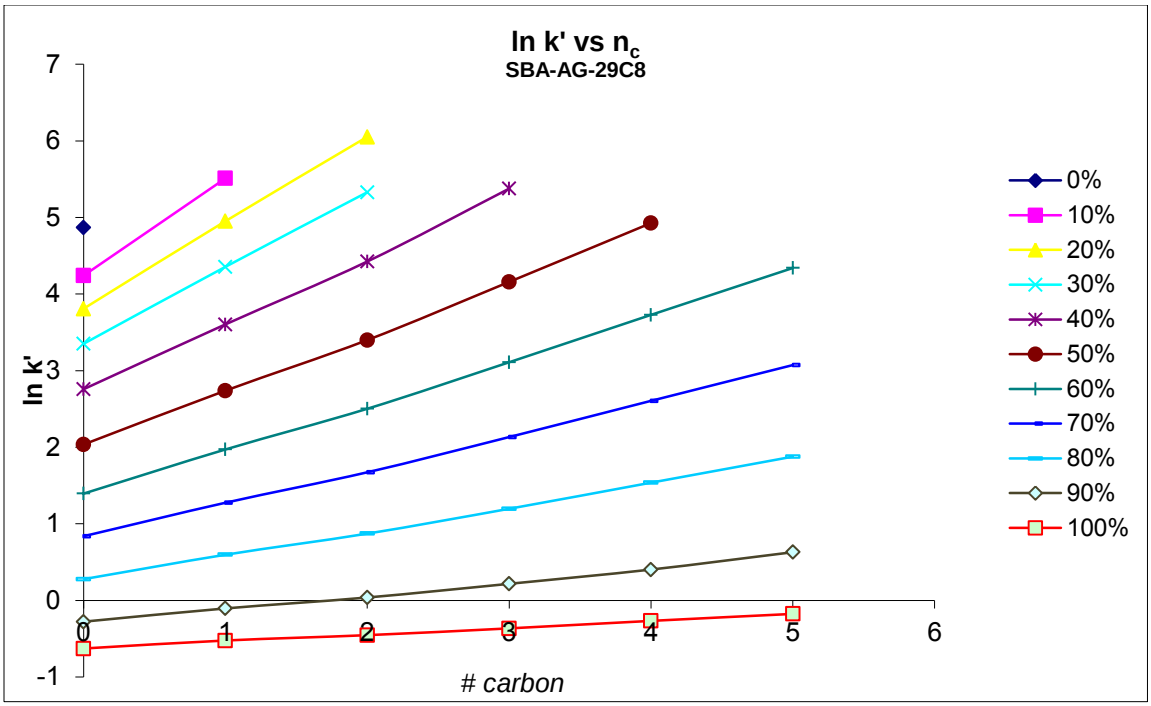

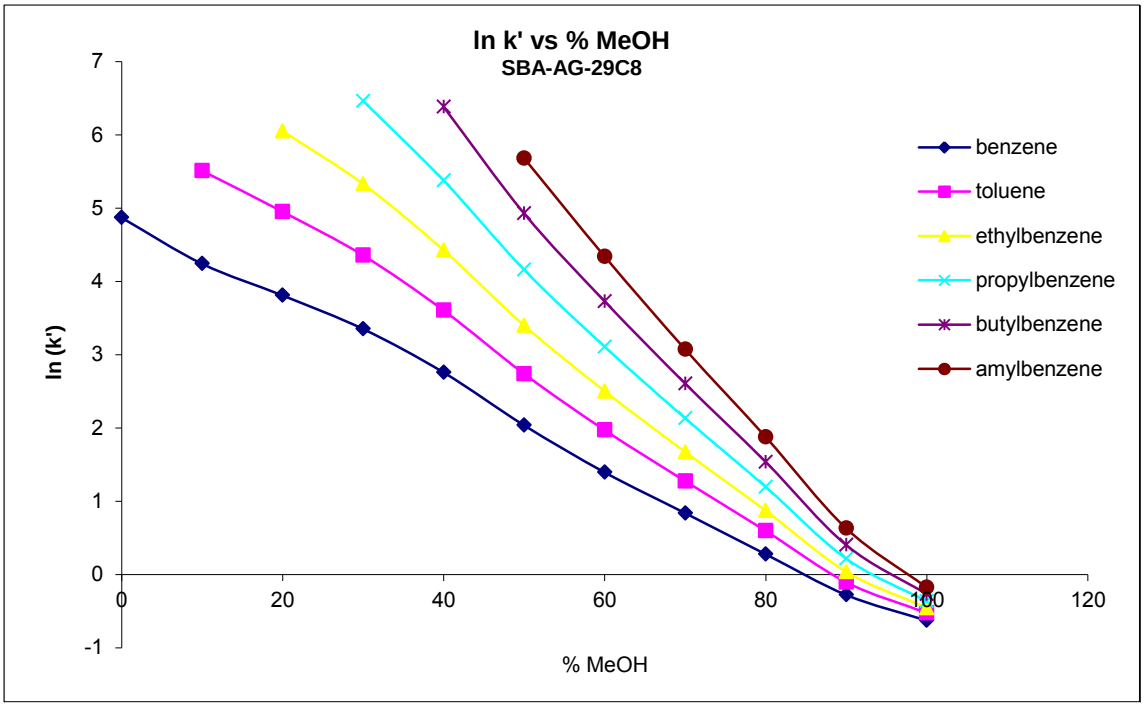

Figure 51. Methylene selectivity plots for SBA-29C8

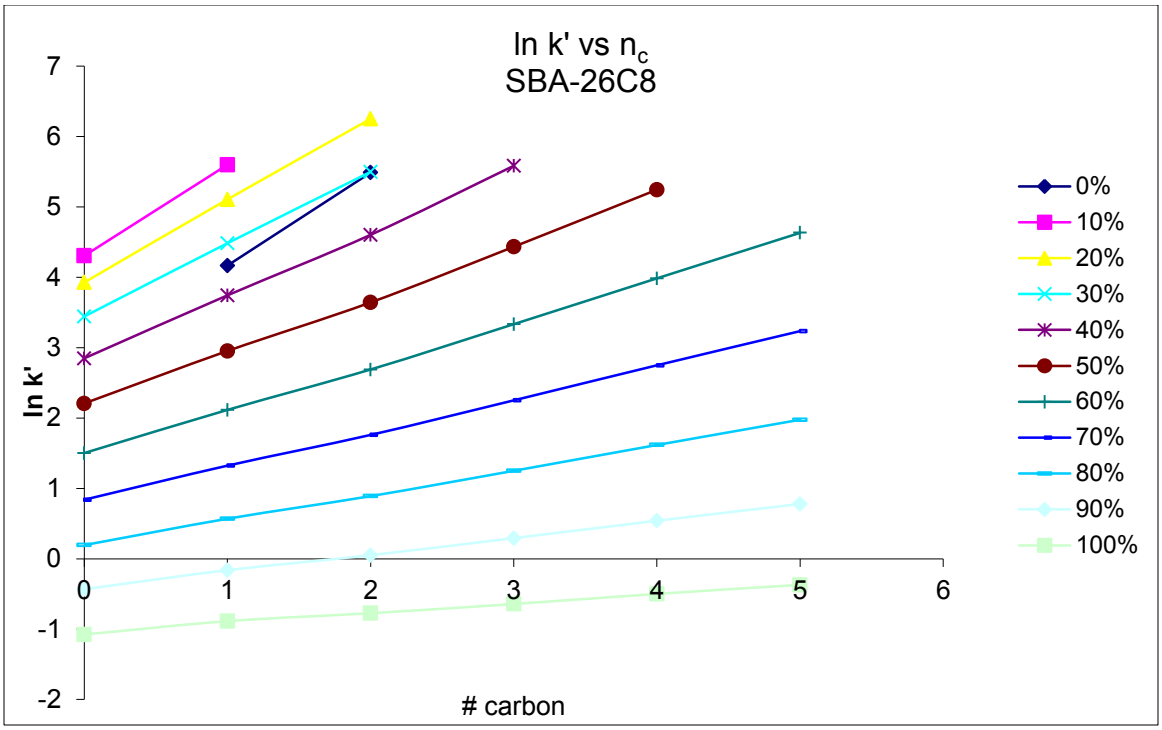

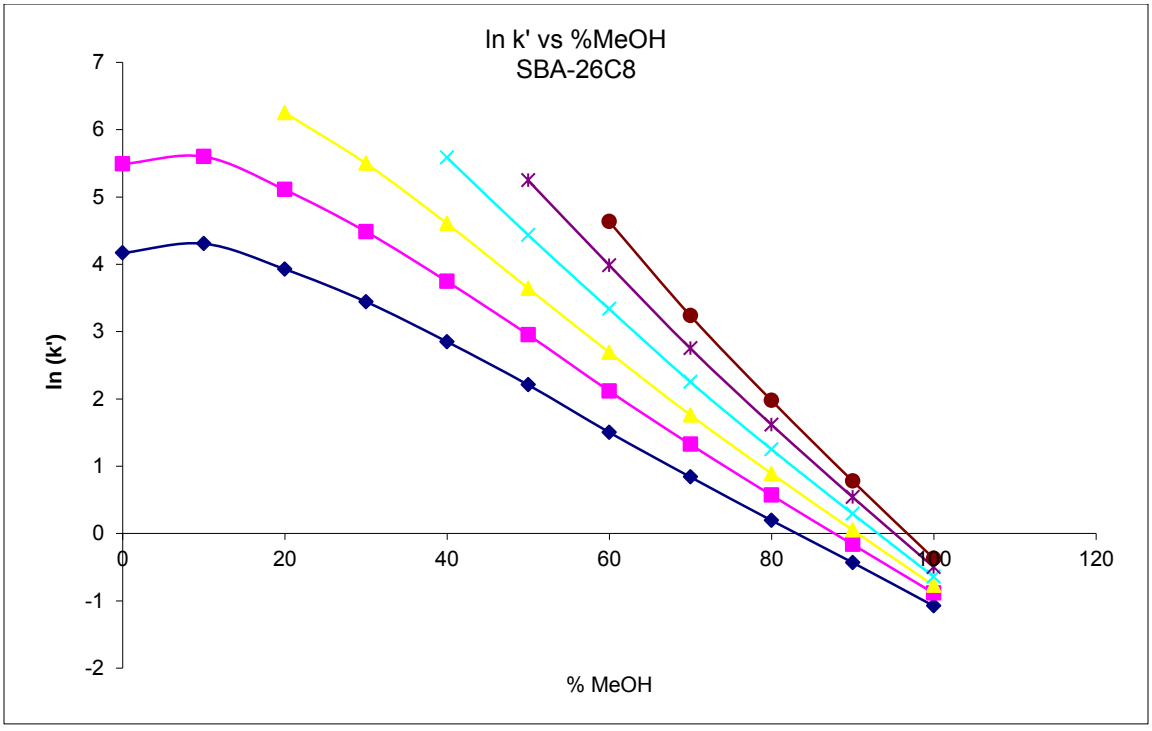

Figure 52. Methylene selectivity plots for SBA-26C8

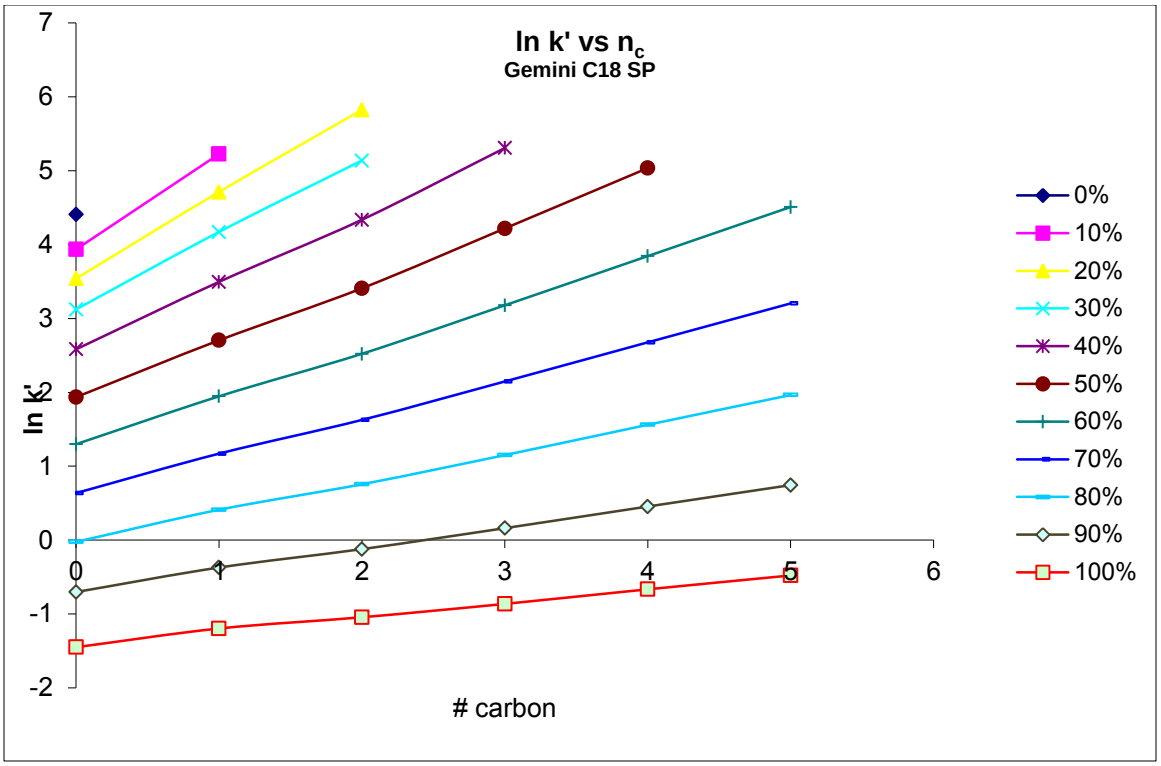

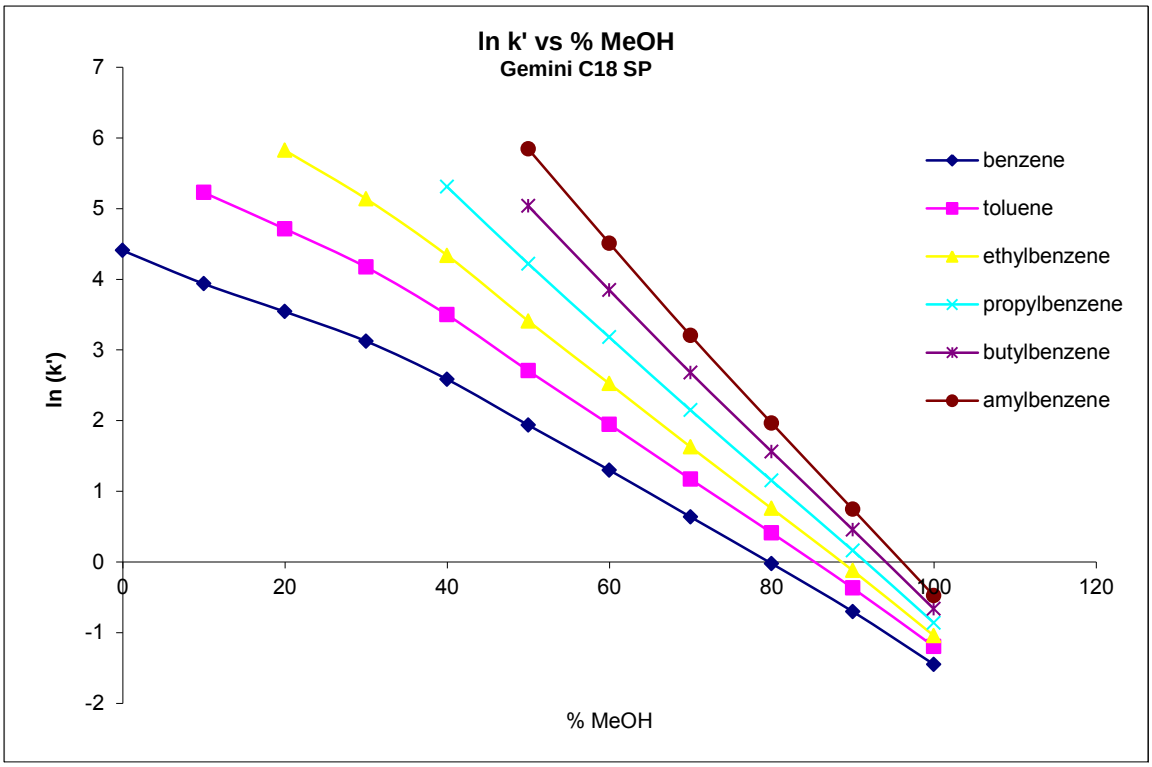

Figure 53. Methylene selectivity plots for Gemini C18

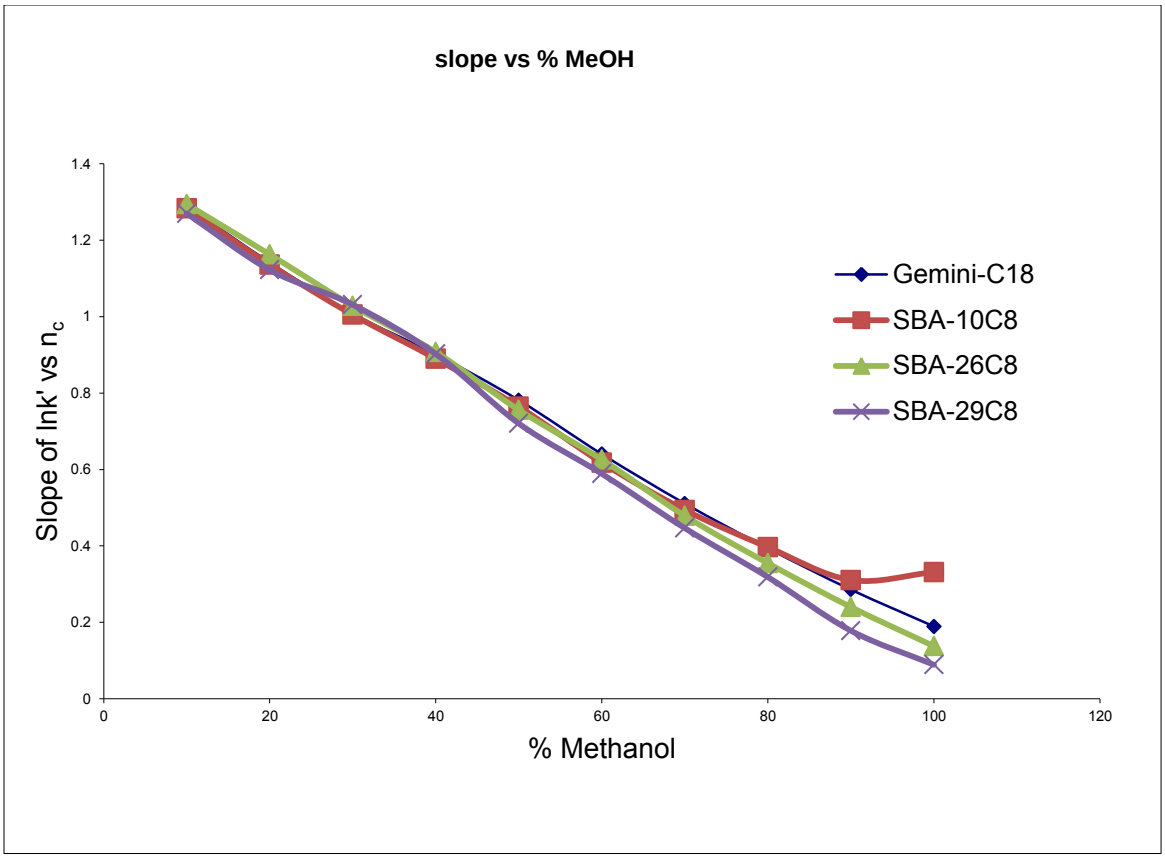

Figure 54. Methylene selectivity vs %MeOH for Gemini C18 and SBA -10C8, -26C8, and -29C8.

50-53, we can see the slight linear deviation of the lines corresponding to benzene and toluene. Plots of the logarithm of the retention factor should yield straight lines, however, the slight deviation from linear behavior for the first members of the homologous series can be expected [14]. Likewise the plot of the logarithm of the retention factor against the number of carbons in adjacent alkylbenzenes shows that for 100% methanol, there is a slight deviation from linear behavior for the data point associated with benzene. The overall increase in selectivity with increasing aqueous composition in the mobile phase can be mainly attributed to the analyte partition coefficient with the adsorbed organic layer [21]. The analytes show an increased energetic preference to distribute into the adsorbed organic layer on the surface of the modified silica as the organic concentration decreases in the mobile phase[21].

The plot of the selectivity (EB/T) vs % Methanol between SBA-10C8 and the Gemini C18 column show close comparability (Figure 55). Similar results are observed for the methylene selectivity performed with acetonitrile as the mobile phase (Figure 56). These results seem to confirm the conclusion of Engelhardt [71] that the dependence of methylene selectivity on the carbon load reaches a limit at around 12%. The % carbon of C8 modified silica (at least in this study) is roughly 18%. Therefore, it is clear that methylene selectivity does not discriminate between surfaces modified with C8 or C18.

It is interesting to note the similarities between the minor deviations seen with both methanol and acetonitrile as the mobile phase. The ln k vs organic and number of carbons show minor deviations at high organic content in the mobile phase, especially for benzene and toluene, the first members of the series. At high acetonitrile content, the analyte partition coefficient is low, meaning there is less energetic preference to penetrate into the organic layer. At these conditions, the retention of benzene and toluene are more governed by the specific dispersion

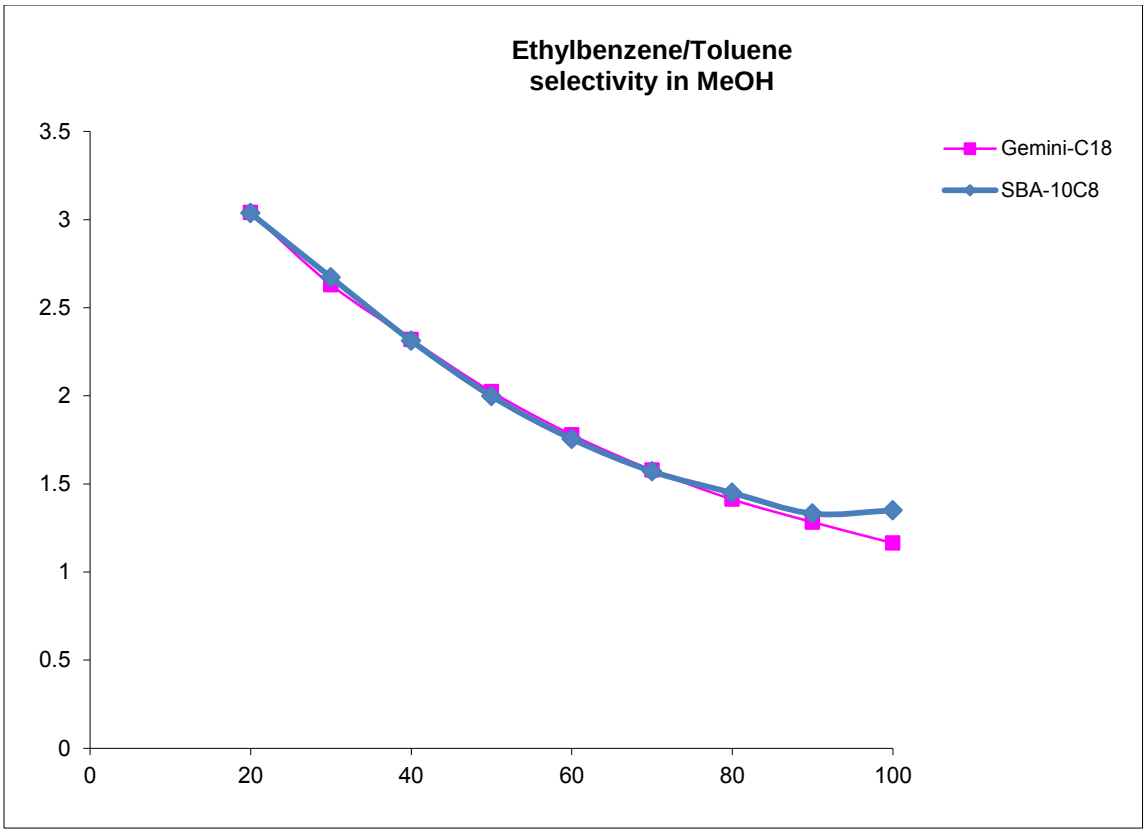

Figure 55. Plot of selectivity of ethylbenzene to toluene for both SBA-10C8 and Gemini C18

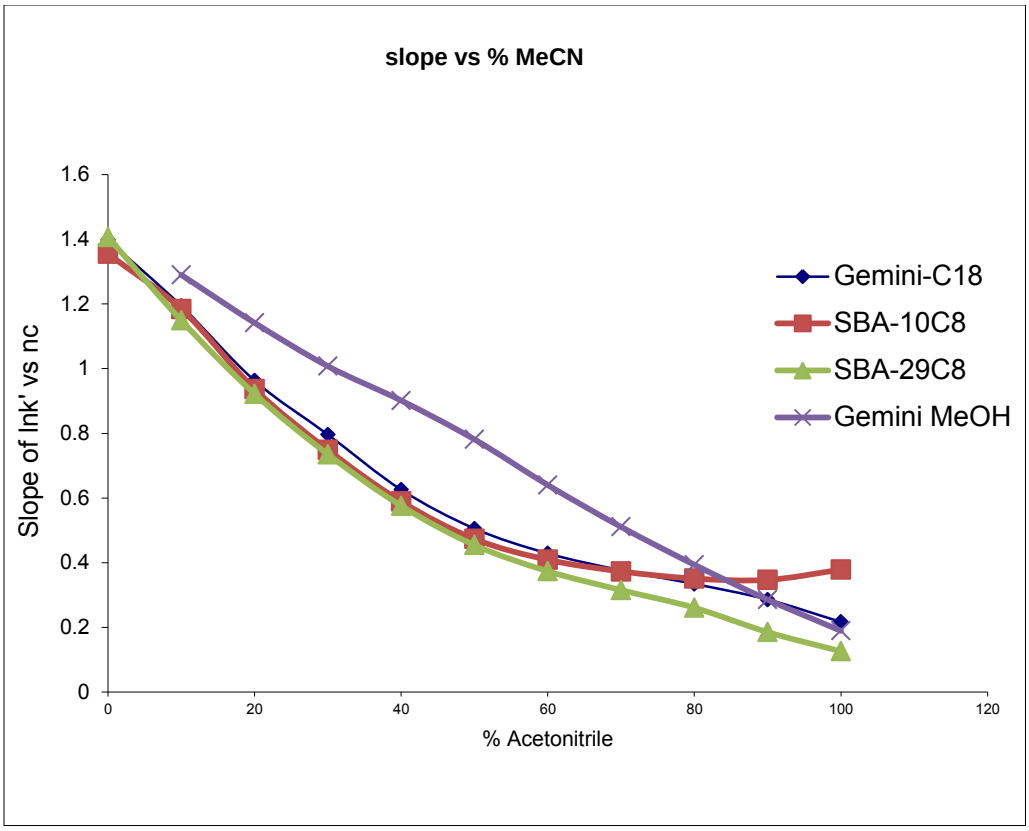

Figure 56. Slope of lnk on n_c versus % MeCN

type interactions with the modified surface and it would seem reasonable that slight differences in the stationary phase structure could influence its ability to retain the analyte. For example, for SBA-10C8, at 100% methanol, the retention of benzene is lower in value than would be expected by trending the values for the other mobile phase compositions and number of carbons, resulting in a lower retention than expected and a higher selectivity of toluene to benzene. This result gives the indication that the SBA-C8 materials show less than expected separation ability at high organic contents, where the stationary phase structure and physio-chemical properties become more of a determining factor as compared to analyte distribution into or out of the bulk mobile phase.

4.5 Surface Specific Retention

From the results of the methylene selectivity, at least to the author, it was clear that something was amiss. For example, the column packed with SBA-batch 10C8 is a 100 x 3.0 mm column with the modified silica having a surface area of roughly 512 square meters per gram. In comparison, the Gemini C18 column, also packed into a 100 x 3.0 mm column using the same packing method, has silica exhibiting a specific surface area of roughly 244 square meters per gram. However, the retention of alkylbenzenes in both columns were closely comparable. In theory, according to Eq. (16), the retention of alkylbenzenes in the SBA column should have been roughly twice the retention observed for the Gemini C18 column as retention is proportional to the total surface area in the column

The retention data for column SBA-26C8, SBA-29C29, and SBA-10C8 were compared to the slurry packed Gemini C-18 column as well as two other commercial silica batches for which we

obtained data on the column and adsorbent geometry. Table V shows the adsorbent and column characteristics of the two additional commercial columns (Prodigy and Luna) used as comparators in this study. Using the retention data obtained from the methylene selectivity experiments, as well as the calculated mass of adsorbent in each column (and thus total surface area), surface specific retention factors for each column were calculated. Additional retention data for the SBA-26C8 column performed at a second date was also included to show the reproducibility of the results.

It has been previously shown [20] that the use of surface specific retention factors across different columns provides a superior way to compare retention properties of adsorbent. Traditional retention factors describe the adjusted retention volume related to the column void volume. This could be misleading in columns that have similar void volumes but different total surface areas. Alternatively, the surface specific retention factor relates the adjusted retention volume to the total surface area in the column. It was previously shown that while the distribution of retention factors across several columns with the same chromatographic conditions exceeded 30%, the relative standard deviation of the surface specific retention factors was roughly 3% [20]. The comparison of the SBA C8 columns to the commercial columns in this study exhibited quite the opposite phenomenon. Although the retention of alkylbenzenes on the Gemini-C18 and other commercial columns studied showed close comparison in both the acetonitrile and methanol chromatographic systems when using the surface specific retention factors, the SBA C8 columns exhibited surface specific retention factors with relative standard deviations of about 20% (Figures 57-60).

From the plots, it is clear that surface specific retention factors of the SBA columns show more deviation than the comparison of the traditional retention factors. The surface specific retention

TABLE V. Column characteristics for commercial and SBA-15 (batch 26) columns

	SILICA CHARACTERISTICS			
Silica	S_{BET}	R_{pore}	2*Vp/R	V_{pore}
	m^2/g	Å	m^2/g	mL
Prodigy	228	55.1	221	0.256
Luna	270	41.5	288.2	0.598
SBA-15	479	29.7	409	0.608

	COLUMN CHARACTERISTICS				**Adsorbent**		**S_{total}**	
Silica	Dimensions	Vo	Vip	Vpore			(calc.)	(weighed)
	mm	mL	mL	mL	(calc, g)	(weighed,g)	m^2	m^2
Prodigy	50 x 4.6	0.526	0.270	0.256	0.4197	0.4473	96	102
Luna	100 x 4.6	1.062	0.545	0.517	0.865	0.9424	234	254
SBA-15	50 x 3.0	0.229	0.181	0.048	0.079	0.1813	38	87

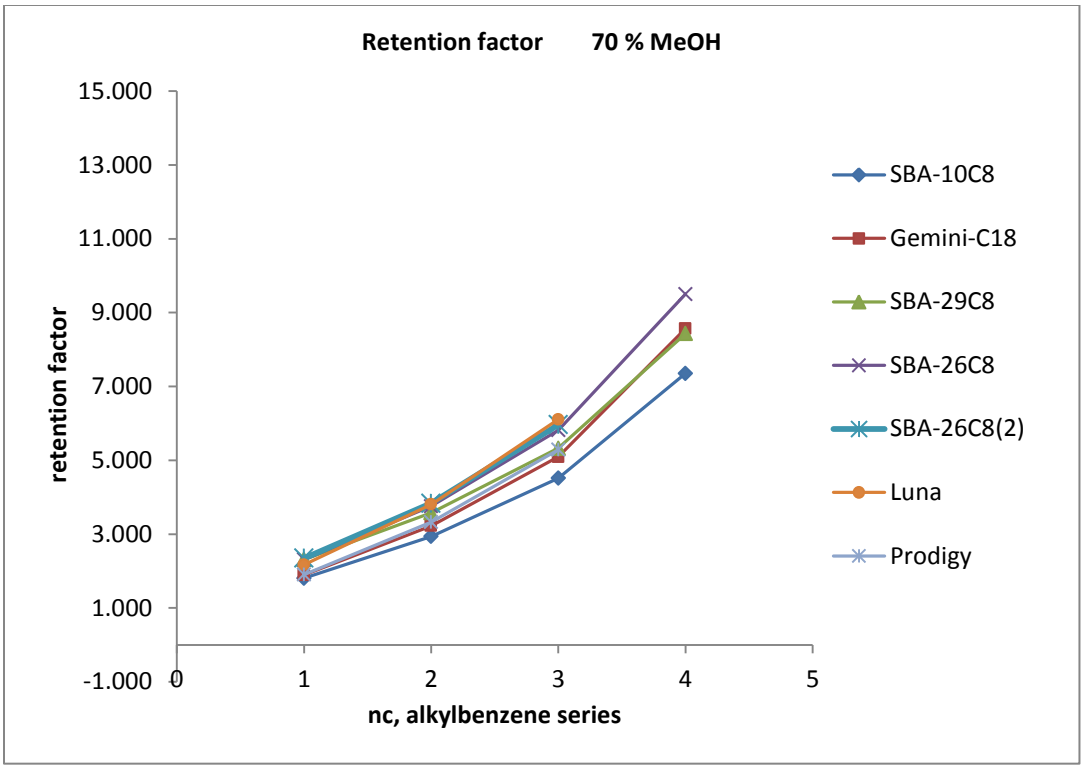

Figure 57. Comparison of traditional retention factors at 70% MeOH

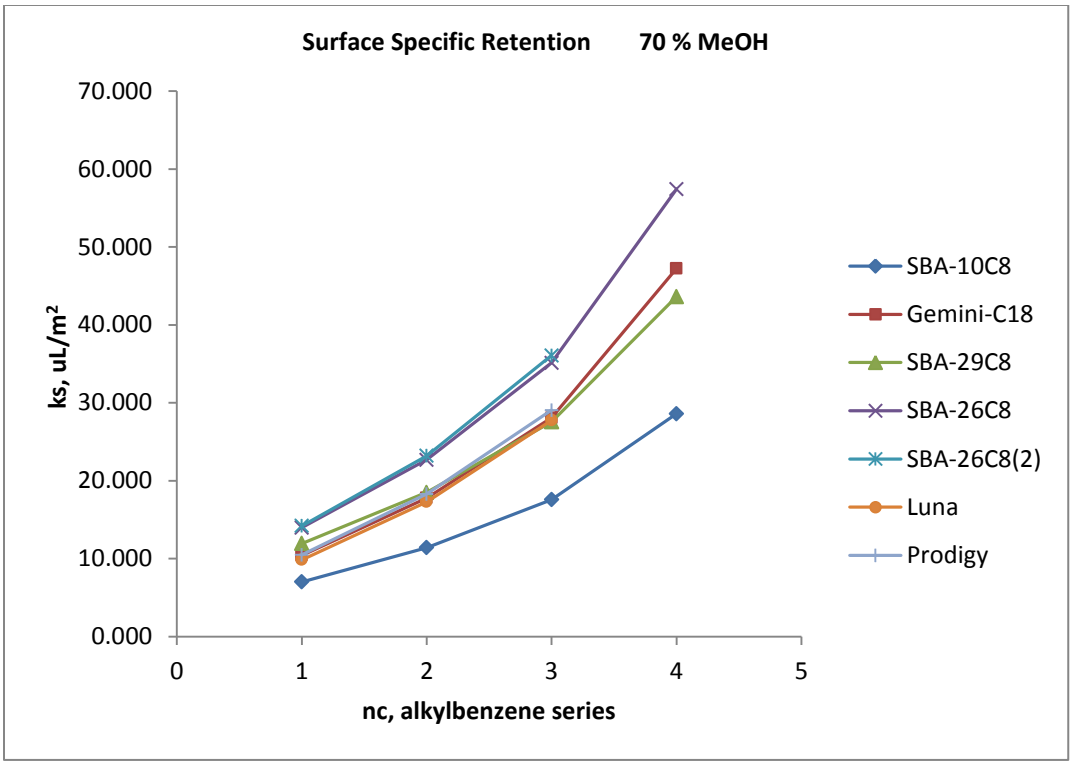

Figure 58. Comparison of surface specific retention factors at 70% MeOH

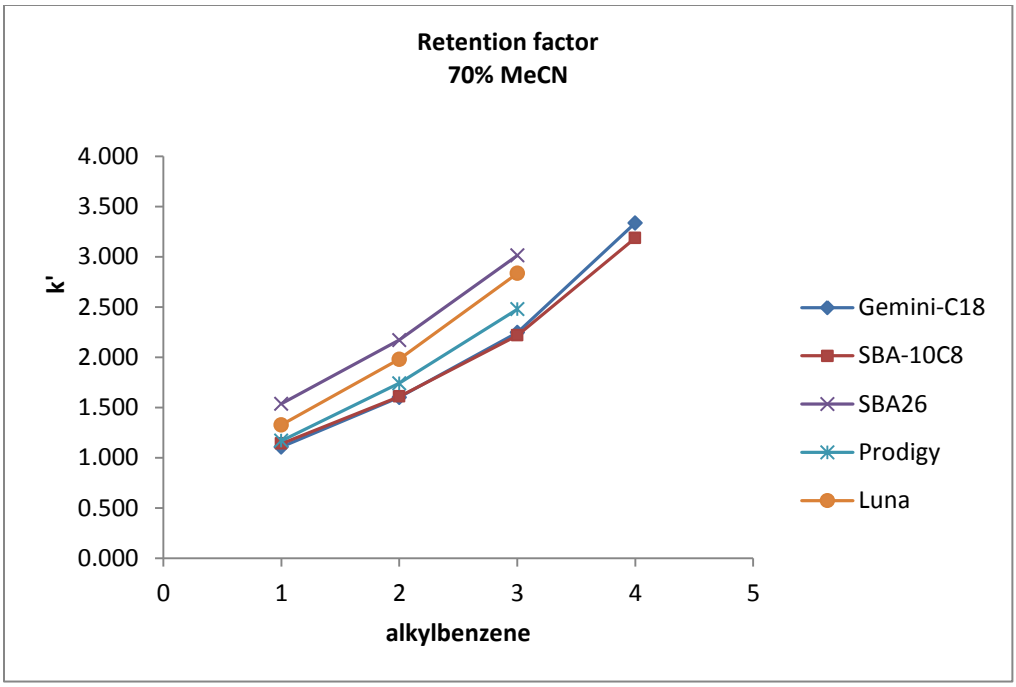

Figure 59. Comparison of traditional retention factors at 70% MeCN

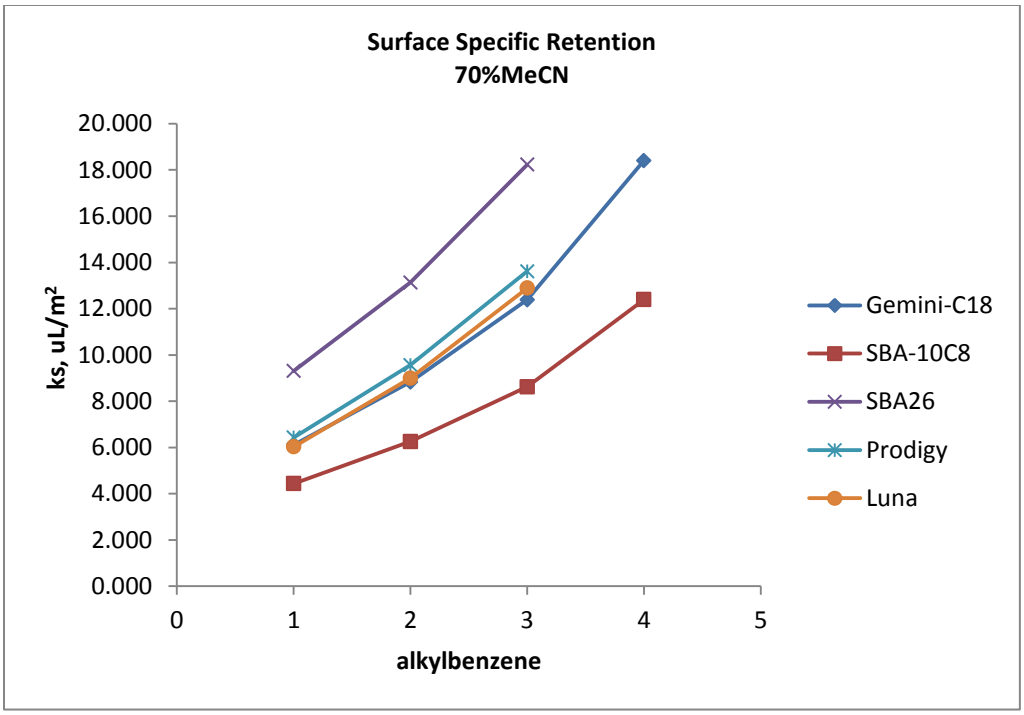

Figure 60. Comparison of surface specific retention factors at 70% MeCN

factors were calculated using the total surface area in the column determined by calculating the mass inside the column using Eq (22).

$$m_{ads} = \frac{V_O - V_{ip}}{V_P}$$

This relationship of the column pore volume to the specific pore volume as determined by low temperature nitrogen adsorption involves the characterization of the columns as described in 4.1. The fact that the calculated mass and total surface area inside the commercial silica columns provided similar surface specific retention factors demonstrates the validity of the method. Similarly, the opposite situation as seen with the SBA C8 columns points to an error in the estimation of the column mass and total surface area inside the column. The determination of the column pore volume comes through the measurement of the void volume and interparticle volume of the column. While there is evidence, through the calculated packing densities of the columns (Table I), that the value of the interparticle volume is correct, it is reasonable to suspect that the determination of the void volume resulted in an underestimation of the column pore volume.

In order to determine the actual mass of adsorbent inside the column, the SBA-26C8 as well as the Prodigy and Luna column, were unpacked and dried to constant weight before weighing. As can be seen in Table VI, the actual mass of adsorbent for the commercial columns obtained match closely with the theoretical masses estimated through Eq (22). Conversely, the SBA-26C8 column has an actual mass of adsorbent more than twice the estimated value. Figures 61 and 62 shows a comparison of the surface specific retention factor of SBA-26C8 obtained from weighing the adsorbent as opposed to using the estimated value. From this it is clear that roughly half of the surface area of the SBA C8 material is not seen by the HPLC

TABLE VI. Surface specific Retention for SBA batch 26 calculated with weighed column mass.

	Surface Specific Retention Factors					
Silica	**70/30 MeOH**			**70/30MeCN**		
	With calculated mass					
	benzene	toluene	ethylben	benzene	toluene	ethylben
Prodigy	10.5	18.3	29.1	6.4	9.56	13.6
Luna	9.86	17.3	27.8	6.0	9.00	12.9
SBA-15	14.2	23.2	36.1	9.3	13.1	18.2

	Surface Specific Retention Factors					
Silica	**70/30 MeOH**			**70/30MeCN**		
	With weighed mass					
	benzene	toluene	ethylben	benzene	toluene	ethylben
Prodigy	9.83	17.2	27.3	6.03	8.97	12.8
Luna	9.05	15.9	25.5	5.53	8.26	11.8
SBA-15	6.20	10.1	15.7	4.05	5.72	7.95

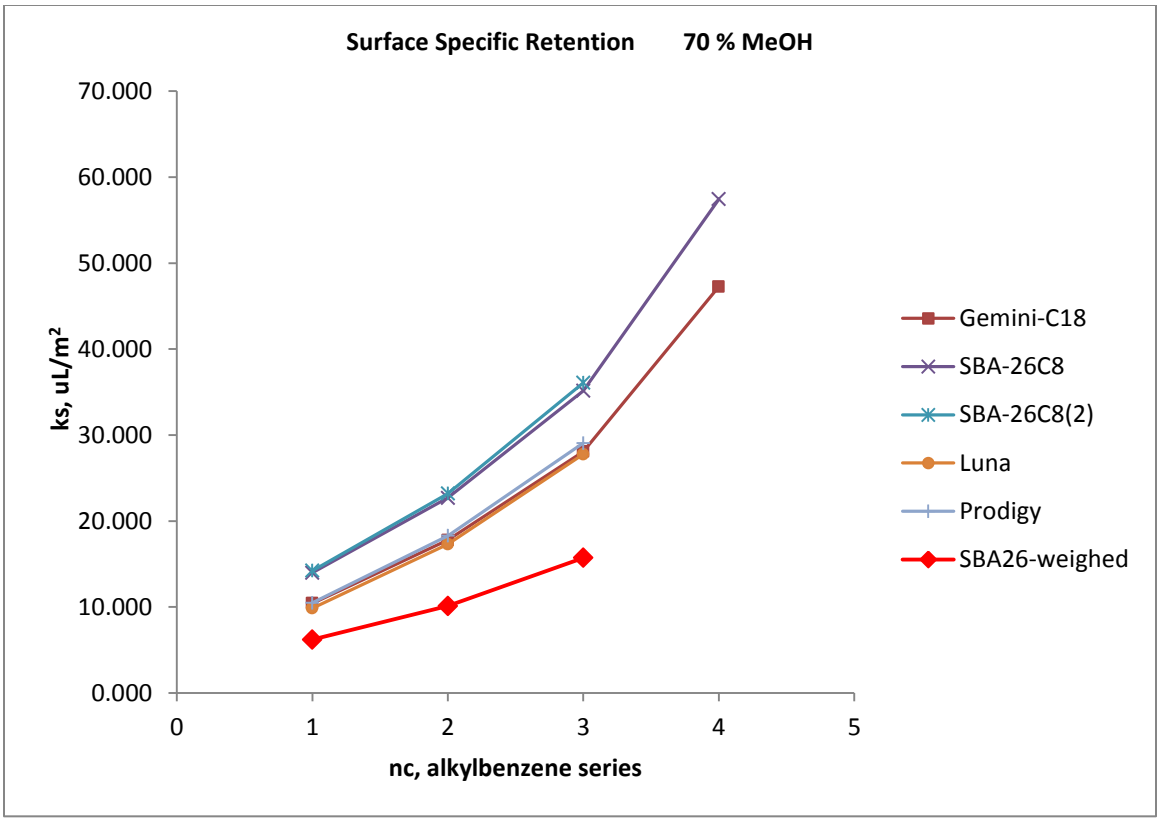

Figure 61. Comparison of Surface specific retention factor for SBA-26C8 after weighing the adsorbent

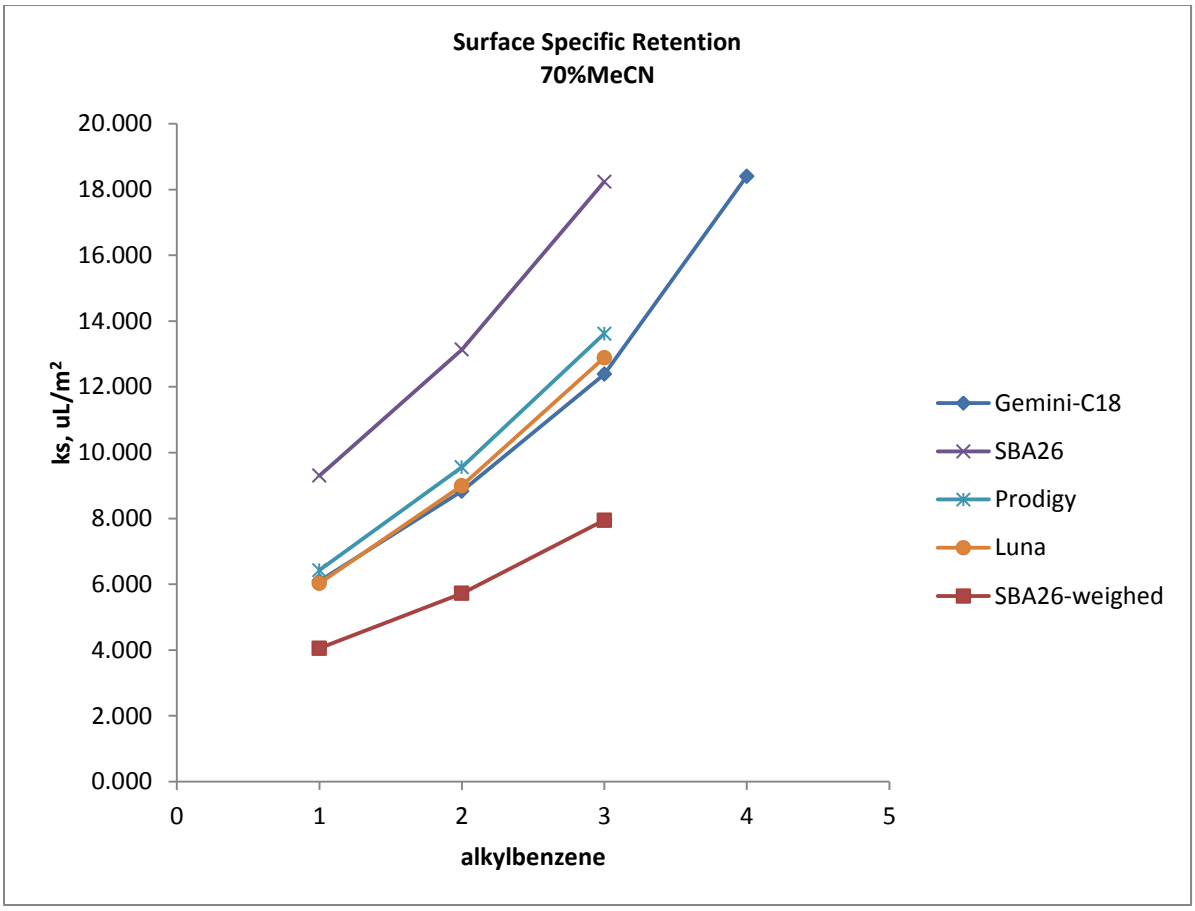

Figure 62. Comparison of surface specific retention for SBA 26C8 after weighing the adsorbent in the column

chromatographic system. Now it makes sense why the SBA-10C8 column with twice the surface area showed the same retention as compared to the Gemini C18 column.

To answer the question of how half of the pore volume/surface area is not being seen in the SBA C8 column requires a discussion of microporosity, pore structure and modification. The most obvious reason for the apparent disparity between the surface areas as seen by chromatography and low temperature nitrogen adsorption would be the presence of micropores. However, as was seen in the discussion of the synthesis of the spherical SBA-15 materials, t-plots showed the absence of micropores. In fact, as seen between the single and dual ageing schemes, the hydrothermal treatment obtained during the second ageing was responsible for the development of the pore structure and the absence of micropores.

In terms of the pore size, all of the modified spherical SBA silicas exhibit pore diameters ranging from 50Å to 60Å. Although this is on the low range of desirable pore sizes for adsorbents in chromatography [6], it should still allow the complete penetration of mobile phase into the porous space. Since the estimation of mass inside the columns under estimated the mass by roughly two times, there must be a significant obstruction to the mobile phase penetration into the pores, as the void volume is determined by a deuterated component of the mobile phase. As we saw with the determination of the effective diffusion coefficient, the determination of γ provided an insight into the porous structure of the modified material. Perhaps the reason for the high level of obstruction arose from a combination of the porous structure and modification. Figure 63 shows an overlay of the nitrogen adsorption isotherms for the bare silica and C1 through C18 modified samples of batch 29. Through the shift of the desorption branch along the P/Ps axis, we can determine with the Kelvin equation the relative range of the pore sizes calculated. In the case of the spherical SBA silicas, modification resulted in a significant

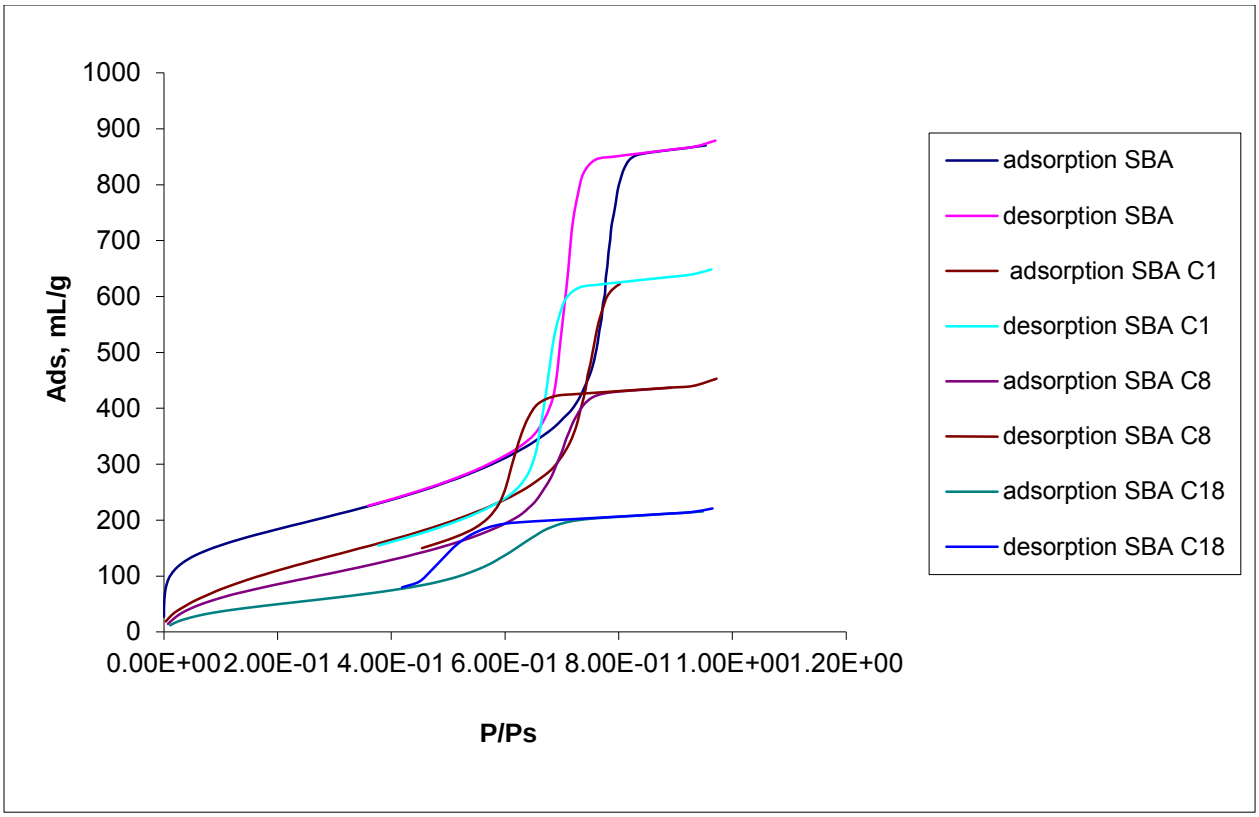

Figure 63. Overlay of isotherms for bare SBA 29 and C1-C18 modified samples. Shows the shift of the desorption isotherm

variation of the modified layer height yielding pore radii from 25Å to 12Å. Therefore, modified spherical SBA silicas may have situations where constricted pore sizes of around 20Å diameter could be present. In addition to this, it is evident from the discussion of the synthesis results, that a loss of pore structure was inevitable with change in morphology to spherical particles. Although we have no direct evidence of the exact pore structure inside of the particles, it seems with the data at hand, that spherical SBA silicas most likely exhibit the long narrow pores, perhaps slightly more interconnected than in the fibrous SBA, with the possible "wrapping-around" of the pores from the curvature of the spherical particles. The effect of curvature, in combination with modification may produce a scenario where severe restriction of the pore volume is confronted for liquid probes, i.e. HPLC mobile phase as opposed to the much smaller nitrogen molecule.

In order to possibly confirm the differences between modified and unmodified spherical SBA silicas in chromatography, the unmodified SBA 36 column was unpacked and weighed in order to compare the actual weight to the estimated value. Table VII shows the actual mass inside the column for SBA 36 compares closely to the estimated weight. Therefore the void volume determination was accurately able to determine the volume of liquid inside the column which includes the liquid inside the pores. From this result it seems more likely that the loss of available surface is due to a loss of pore volume under chromatographic conditions from the constriction of pore diameters as consequence of the combination of the tortuous pore structure inside the spherical particle and modification.

TABLE VII. Weighed mass of adsorbent for SBA Batch 26 and 36

Column Characterization	Vo mL/column	Vpore mL/column	Vpore mL/g	calculated mass ads g	weighed mass ads g
SBA-AG-26 C8	0.229	0.048	0.61	0.079	0.1813
SBA-AG-36	0.151	0.088	1.09	0.0564	0.0688

V. Conclusions

1. Initial experiments to study the effect of flow rate on retention did not yield the expected increase in retention. However, in light of the limited accessible surface when using spherical SBA-15 stationary phased, it is reasonable that such increase in retention was not possible given the limited surface area available for the process of retention.

2. Due to the obstruction and or tortuosity observed in the SBA columns, the atypical peak shape observed at fast flow rates which became Gaussian at slow flow rates could be indicative of the obstruction encountered by analyte molecules at the different velocities. Under fast velocity, the obstruction would lead to only partial penetration in to the tortuous pores, yielding a bimodal peak shape from the difference in those analytes penetrating the porous space to those pushed through the column. On the other hand, the Gaussian peak shape observed at slow flow rates could be a result of the increased ability of analyte molecules to diffuse into the tortuous or obstructed pores at the very slow flow.

4. Kinetic studies showed the increased resistance to mass transfer for the SBA columns as compared to commercial columns.

5. Kinetic studies also showed the successful calculation of the obstructive parameter, γ, which was confirmed with the comparison of the commercial column obstructive parameter to typical values found for columns in literature. The presence of ordered pores, with known reduction in interconnectivity, may present the liquid system with difficulites in terms of analyte diffusive paths. SBA silicas with smaller diffusive paths, i.e. monoliths or superficially porous particels may present a better opportunity to evaluate the effect of ordered pores on retention.

6. Methylene selectivity data showed close caomparability to the commercial silica, indicating a well-modified and functional surface. However, when compared between columns, a loss of retention was observed in relation to the supposed surface area in the SBA columns.

7. Surface specific retention studies were able to show the ineffectiveness of spherical SBA-15 as a stationary pahse for anything other than academic research. Up to half of the surface area as seen with LTNA was not accessible in chromatography. Evaluation of the bare silica show the absence of microporosity. It is proposed that the long, narrow pores, which may bend and turn, can produce a situation – especially when modified – as we saw evidence of the variation of bonded layer height. Bare SBA silica showed an ability to be accurately characterized through chromatography. Therefore, the modification in combination with the nature of the pores results in a system not indicative to liquid accessibility.

   Another , however more remote possibility, is perhaps in these long narrow pores, there is only diffusion, and nothing else. And perhaps in silica gel – although it is popularly believed there is only diffusion inside the "stagnant" pores-perhaps there is a measure of convective flow inside the super connected intraparticle spaces. Perhaps the great difference in the available surface area is really only because we never had any other real structure to judge the mechanism of chromatography against- instead of mathematical models. Although a long-shot, it is reasonable that we could be actually observing what a stagnant pore really does to chromatography.

VI. References

1. Y. Kazakevich, J Chrom A 1126 (2006) 232-243
2. F Gritti, Y. Kazakevich, G. Guiochon, J Chrom A 1169 (2007) 111-124
3. F. Chan, L.S. Yeung, R. LoBrutto, Y.V. Kazakevich, J Chrom A 1069 (2005) 217-224
4. I. Rustamov, T. Farcas, F. Ahmed, F. Chan, R. LoBrutto, H.M. McNair, Y.V. Kazakevich, J Chrom A 913 (2001) 49-63
5. A. Vailaya, Cs. Horvath, J Chrom A 829 (1998) 1-27
6. Y.V. Kazakevich, R. LoBrutto, HPLC for Pharmaceutical Scientists, Wiley-Interscience, NJ, 2007 (Chapters 1,2,3 and 17)
7. A.V. Kiselev, J Chrom 49 **1970**, 84-129
8. A. Cavazzini, F. Gritti, K. Kaczmarski, N. Marchetti, G. Guichon, Anal. Chem., 2007, 79 (15) 5972-5979.
9. K.K. Unger, R. Skudas, M.M. Schulte, J Chrom A 1184 (2008) 393
10. J. Zhao, F. Gao, Y. Fu, W. Jin, P. Yang, D. Zhao, Chem Comm. 18 March 2002.
11. M. Ide, E Wallaert, I. Van Driessche, F. Lymen, P. Sandra, P. Van Der Voort, Micro. Meso. Mater. 142 (2011) 282-291
12. F. Gritti, G. Guiochon, J Chrom A 1075 (2005) 117-126
13. H. Colin, G. Guiochon, J Chrom 1977, 141, 289-312
14. Cs. Horvath, Melander W. Reversed Phase Chromatography In HPLC: Advances and Perspectives; Horvath, Ed. Academic Press: NY, 1980, vol.2, 113-303.
15. J.J. Kirkland, Modern Practice of liquid chromatography, Wiley-Interscience, NY, 1971., chapter 1.
16. G. Guiochon, J Chrom A 1126 (2006) 6-49.

17. G. Guiochon, A. Felinger, A.M. Katti, D. Shirazi, Fundamentals of Preparative and Non-Linear Chromatography, 2nd ed., Elsevier, Amsterdam, Netherlands, 2006.
18. G. Guiochon J Chrom A 965 (2002) 129-161.
19. E. Wen, R. Asiaie, Cs. Horvath, J Chrom A 855 (1999) 349-366.
20. A. Giaquinto, Z. Liu, A. Bach, Y.V. Kazakevich, Anal. Chem 2008 80 6358-6364
21. Y.V. Kazakevich, R. LoBrutto, F. Chan, T. Patel, J Chrom A 913 (2001) 75-87
22. M. Jaroneic, J Chrom A 656 (1993) 37-50
23. G. Foti, M. Belvito, A. Alvarez-Zepeda, E. Kovats, J Chrom A 630 (1993)
24. K. Unger, J Chrom A 1060 (2004) 1-7.
25. J.J Kirkland, F.A. Truszkowski, R.D. Ricker, J Chrom A 965 (2002) 25-34
26. K. Unger et al., J Chrom A 892 (2000) 47-55.
27. L.R. Snyder, J.L. Glajch, J.J. Kirkland, in Practical Method Development, 2nd Ed., Wiley, N.Y., 1997, Chp.5.
28. J.J. Kirkland J Chrom A 1060 (2004) 9-21.
29. J.J Kirkland, J.J. DeStefano, J Chrom A 1126 (2006) 50-57.
30. F. Gritti, G. Guiochon, J Chrom A 1217 (2010) 5069-5083.
31. D. Cabooter, A. Fanigliulo, G. Bellazzi, A. Rottigini, G. Desmet, J Chrom A 1217 (2010) 7074-7081.
32. C. Dawaele, M. Verzela, J Chrom 260 (1993) 13.
33. F. Gritti, G. Guiochon, J Chrom A 1166 (2007) 30-46.
34. M. Kele, G. Guiochon, J Chrom A 855 (1999) 423-453.
35. F. Gritti, G. Guiochon, J Chrom A 1176 (2007) 107-122.

36. L. Hong, A. Felinger, K. Kaczmarski, G. Guiochon, Chem. Eng. Sci 59 (2004) 3399-3412.
37. A. Felinger J Chrom A 1126 (206) 120-28.
38. K. Miyabe J Chrom A 1183 (2008) 49-64.
39. J.C. Giddings, Dynamics of Chromatography, Principles and Theory, Marcel Dekker, N.Y., 1965.
40. K. Miyabe, A. Cavazzini, F. Gritti, M. Kele, G. Guiochon, Anal. Chem. 2003, 75 (24), 6975-6986.
41. F. Gritti, G. Guiochon, Chem. Eng. Sci. 61 (2006) 7636-7650.
42. J.J. Meyers, S. Nahar, D.K. Ludlow, A.I. Liapis, J Chrom A 907 (2001) 57-21.
43. J.J Meyers, A.I. Liapis, J Chrom A 827 (1998) 197-213.
44. J.J. Meyers, O.K. Crosser, A.I. Liapis, J Chrom A 908 (2001) 35-47.
45. J.F. Langsford, M.R. Schure, Y. Yao, S.F. Maloney, A.M. Lenhoff, J Chrom A 1126 (2006) 95-106.
46. A.I. Liapis, J.J. Meyers, O.K. Crosser, J Chrom A 865 (1999) 12-25.
47. K.C. Loh, D. Wang, J Chrom A 718 (1995) 239-255.
48. A. Cavazinni, F. Gritti, K. Kaczmarski, N. Marchetti, G. Guiochon, Anal. Chem. 2007, 79 (15), 5972-5979.
49. K. Miyabe, G. Guiochon, J Chrom A 1217 (2010) 1713-1734.
50. F. Gritti, A. Cavazzini, N. Marchetti, G. Guiochon, J Chrom A 1157 (2007) 289-303.
51. K. Miyabe, Anal. Chem. 2007, 79 (19), 7457-7472.
52. K. Miyabe, A. Cavazzini, F. Gritti, M. Kele, G. Guiochon, Anal. Chem. 2003, 75 (24), 6975-6986.

53. K. Miyabe, N. Ando, G. Guiochon, J Chrom A 1216 (2009) 4377-4382.

54. D.J. Richard, A.M. Striegel, J Chrom A 1217 (2010) 7131-7137.

55. A. Liekens, J. Denayer, G. Desmet, J Chrom A 1218 (2011) 4406-4416.

56. V. Wernet, R. Bouchet, R. Denyol, Micropor. Mesopor. Mater. 140 (2011) 97-102.

57. C.T. Kresge, M.E. Leonowicz, W.J. Roth, J.C. Vortuli, J.S. Beck, Nature 359 (1992) 710.

58. D. Zhao, J. Feng, Q. Huo, N. Melosh, G.H. Frederickson, B.F. Chemelka, G.D. Stucky, Science 279 (1998) 548.

59. Y. Ma, L. Qi, J. Ma, Y. Wu, O. Liu, H. Cheng, Colloids and Surfaces A: Phys. Chem Eng. Aspects 229 (2003) 1-8.

60. T. Martin, A. Galarneau, F. DiRenzo, D. Brunel, F. Fajula, Chem. Mater. 2004, 16, 1725-1713.

61. F. Fajula, A. Galarneau, F. DiRenzo, Micropor. Mesopor. Mater. 82 (2005) 227-239.

62. A. Galarneau, J. Iapichella, D. Brunel, F. Fajula, Z. Bayram-Hahn, K. Unger, G. Puy, C. Demesmay, J. Rocca, J. Sep. Sci. 2006, 29, 844-855.

63. R. Tian et al., Electrophoresis 2006, 27, 742-748.

64. G. Zhu, Q. Yang, D. Jiang, J. Yang, L. Zhang, Y. Li, C. Li, J Chrom A 1103 (2006) 257-264.

65. M. Bruzzoniti, R. DeCarlo, S. Fiorilli, B. Onida, C. Sarzanini, J. Chrom A 1216 (2009) 5540-5547.

66. H. Wan, L. Liu, C. Li, X. Xue, X. Liang, J. Coll. Inter. Sci. 337 (2009) 420-426.

67. X. Liu, L. Li, Y. Du, Z. Gao, T. Ong, Y. Chen, S. Ng, Y. Yang, J Chrom A 1216 (2009) 7767-7773.

68. T. Yasmin, K. Muller, J Chrom A 1218 (2011) 6464-6475.

69. A. Sardi, L. Szepesy, J Chrom A 818 (1998) 19-30.

70. A. Sardi, L. Szepesy, J Chrom A 845 (1999) 113-131.

71. H. Englelhardt, M. Jungheim, Chromatographia 29 (1990) 59.

72. J. Li, P.W. Carr, Anal. Chem. 1997 (69) 2530-2536.

73. T.H. Walter, P. Iraneta, M. Capparella, J Chrom A 1075 (2005) 177-183.

Appendix A1

Table AI. Experimental values for Gemini C18 cloumn (Methylene selectivity)

Retention Summary Gemini C18						
	VR					
%MeOH	Benzene	Toluene	Ethylben	Propylben	Butylben	Amylben
0	38.333	153.679				
10	22.264	72.407				
20	12.599	32.628	83.727			
30	6.353	13.097	28.668	62.241	143.069	
40	3.365	5.732	9.888	18.603	35.017	66.173
50	1.983	2.929	4.387	7.128	11.690	19.403
60	1.320	1.759	2.377	3.465	5.138	7.758
70	0.975	1.204	1.503	2.008	2.743	3.829
80	0.775	0.899	1.050	1.296	1.640	2.127
90	0.653	0.717	0.789	0.903	1.053	1.263
100	0.581	0.612	0.642	0.689	0.744	0.815

Gemini C18						
	Surface Specific Retention					
%MeOH	Benzene	Toluene	Ethylben	Propylben	Butylben	Amylben
0	451.177	1825.391				
10	259.734	857.129				
20	144.580	383.209	991.988			
30	70.167	150.513	336.024	736.007	1698.985	
40	34.568	62.768	112.282	216.111	411.671	782.852
50	18.103	29.374	46.744	79.406	133.757	225.642
60	10.210	15.440	22.803	35.759	55.691	86.905
70	6.100	8.828	12.384	18.401	27.158	40.096
80	3.717	5.188	6.987	9.924	14.017	19.825
90	2.264	3.026	3.884	5.242	7.023	9.531
100	1.406	1.775	2.133	2.687	3.348	4.188

Appendix A2

Table AII. Retention data for SBA batch 10C8

Retention Summary SBA-10C8						
	VR					
%MeOH	Benzene	Toluene	Ethylben	Propylben	Butylben	Amylben
0	33.718	129.016				
10	29.043	93.598				
20	15.735	39.259	99.280			
30	7.760	15.468	31.256	69.101		
40	3.967	6.540	11.000	19.852	35.776	64.491
50	2.263	3.263	4.786	7.469	11.787	18.576
60	1.462	1.913	2.544	3.591	5.126	7.394
70	1.057	1.288	1.589	2.068	2.737	3.680
80	0.828	0.950	1.097	1.325	1.628	2.033
90	0.688	0.749	0.818	0.920	1.049	1.211
100	0.611	0.637	0.663	0.704	0.751	0.805

SBA-10C8						
	Surface Specific Retention					
%MeOH	Benzene	Toluene	Ethylben	Propylben	Butylben	Amylben
0	261.652	1012.172				
10	224.834	733.241				
20	120.027	305.294	777.990			
30	57.226	117.924	242.266	540.315		
40	27.352	47.615	82.740	152.454	277.864	504.005
50	13.928	21.803	33.798	54.928	88.938	142.405
60	7.623	11.175	16.141	24.390	36.475	54.337
70	4.437	6.256	8.621	12.393	17.667	25.094
80	2.630	3.589	4.749	6.547	8.928	12.118
90	1.528	2.008	2.552	3.355	4.371	5.647
100	0.921	1.129	1.331	1.654	2.024	2.449

Appendix A3

Table AIII Methylene selectivity data in MeOH; SBA 29C8

Retention Summary SBA-29C8						
	VR					
%MeOH	Benzene	Toluene	Ethylben	Propylben	Butylben	Amylben
0	22.559	91.463				
10	14.343	45.538	140.906			
20	7.900	19.605	48.814			
30	3.880	7.671	15.430	33.759		
40	1.985	3.257	5.450	9.787	17.545	31.420
50	1.149	1.650	2.408	3.752	5.867	9.255
60	0.752	0.978	1.293	1.817	2.580	3.698
70	0.548	0.662	0.810	1.048	1.379	1.835
80	0.435	0.497	0.571	0.686	0.837	1.038
90	0.352	0.379	0.408	0.452	0.504	0.569
100	0.318	0.328	0.341	0.362	0.384	0.411

SBA-29C8						
	Surface Specific Retention					
%MeOH	Benzene	Toluene	Ethylben	Propylben	Butylben	Amylben
0	550.525	2247.802				
10	348.143	1116.544	3465.726			
20	189.434	477.744	1197.241			
30	90.394	183.777	374.902	826.412		
40	43.711	75.056	129.063	235.895	426.996	768.787
50	23.130	35.459	54.143	87.237	139.347	222.803
60	13.351	18.906	26.677	39.585	58.380	85.907
70	8.326	11.134	14.788	20.650	28.796	40.036
80	5.551	7.078	8.901	11.725	15.445	20.404
90	3.498	4.171	4.885	5.953	7.234	8.843
100	2.669	2.907	3.227	3.744	4.294	4.951

Appendix A4

Table AIV Retention data Methylene Selctivity in MeCN (GeminiC18)

Retention Summary Gemini C18						
	VR					
%MeCN	Benzene	Toluene	Ethylben	Propylben	Butylben	Amylben
0	38.333	153.679				
10	22.264	72.407				
20	12.599	32.628	83.727			
30	6.353	13.097	28.668	62.241	143.069	
40	3.365	5.732	9.888	18.603	35.017	66.173
50	1.983	2.929	4.387	7.128	11.690	19.403
60	1.320	1.759	2.377	3.465	5.138	7.758
70	0.975	1.204	1.503	2.008	2.743	3.829
80	0.775	0.899	1.050	1.296	1.640	2.127
90	0.653	0.717	0.789	0.903	1.053	1.263
100	0.581	0.612	0.642	0.689	0.744	0.815

Gemini C18						
	Surface Specific Retention					
%MeCN	Benzene	Toluene	Ethylben	Propylben	Butylben	Amylben
0	451.177	1825.391				
10	259.734	857.129				
20	144.580	383.209	991.988			
30	70.167	150.513	336.024	736.007	1698.985	
40	34.568	62.768	112.282	216.111	411.671	782.852
50	18.103	29.374	46.744	79.406	133.757	225.642
60	10.210	15.440	22.803	35.759	55.691	86.905
70	6.100	8.828	12.384	18.401	27.158	40.096
80	3.717	5.188	6.987	9.924	14.017	19.825
90	2.264	3.026	3.884	5.242	7.023	9.531
100	1.406	1.775	2.133	2.687	3.348	4.188

Appendix A5

Table AV Methylene selectivity data in MeCN (SBA 10C8)

Retention Summary SBA-10C8						
	VR					
%MeCN	Benzene	Toluene	Ethylben	Propylben	Butylben	Amylben
0	33.718	129.016				
10	29.043	93.598				
20	15.735	39.259	99.280			
30	7.760	15.468	31.256	69.101		
40	3.967	6.540	11.000	19.852	35.776	64.491
50	2.263	3.263	4.786	7.469	11.787	18.576
60	1.462	1.913	2.544	3.591	5.126	7.394
70	1.057	1.288	1.589	2.068	2.737	3.680
80	0.828	0.950	1.097	1.325	1.628	2.033
90	0.688	0.749	0.818	0.920	1.049	1.211
100	0.611	0.637	0.663	0.704	0.751	0.805

SBA-10C8						
	Surface Specific Retention					
%MeCN	Benzene	Toluene	Ethylben	Propylben	Butylben	Amylben
0	261.652	1012.172				
10	224.834	733.241				
20	120.027	305.294	777.990			
30	57.226	117.924	242.266	540.315		
40	27.352	47.615	82.740	152.454	277.864	504.005
50	13.928	21.803	33.798	54.928	88.938	142.405
60	7.623	11.175	16.141	24.390	36.475	54.337
70	4.437	6.256	8.621	12.393	17.667	25.094
80	2.630	3.589	4.749	6.547	8.928	12.118
90	1.528	2.008	2.552	3.355	4.371	5.647
100	0.921	1.129	1.331	1.654	2.024	2.449

Appendix A6

Table A VI Methylene Selectivty MeCN (SB29C8)

Retention Summary SBA-29C8						
	VR					
%MeCN	Benzene	Toluene	Ethylben	Propylben	Butylben	Amylben
0	22.559	91.463				
10	14.343	45.538	140.906			
20	7.900	19.605	48.814			
30	3.880	7.671	15.430	33.759		
40	1.985	3.257	5.450	9.787	17.545	31.420
50	1.149	1.650	2.408	3.752	5.867	9.255
60	0.752	0.978	1.293	1.817	2.580	3.698
70	0.548	0.662	0.810	1.048	1.379	1.835
80	0.435	0.497	0.571	0.686	0.837	1.038
90	0.352	0.379	0.408	0.452	0.504	0.569
100	0.318	0.328	0.341	0.362	0.384	0.411

SBA-29C8						
	Surface Specific Retention					
%MeCN	Benzene	Toluene	Ethylben	Propylben	Butylben	Amylben
0	550.525	2247.802				
10	348.143	1116.544	3465.726			
20	189.434	477.744	1197.241			
30	90.394	183.777	374.902	826.412		
40	43.711	75.056	129.063	235.895	426.996	768.787
50	23.130	35.459	54.143	87.237	139.347	222.803
60	13.351	18.906	26.677	39.585	58.380	85.907
70	8.326	11.134	14.788	20.650	28.796	40.036
80	5.551	7.078	8.901	11.725	15.445	20.404
90	3.498	4.171	4.885	5.953	7.234	8.843
100	2.669	2.907	3.227	3.744	4.294	4.951

Appendix A7

Interparticle Volume Determination

Column	SBA-AG-29 C8						
length	5	cm					
ID	0.3	cm					
			Vol.packing	**0.200338**	0.567127		
Col.V	**0.35325**	mL					
Flow	**0.5**	mL/min	V ext.col	**21**	**uL**		
			(MW)^1/3		Ret volume		Average
	114200		48.51641	0.169	0.169	0.169	0.1690
	194000		57.8896	0.168	0.168	0.169	0.1682
	410000		74.28959	0.167	0.167	0.167	0.1670
	560000		82.42571	0.166	0.166	0.166	0.1658
	860000		95.09685	0.165	0.165	0.164	0.1643
	994000		99.7996	0.164	0.163	0.164	0.1633
	1850000		122.7601	0.162	0.162	0.162	0.1620

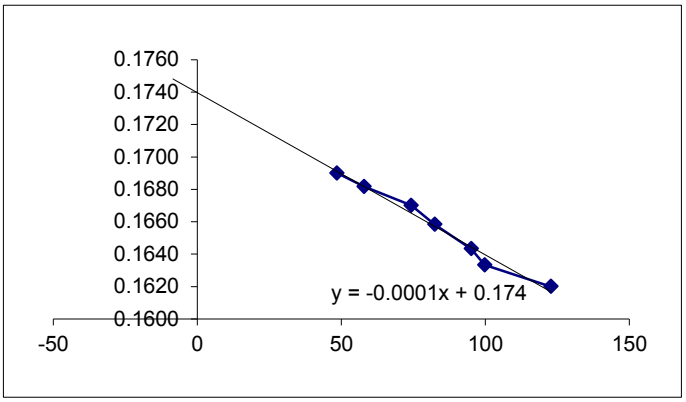

intercept	**0.173912434**	
V int	0.152912434	mL
Vo	0.21	mL
Vpore	0.057	mL/col
Vpore	0.676	mL/g
adsorbant (grams)	0.084449062	g

ADSORPTION CALCULATIONS

Full isoterm

$$\begin{pmatrix} m_{ads} \\ p_{cal} \\ p_{ads} \\ p_{des} \end{pmatrix} :=$$

########	########	########
SBA-AG-3	SBA-AG-3	SBA-AG-3
A40D80	A40D80	A40D80

EXCEL component
experimental data
(paste exp. data in columns:
helium cal.- COL**A**;
adsorption - COL**B**;
desorption - COL**C**.
In the Output dialog box set address regions (e.g. A10:A302) etc.

$m_{ads} := m_{ads} \cdot g \qquad m_{ads} = 0.0542 \cdot g$

Experimental parameters

Manifold volume $V_{man} := 25.3417 \cdot mL$

Sample temperature $T_s := 77.2 \cdot K$

Manifold temperature $T_m := (25 + 273.2) \cdot K$

Nitrogen surface tension $\gamma := 8.72 \cdot \frac{dyne}{cm}$

Definitions

$nm := 10^{-9} \cdot m \qquad Å := 10^{-10} \cdot m$

$N_A := 6.022 \cdot 10^{23} \cdot \frac{1}{mole} \qquad mmole := 10^{-3} \cdot mole$

$R := 8.314472 \cdot \frac{joule}{mole \cdot K} \qquad \mu mole := 10^{-6} \cdot mole$

Liq. nitrogen molar volume $V_L := 34.68 \cdot \frac{mL}{mol}$

Sample vial volume calibration

$p := p_{cal} \cdot torr \qquad n := \left| \frac{last(p) - 2}{3} \right|$

number of calibration points $n = 14$

$i := 0 .. \left| \frac{last(p) - 2}{3} \right| \qquad j_h := 1 .. n \qquad Poh_i := p_{3 \cdot i} \qquad Peh_i := p_{3 \cdot i + 1}$

$$V_{v_0} := \frac{T_s \cdot V_{man}}{T_m} \cdot \left(\frac{Poh_0}{Peh_0} - 1 \right) \qquad V_{vj_h} := \frac{T_s \cdot V_{man}}{T_m} \cdot \frac{Peh_{j_h} - Poh_{j_h}}{Peh_{j_h - 1} - Peh_{j_h}}$$

$V_{av} := mean(V_v)$ $V_{av} = 9.006 \cdot mL$ Vial volume

$rsd\_V := \frac{stdev(V_v)}{V_{av}} \cdot 100$ $rsd\_V = 0.352$ RSD%

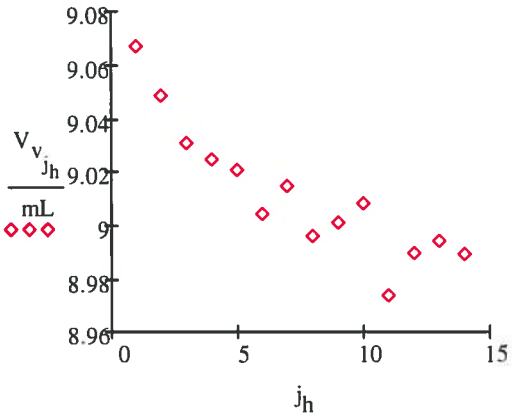

Adsorption Isotherm

$p_{ads} := p_{ads} \cdot torr \qquad n_a := \left| \frac{last(p) - 2}{3} \right| \qquad i := 0 .. n_a \qquad i2 := 1 .. n_a$

Split of a raw data series separate vectors: Po, Pe, Ps (adsorption data)

$p_{o_i} := p_{3 \cdot i} \qquad p_{e_i} := p_{3 \cdot i+1} \qquad p_{s_i} := p_{3 \cdot i+2}$

$sm_i := i \qquad p_{ss} := ksmooth(sm, p_s, 11) \qquad p_{ps_i} := \frac{p_{e_i}}{p_{ss_i}}$

Smoothing of Ps data

$$a_{ads_0} := \frac{p_{o_0} \cdot V_{man}}{T_m} - \frac{p_{e_0} \cdot V_{man}}{T_m} - \frac{p_{e_0} \cdot V_{av}}{T_s}$$

$$a_{ads_{i2}} := \frac{V_{man}}{T_m} \cdot \left(p_{o_{i2}} - p_{e_{i2}} \right) + \frac{V_{av}}{T_s} \cdot \left(p_{e_{i2-1}} - p_{e_{i2}} \right)$$

$$ads_i := \frac{\sum_{j2=0}^{i} a_{ads_{j2}}}{R \cdot m_{ads}}$$

$a_{max} := max(ads) \qquad a_{max} = 35.308 \cdot \frac{mmole}{g}$

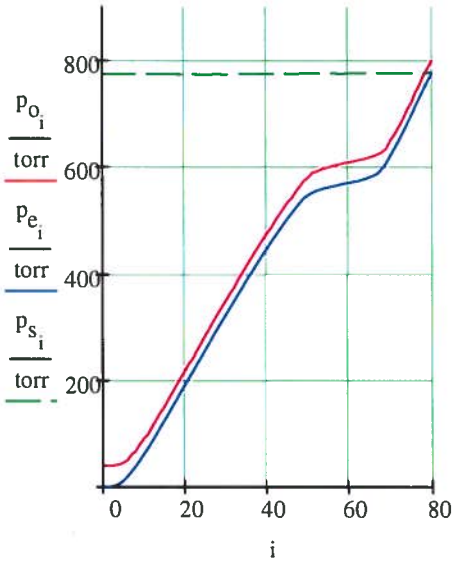

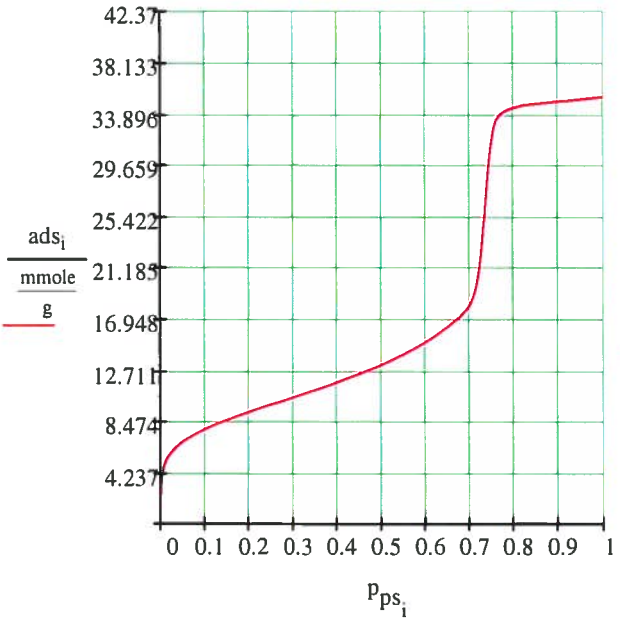

$Ads(x) := linterp(p_{ps}, ads, x)$

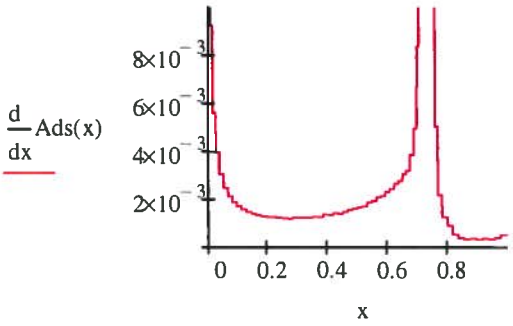

$V_{pore} := \frac{34.7}{1000} \cdot 34.851 \qquad V_p := V_{pore} \cdot \frac{mL}{g}$

$V_p = 1.209 \cdot \frac{mL}{g}$

$\sqrt{\blacksquare}$

$$n_b(p_{ps}, n_a, mi, ma) := \begin{| i \leftarrow 0 \\ \text{for } j \in 0..n_a \\ \quad i \leftarrow i + 1 \text{ if } mi < p_{ps_j} < ma \\ i |}$$

$$n_s(p_{ps}, t) := \begin{| i \leftarrow 0 \\ \text{while } p_{ps_i} < t \\ \quad i \leftarrow i + 1 |}$$

BET calculations

Select BET region (str - start; en - end)

str := .1 $n_{ss} := n_s(p_{ps}, str)$ $n_s = 12$ en := .2 $n_{bs} := n_b(p_{ps}, n_a, str, en)$ $n_b = 6$ $i_b := 0..n_b - 1$

$PP_{b_{i_b}} := p_{ps_{n_s+i_b}}$ $ads_{b_{i_b}} := ads_{n_s+i_b}$ $Bet_{i_b} := \dfrac{PP_{b_{i_b}}}{ads_{b_{i_b}} \cdot (1 - PP_{b_{i_b}})}$

$slp := slope(PP_b, Bet)$ $icpt := intercept(PP_b, Bet)$ $C := \dfrac{slp}{icpt} + 1$ $N_{max} := \dfrac{1}{slp + icpt}$

$\omega := 16.2 \cdot Å^2$ $S := \omega \cdot N_A \cdot N_{max}$

C = 97.558 Constant C of BET equation

S = 752.427 $\frac{m^2}{g}$ **surface area [m^2/g]**

$$ad_i := \frac{N_{max} \cdot C \cdot p_{ps_i}}{(1 - p_{ps_i}) \cdot [1 + (C - 1) \cdot p_{ps_i}]}$$

BET graph

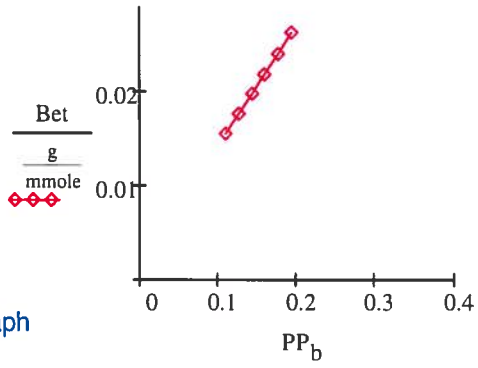

$p := p_{des} \cdot torr$ **Pore volume calculations**

$$n_p := \left| \frac{\text{last}(p) - 2}{3} \right| \qquad i3 := 0 .. n_p \qquad Ppo_{i3} := p_{3 \cdot i3} \qquad Ppe_{i3} := p_{3 \cdot i3+1} \qquad Pps_{i3} := p_{3 \cdot i3+2}$$

$st_{i3} := i3$ $\qquad P_{ds} := \text{ksmooth}(st, P_{ps}, 10)$ Split and smooth of desorption raw data $\qquad P_{start} := Pe_{n_a}$

$$PPps_{i3} := \frac{Ppe_{i3}}{P_{ds_{i3}}} \qquad k := 1 .. n_p \qquad PP_{ps} := PPps \qquad n_p = 26$$

$$v_{des_0} := \left[Ppe_0 \cdot \left(\frac{V_{man}}{T_m} + \frac{V_{av}}{T_s} \right) - Ppo_0 \cdot \frac{V_{man}}{T_m} - P_{start} \cdot \frac{V_{av}}{T_s} \right] \cdot \frac{273.2 \cdot K}{760 \cdot torr \cdot m_{ads}}$$

$$v_{des_k} := \left[Ppe_k \cdot \left(\frac{V_{man}}{T_m} + \frac{V_{av}}{T_s} \right) - Ppo_k \cdot \frac{V_{man}}{T_m} - Ppe_{k-1} \cdot \frac{V_{av}}{T_s} \right] \cdot \frac{273.2 \cdot K}{760 \cdot torr \cdot m_{ads}} \qquad V_{des_k} := \left(\sum_{j=0}^{k} v_{des_j} \right)$$

$$ads_{stp} := ads \cdot 273.2 \cdot K \cdot \frac{R}{1 \cdot atm}$$

Full isotherm
adsorption and desorption branches
are shown in N2 volume at STP cond.

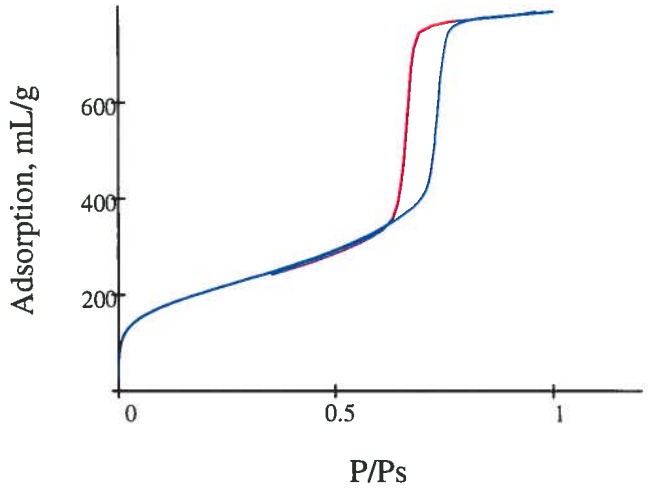

Evaluation of the adsorbtion thickness

$$opt := much(p_{ps}, 0.6) \qquad j_o := 0..opt - n_s \qquad vg := \begin{pmatrix} 3 \\ 2 \end{pmatrix}$$

$$ads_{u_{j_o}} := \frac{ads_{n_s + j_o}}{N_{max}} \qquad pp_{u_{j_o}} := p_{ps_{n_s + j_o}}$$

$$P := genfit(pp_u, ads_u, vg, F) \qquad P = \begin{pmatrix} 2.356 \\ 2.453 \end{pmatrix} \qquad ad_u(r) := F(r, P)_0$$

$$F(z,u) := \begin{bmatrix} \exp\left(\frac{\ln\left(\frac{u_1}{\ln\left(\frac{1}{z}\right)}\right)}{u_0}\right) \\ \frac{-\ln\left(\frac{u_1}{\ln\left(\frac{1}{z}\right)}\right)}{(u_0)^2} \cdot \exp\left(\frac{\ln\left(\frac{u_1}{\ln\left(\frac{1}{z}\right)}\right)}{u_0}\right) \\ \frac{1}{u_1 \cdot u_0} \cdot \exp\left(\frac{\ln\left(\frac{u_1}{\ln\left(\frac{1}{z}\right)}\right)}{u_0}\right) \end{bmatrix}$$

Nitrogen adsorbed layer thickness $\tau := 3.54 \cdot Å$

Pore size distribution calculations

$$A_{des} := reverse(V_{des}) \qquad \tau_{des_{i3}} := ad_u\left(PP_{ps_{i3}}\right) \cdot \tau \qquad R_{ds} := -\frac{\frac{2 \cdot \gamma \cdot V_L}{R \cdot T_s}}{\ln(PP_{ps})} \qquad R_{des_{i3}} := \tau_{des_{i3}} + R_{ds_{i3}}$$

$$r_{des} := reverse(R_{des}) \qquad Pore(x) := linterp\left(\frac{r_{des}}{Å}, \frac{A_{des}}{\frac{mL}{g}}, x\right)$$

Distribution (integral form)

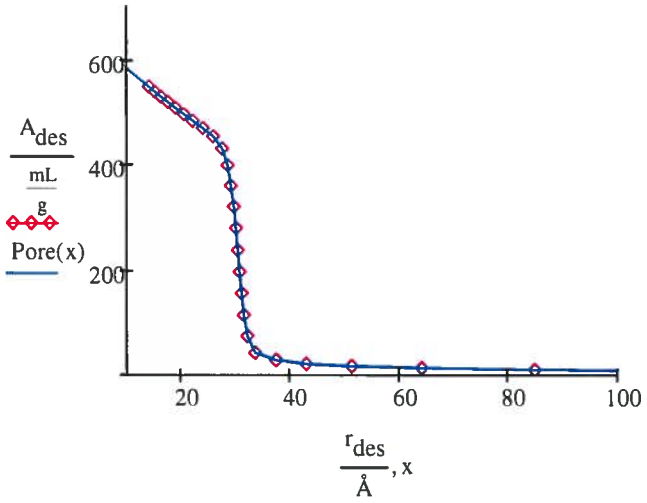

$$dis(x) := \frac{d}{dx}Pore(x)$$

$$Dist_{i3} := -dis\left(\frac{r_{des_{i3}}}{Å}\right)$$

$$R_{max} := r_{des_{much(Dist,\,max(Dist))+1}}$$

$$R_{max} = 30.417 \cdot Å$$

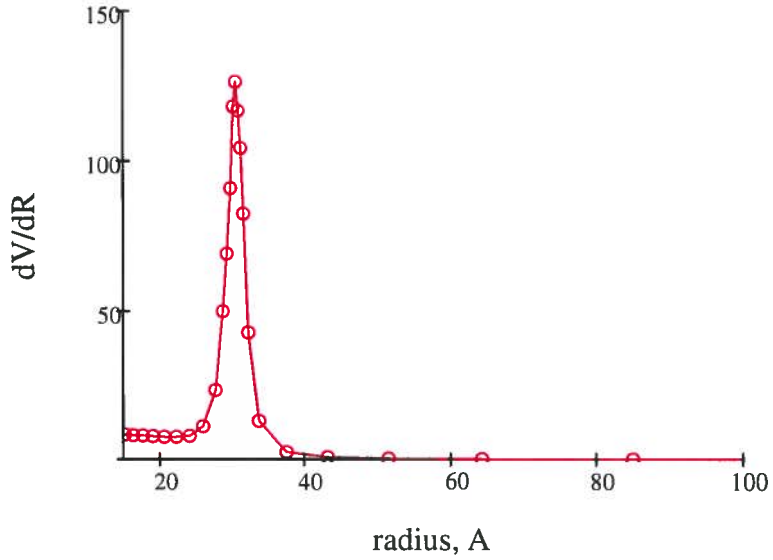

Cylindrical pore correlation check

$$d_{Si} := 2.2 \cdot \frac{g}{mL} \qquad S = 752.427 \cdot \frac{m^2}{g} \qquad V_p = 1.211 \cdot \frac{mL}{g}$$

Radius from desorbtion

$$R_{max} = 30.417 \cdot Å$$

Radius from surface

$$2 \cdot \frac{V_p}{S} = 3.22 \cdot nm$$

$$\frac{R_{max} - 2 \cdot \frac{V_p}{S}}{R_{max}} \cdot 100 = -5.848$$

find number for vector element < x

$$\text{much}(ads, x) := \begin{| i \leftarrow 0 \\ \text{while } ads_i < x \\ \quad i \leftarrow i + 1 \\ i - 1 |$$

$$\Delta Bet\%_{i_b} := \left[1 - \left(\frac{slp \cdot PP_{b_{i_b}} + icpt}{Bet_{i_b}}\right)\right] \cdot 100 \qquad N_{max} = 7.713 \cdot \frac{mmole}{g}$$

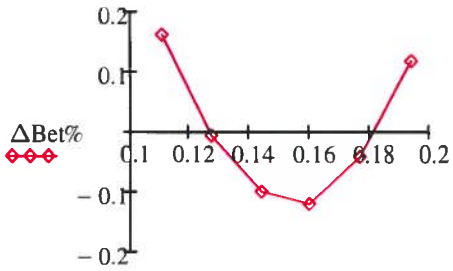

PP_b

t graph (relative to the standard isotherm from Gregg and Sing

$$\begin{pmatrix} pp_s \\ t_{val} \end{pmatrix} :=$$

1.00E-03	1.389
5.00E-03	1.875
0.01	2.152
0.02	2.673
0.03	2.951
0.04	3.124
0.05	3.229
0.06	3.263
0.07	3.367
0.08	3.472

$n_m := 5.381 \qquad t(x) := \text{linterp}\left(\frac{t_{val}}{n_m}, pp_s, x\right)$

$Tf(x) := Ads(t(x))$